Quarterly Reviews of Biophysics **39**, 3 (2006), pp. 227–324. © 2006 Cambridge University Press
doi:10.1017/S0033583506004434 Printed in the United Kingdom
First published online 12 October 2006


# The architecture and function of the light-harvesting apparatus of purple bacteria: from single molecules to *in vivo* membranes

Richard J. Cogdell[1]*, Andrew Gall[2] and Jürgen Köhler[3]

[1] Biomedical Research Building, Institute of Biomedical and Life Sciences, University of Glasgow, Glasgow, UK
[2] Service de Biophysique et des Fonctions Membranaires, Département de Biologie Joliot-Curie/CEA, et Protéines Membranaires Transductrices d'Energie URA2096/CNRS, Centre d'Etudes de Saclay, Gif-sur-Yvette, France
[3] Lehrstuhl für Experimentalphyik IV and Bayreuth Institute for Macromolecular Research (BIMF), Universität Bayreuth, Germany

**Abstract.** This review describes the structures of the two major integral membrane pigment complexes, the RC–LH1 'core' and LH2 complexes, which together make up the light-harvesting system present in typical purple photosynthetic bacteria. The antenna complexes serve to absorb incident solar radiation and to transfer it to the reaction centres, where it is used to 'power' the photosynthetic redox reaction and ultimately leads to the synthesis of ATP. Our current understanding of the biosynthesis and assembly of the LH and RC complexes is described, with special emphasis on the roles of the newly described bacteriophytochromes. Using both the structural information and that obtained from a wide variety of biophysical techniques, the details of each of the different energy-transfer reactions that occur, between the absorption of a photon and the charge separation in the RC, are described. Special emphasis is given to show how the use of single-molecule spectroscopy has provided a more detailed understanding of the molecular mechanisms involved in the energy-transfer processes. We have tried, with the help of an Appendix, to make the details of the quantum mechanics that are required to appreciate these molecular mechanisms, accessible to mathematically illiterate biologists. The elegance of the purple bacterial light-harvesting system lies in the way in which it has cleverly exploited quantum mechanics.



* Author to whom correspondence should be addressed: Professor R. J. Cogdell, Biomedical Research Building, Institute of Biomedical and Life Sciences, University of Glasgow, 126 University Place, Glasgow G12 8TA, UK.
Tel.: +44 (0)141-330-4232; Fax: +44 (0)141-330-4620; Email: R.cogdell@bio.gla.ac.uk

## 1. Introduction

Photosynthesis usually starts with the absorption of a photon by the light-harvesting (LH) apparatus. This absorbed energy is then rapidly and efficiently transferred to a reaction centre (RC), where it is used to drive a transmembrane charge separation. At this point the light-energy has been 'trapped' and chemistry begins. The result of having a LH or antenna system is to increase the effective cross-section for light absorption of each RC. This then allows photosynthesis to operate effectively over a wide range of incident light-intensities. To put this another way, the antenna system acts to concentrate diffuse solar energy at the RC, where it can be transduced into useful chemical energy. The concept of the photosynthetic unit (PSU), where the LH apparatus funnels energy to a trap, was experimentally demonstrated by Duysens (1952).

This review describes how the LH apparatus, present in purple non-sulphur photosynthetic bacteria, works. We have set out to try to make this review accessible to both biologists and physicists. This is especially challenging when trying to present the theoretical ideas, which have been developed to explain the spectroscopic and energy-transfer properties of the LH complexes, in a way that allows a biologist to understand the main concepts that come out from a detailed quantum mechanical analysis. The beauty of how the purple bacteria have evolved a solution to the problem of efficiently harvesting light energy comes, as we show below, from how they have, by trial and error, been able to elegantly exploit quantum mechanics. We find that this is a truly remarkable outcome.

The purple bacteria are anaerobic photosynthetic organisms and live in the anaerobic layers in ponds, lakes and streams (Pfennig, 1978). This ecological niche is depicted in Fig. 1. The key point in this figure is that the spectrum of the solar energy that reaches the purple bacteria has been filtered by the chlorophyll contained in the oxygenic phototrophs that are located above them, nearer to the sun. This filtering removes the blue and red light (up to $\sim$750 nm). The purple bacteria, therefore, must 'make their living' by utilizing green light and far-red light of wavelengths above 750 nm. They achieve this by having a photosynthesis that is based on bacteriochlorophyll (Bchl) and carotenoids (Car) and examples of the molecular structures of these pigments are shown in Fig. 2. The absorption spectra of these two types of pigments are given in Fig. 3. Cars harvest the green light and the Bchls harvest the near infra-red (NIR) wavelengths.

These light-absorbing pigments function in both the LH system and the RCs. Which of these two functions they actually perform is controlled by the type of protein they are associated with. If they are bound to RC polypeptides they will be involved in electron-transfer reactions, whereas if they are complexed with LH apoproteins they will only participate in energy-transfer reactions. In both of these cases the pigments are non-covalently attached to their binding proteins and these proteins are integral membrane proteins. The interaction of the pigments with these proteins induces a red shift in their major absorption bands, as illustrated in Fig. 3*c*. The physical mechanisms, which underline these spectral shifts, will be discussed in detail later in this review. At this point though, it is important to note that these red shifts provide the proteins with mechanisms for tuning the position of the pigments' absorption bands and this allows both a broadening of the range of wavelengths over which light can be absorbed to power the photosynthetic process and for the establishment of spectral (and therefore energy) gradients that can direct, or 'funnel', the absorbed energy, downhill, towards the RC (Zuber & Cogdell, 1995).

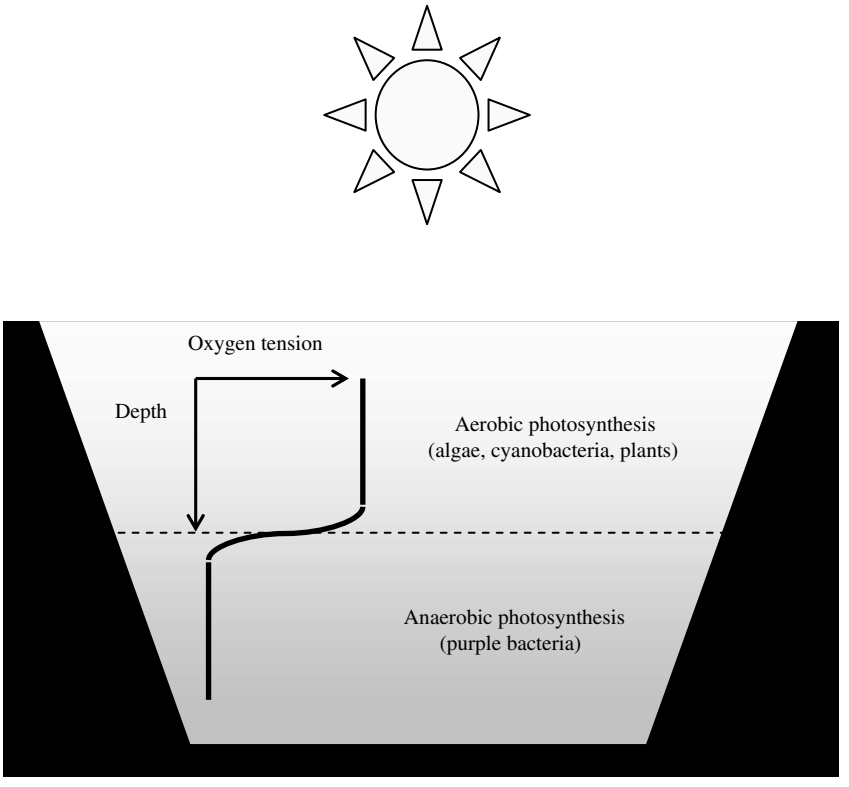


**Fig. 1.** A stylized representation of a lake containing both aerobic and anaerobic phototrophic organisms. Note that purple bacterial photosynthesis is restricted to the lower anaerobic layer and so they only receive solar energy that has been filtered, mainly by chlorophyll. At the interface between the aerobic and anaerobic layers the oxygen tension falls to zero.

Figure 4 shows a cartoon of the photosynthetic membrane of a typical purple bacterium. Remarkably now there are X-ray crystal structures for all of the components shown, or at least very close homologues (Deisenhofer *et al.* 1984, 1985; Allen *et al.* 1986, 1987, 1988; Yeates *et al.* 1987, 1988; Komiya *et al.* 1988; Abrahams *et al.* 1994; McDermott *et al.* 1995; Freer *et al.* 1996; Koepke *et al.* 1996; Prince *et al.* 1997; Stock *et al.* 1999; McLuskey *et al.* 2001; Katona *et al.* 2003; Kurisu *et al.* 2003; Papiz *et al.* 2003; Roszak *et al.* 2003; Stroebel *et al.* 2003; Cramer *et al.* 2005). The primary reactions of purple bacterial photosynthesis, i.e. LH and the RC electron-transfer reactions, all take place within two well-defined pigment–protein complexes, called LH2 and the RC–LH1 'core' complex. Starting with the photosynthetic membranes, it is rather easy to solubilize these complexes and then to independently isolate and purify them. The first step in this process is shown in Fig. 5, where we have used *Rhodopseudomonas* (*Rps.*) *acidophila* 10050 membranes as an example. The two complexes are well resolved on the sucrose gradients and clearly visible by eye. Since the eye is not sensitive in the NIR, where the long wavelength absorption bands of the Bchls are located, the complexes appear red/brown in colour due to the strong absorption of the Cars. The colours of the two bands are different due to the preferential uptake of different Car molecules into the different LH antennae (see Table 1; Gall *et al.* 2005). Figure 5 also shows the absorption spectra of these two complexes.

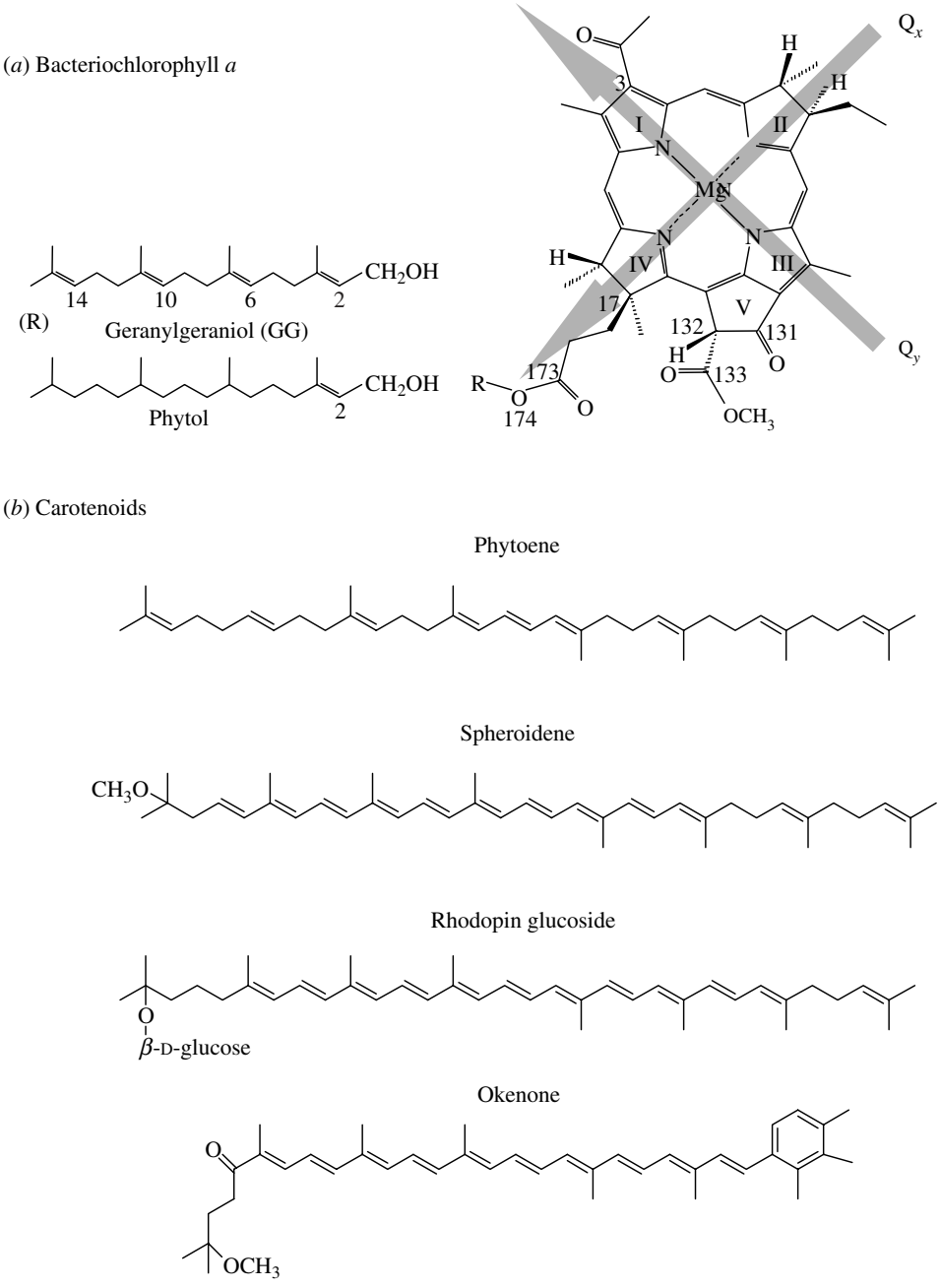


**Fig. 2.** Structures of the (*a*) bacteriochlorophyll *a* and (*b*) carotenoid pigments found in the LH systems of purple bacteria. Different bacteria can produce different Bchl*a* and Car molecules. In most cases the esterifying alcohol in Bchl*a* is phytol, however, geranylgeraniol (gg) is also sometimes present. The different Car molecules are built from the $C_{40}$ molecule phytoene and three examples are depicted: spheroidene (from *Rb. sphaeroides*), rhodopin-glucoside (from *Rps. acidophila*) and okenone (from *Chr. purparatum*). (For detailed descriptions of Bchl and Car structures and their biosynthetic pathways see Scheer, 1991; Takaichi, 1999.) The numbering scheme of the bchl molecule conforms to the IUPAC standard (IUPAC, 1987). The directions of the $Q_x$ and $Q_y$ transition dipoles within the molecular frame of the bacteriochlorin ring are shown by the arrows.

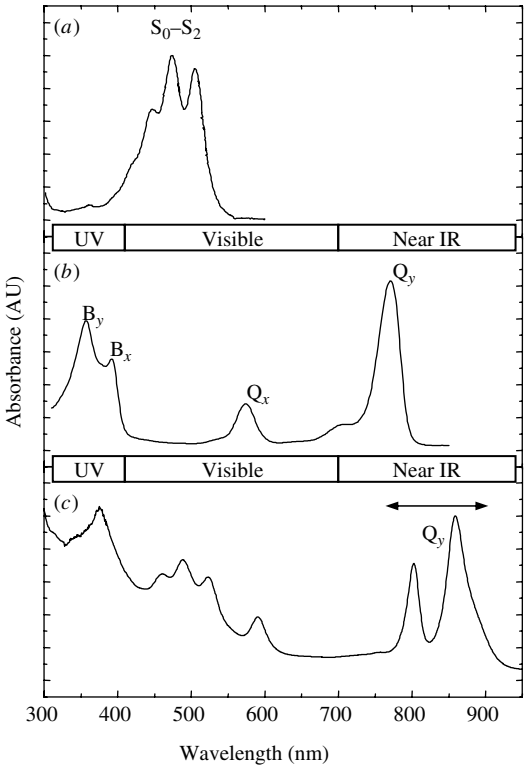


**Fig. 3.** Room-temperature absorption spectra of the Bchl and Car pigments from *Rps. acidophila*. (*a*) Characteristic ground state ($S_0$–$S_2$) absorption peaks of solvent-extracted Car rhodopin-glucoside in hexane. (*b*) Monomeric Bchl*a* in 7:2 (v/v) acetone:methanol showing its Soret ($B_x$ and $B_y$), $Q_x$ (590 nm) and $Q_y$ (772 nm) electronic transitions. (*c*) *In vivo* absorption spectrum of isolated membranes. The absorption spectra of both the Cars and $Q_y$ transitions of the bacteriochlorphylls (and bacteriophyophytins) are red-shifted when the pigments are bound to their apoproteins in the photosynthetic membrane. This is especially noticeable for the $Q_y$ transition, which shifts from 772 nm (in organic solvent) to between ~800 nm and ~900 nm (see double-headed arrow), *in vivo*.

In the NIR LH2 has two strong absorption bands at ~800 and 850 nm, while the RC–LH1 complex has a single strong absorption band at ~875 nm. As a result LH2 and LH1 complexes can also be referred to as the B800–850 and B875 complexes respectively (Cogdell *et al.* 1985). Both the LH1 and the LH2 complexes are constructed on the same modular principle. The Bchls and Cars are non-covalently attached to two low-molecular-weight, hydrophobic apoproteins, called $\alpha$ and $\beta$. These then oligomerize to produce the intact native structures.

In this review we use the names of many different purple bacteria. Since the nomenclature of purple bacterial species is continually being changed by taxonomists we have chosen to use the names that most workers in the field will recognize. For example, although *Rhodopseudomonas acidophila* has been reclassified as *Rhodoblastus acidophilus* (Imhoff, 2001) we shall continue to use *Rps. acidophila* here. The current nomenclature of purple photosynthetic bacteria is listed in Table 2 and is updated with the publication of each new edition of the *International Journal of Systematic and Evolutionary Microbiology*.

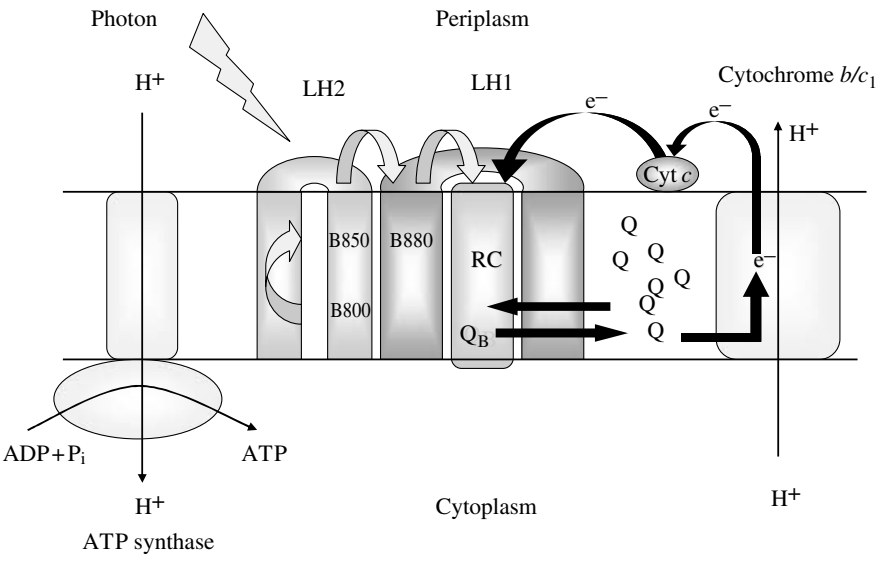


**Fig. 4.** A cartoon of the photosynthetic membrane of a typical purple bacterium. The major integral membrane proteins involved in the light reactions of photosynthesis are shown. The grey arrows indicate energy transfer and the black arrows the redox reactions involved their simple cyclic electron transport pathway. The reaction centre (RC) reduces the secondary electron acceptor (ubiqinone, $Q_B$) which has to pass through the LH1 complex inorder to deliver its reducing equivalents to cyclic electron pathway. Electron transport pumps protons across the membrane and the resultant trans-membrane proton motive force is used by the ATP-synthase to generate ATP.

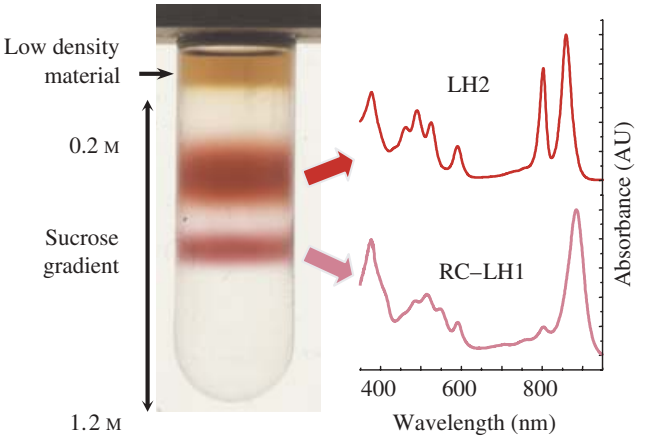


**Fig. 5.** First steps in the isolation and purification of LH2 and RC–LH1 complexes from *Rps. acidophila* strain 10050. The photosynthetic membrane depicted in Fig. 3*c* was solubilized by addition of the detergent LDAO (Fluka Biochemicals). Then the solubilized material was layered onto the top of a sucrose-density gradient and centrifuged at 190 000 ***g*** for 14 h. This separates the two major LH complexes from the rest of the cellular material. The two complexes have a different colour since they preferentially bind different Cars. The Car composition of the two LH complexes are shown in the Table 1. The room-temperature absorption spectra of the LH2 and RC–LH1 complexes are shown in this figure. (For fuller descriptions of the complete isolation and purification processes, see Firsov & Drews, 1977; Cogdell *et al.* 1983; Gall *et al.* 2005.)

**Table 1.** *The composition* (*mol %*) *of coloured carotenoids found in the light-harvesting complexes of* Rps. acidophila *10050* (*redrawn from Gall et al. 2005*)

| Carotenoid | LH2 | RC-LH1 |
|---|---|---|
| Lycopene | 3 | 1 |
| Rhodopin | 17 | 1 |
| Rhodopin-glucoside | 78 | 5 |
| Rhodopinol-glucoside | 1 | 0 |
| Rhodovibrin | 0 | 0 |
| Anhydrorhodovibrin | 1 | 9 |
| OH-spirilloxanthin | 0 | 0 |
| Spirilloxanthin | <1 | 84 |

## 2. Structures

### 2.1 The structure of LH2

The overall structure of LH2 from the purple bacterium *Rps. acidophila* strain 10050 is shown in Fig. 6. This LH2 complex is a circular nonamer and is composed of nine pairs of $\alpha\beta$-apoproteins (McDermott *et al.* 1995). Each of these apoproteins has a single transmembrane $\alpha$-helix. The inner wall of the complex is formed by the 9 $\alpha$-apoprotein helices. The outer wall is formed by the nine $\beta$-apoprotein helices. The structure is capped on either side by the N- and the C-termini of both apoproteins folding over and interacting with one another. The majority of the pigments are complexed in the space between the $\alpha$- and $\beta$-apoproteins. These apoproteins form a scaffold that positions the pigments for optimal functionality. The N-termini of both the apoproteins are located at the cytoplasmic surface of the photosynthetic membrane and the C-terminal at the periplasmic side (see Brunisholz & Zuber, 1992; Zuber & Cogdell, 1995).

Starting from the cytoplasmic side and 'walking' through the complex the first group of pigments encountered are nine monomeric Bchl*a* molecules, one for each $\alpha\beta$-apoprotein pair (Fig. 7). The bacteriochlorin rings of these Bchls lie flat, parallel to the membrane plane and at right angles to the transmembrane $\alpha$-helices. The central $Mg^{2+}$, inside the B800 bacteriochlorin ring, is liganded to the protein *via* an extension of the N-terminal methionine residue of the $\alpha$-apoprotein. In the original structural description of LH2 (McDermott *et al.* 1995), which was at a resolution of 2·5 Å, this extension was modelled as an *N*-formyl group. However the improved structure of 2·0 Å resolution clearly shows that this was incorrect (Papiz *et al.* 2003). The higher resolution electron-density map in this region is best fitted by a carboxyl group suggesting the presence of COO-$\alpha$-Met1 (Fig. 8). Although this is an unusual modification it is not unique (Sage *et al.* 1996; Benini *et al.* 2001). The B800 Bchl molecule also has H-bond interactions with $\beta$-Arg20 and the residues $\beta$-His12 and $\alpha$-Gln3 *via* the $\alpha$-COO ligand. In the nonameric ring the monomeric Bchl*a* molecules are separated, centre-to-centre, by 21·3 Å (Fig. 9*b*). They give rise to the 800 nm absorption band (Fig. 5) and are called the B800 molecules. The B800 Bchls from *Rps. acidophila* are bound rather loosely and can be reversibly removed from the complex (Fraser *et al.* 1999). Interestingly, it has also been possible to reconstitute modified Bchls and indeed Chls into these B800-binding sites (Gall *et al.* 1999, 2001; van Gammeren *et al.* 2005). This has proved to be very useful for functional studies that will be described later.

**Table 2.** *The nomenclature of purple photosynthetic bacteria. Only species that have had their names changed are listed. The bacterial names in parentheses are reclassifications that were derived from the original basonyms but were further renamed, sometimes more than once*

| Basonym | Reclassified as |
|---|---|
| ***Rhodobacter* (*Rb.*)** | |
| *Rhodobacter adriaticus* | *Rhodovulum adriaticum* |
| *Rhodobacter euryhalinus* | *Rhodovulum euryhalinum* |
| *Rhodobacter sulfidophilus* | *Rhodovulum sulfidophilum* |
| ***Rhodopseudomonas* (*Rps.*)** | |
| *Rhodopseudomonas acidophila* | *Rhodoblastus acidophilus* |
| *Rhodopseudomonas adriatica* | *Rhodovulum adriaticum* (*Rhodobacter adriaticus*) |
| *Rhodopseudomonas blastica* | *Rhodobacter blasticus* |
| *Rhodopseudomonas capsulata* | *Rhodobacter capsulatus* |
| *Rhodopseudomonas gelatinosa* | *Rubrivivax gelatinosus* (*Rhodocyclus gelatinosus*) |
| *Rhodopseudomonas globiformis* | *Rhodopila globiformis* |
| *Rhodopseudomonas marina* | *Rhodobium marinum* |
| *Rhodopseudomonas rutila* | *Rhodopseudomonas palustris** |
| *Rhodopseudomonas sphaeroides* | *Rhodobacter sphaeroides* |
| *Rhodopseudomonas sulfidophila* | *Rhodovulum sulfidophilum* (*Rhodobacter sulfidophilus*) |
| *Rhodopseudomonas sulfoviridis* | *Blastochloris sulfoviridis* |
| *Rhodopseudomonas viridis* | *Blastochloris viridis* |
| ***Rhodospirillum* (*Rsp.*)** | |
| *Rhodospirillum centenum* | *Rhodocista centenaria* |
| *Rhodospirillum fulvum* | *Phaeospirillum fulvum* |
| *Rhodospirillum molischianum* | *Phaeospirillum molischianum* |
| *Rhodospirillum sodomense* | *Rhodovibrio sodomensis* |
| *Rhodospirillum tenue* | *Rhodocyclus tenuis* |
| ***Chromatium* (*Chr.*)** | |
| *Chromatium buderi* | *Isochromatium buderi* |
| *Chromatium glycolicum* | *Halochromatium glycolicum* |
| *Chromatium gracile* | *Marichromatium gracile* |
| *Chromatium minus* | *Thiocystis minor* |
| *Chromatium minutissimum* | *Allochromatium minutissimum* |
| *Chromatium purpuratum* | *Marichromatium purpuratum* |
| *Chromatium salexigens* | *Halochromatium salexigens* |
| *Chromatium tepidum* | *Thermochromatium tepidum* |
| *Chromatium vinosum* | *Allochromatium vinosum* |
| *Chromatium violascens* | *Thiocystis violascens* |
| *Chromatium warmingii* | *Allochromatium warmingii* |
| ***Ectothiorhodospira*** | |
| *Ectothiorhodospira abdelm* | *Halorhodospira abdelmalekii* |
| *Ectothiorhodospira halochloris* | *Halorhodospira halochloris* |
| *Ectothiorhodospira halophila* | *Halorhodospira halophila* |
| *Ectothiorhodospira marismortui* | *Ectothiorhodospira mobilis** |
| *Ectothiorhodospira vacuolata* | *Ectothiorhodospira shaposhnikovii** |
| ***Thiocapsa*** | |
| *Thiocapsa halophila* | *Thiohalocapsa halophila* |
| *Thiocapsa pfennigii* | *Thiococcus pfennigii* |
| ***Amoebobacter*** | |
| *Amoebobacter pedioformis* | *Thiolamprovum pedioforme* |
| *Amoebobacter pendens* | *Thiocapsa pendens* |
| *Amoebobacter purpureus* | *Lamprocystis purpurea* (*Pfennigia purpurea*) |
| *Amoebobacter roseus* | *Thiocapsa rosea* |

* Heterotypic synonym of the same species.

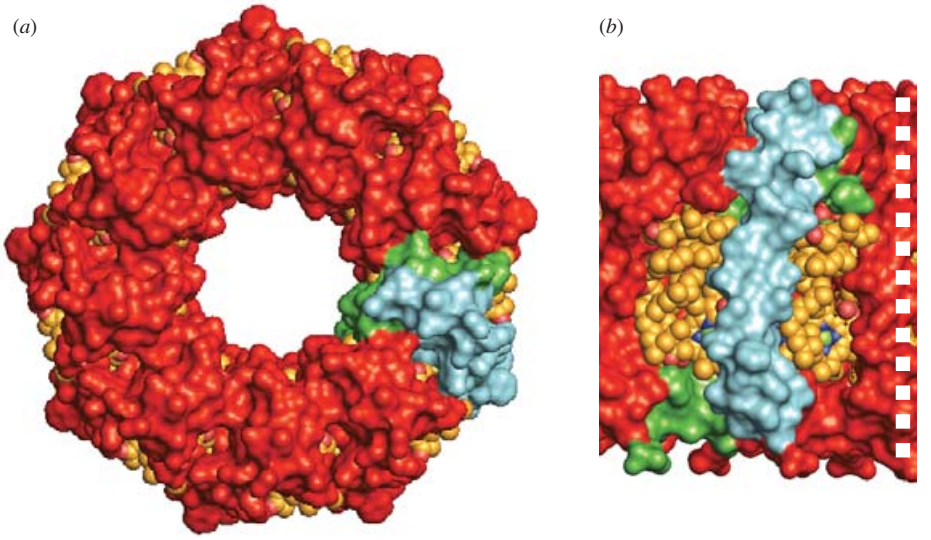


**Fig. 6.** Structure of the LH2 complex from *Rps. acidophila* strain 10050. (*a*) Viewed from the perplasmic side of the photosynthetic membrane. Note the nonameric arrangement. Each 'subunit' is comprised of an inner $\alpha$-apoprotein (green) and an outer $\beta$-apoprotein (cyan). The pigments (yellow) are sandwiched between the apoproteins. (*b*) A view of a small section of LH2 perpendicular to the direction of the transmembrane $\alpha$-helices. The N- and C-terminal domains of the $\alpha$- and $\beta$-apoproteins seal the top and bottom of the complex respectively.

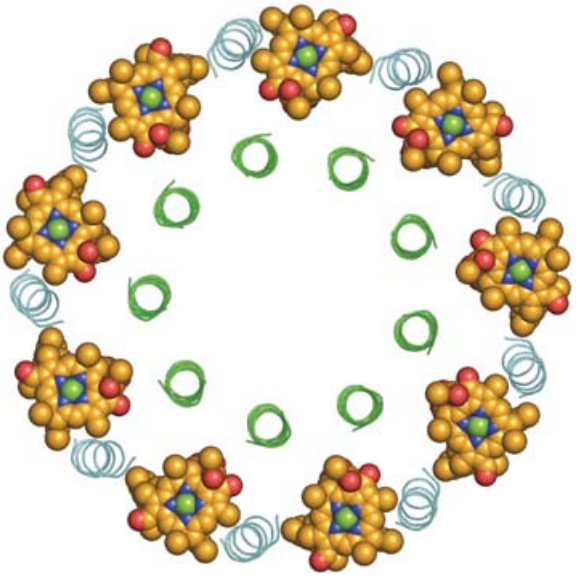

**Fig. 7.** The B800 Bchl molecules in the LH2 complex from *Rps. acidophila* viewed looking in a direction parallel to the direction of the transmembrane $\alpha$- helices. The BChls are sandwiched between the $\alpha$-and $\beta$-apoproteins which are coloured green and cyan respectively. Key to Bchl atom colours: yellow/grey, carbon; green, magnesium; blue, nitrogen; red, oxygen. For clarity, the phytol chains have been removed from the Bchl molecules.

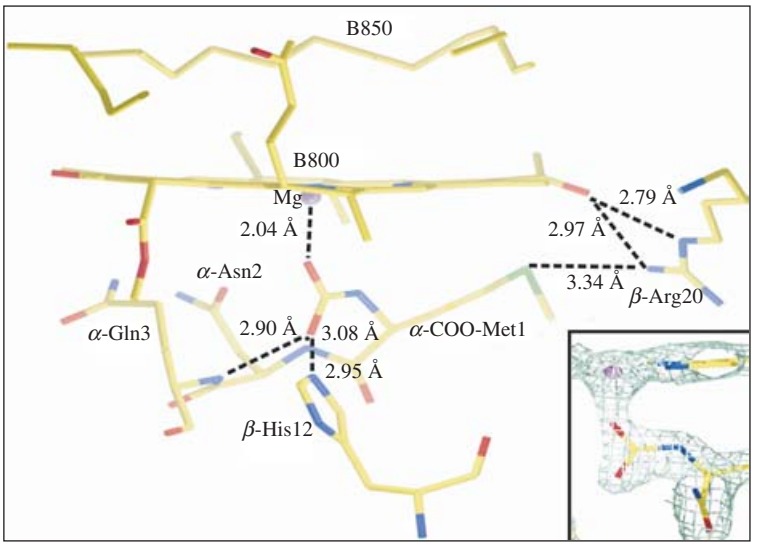


**Fig. 8.** A diagram showing the ligation of the Bchl–B800 molecules *via* a carboxyl group extension of the N-terminal methionine residue of the $\alpha$-apoprotein. Inset: electron density in the region of COO-$\alpha$Met1 and B800 superimposed with the atomic model. (Redrawn from Papiz *et al.* 2003.)

Proceeding down further into the complex a second group of Bchl molecules are encountered (Fig. 9). There are 18 Bchls in this group, two per $\alpha\beta$-apoprotein pair. Their central $Mg^{2+}$ atoms are liganded to the protein by histidine residues and the plane of their bacteriochlorin rings are parallel to the trans-membrane $\alpha$-helices, i.e. at right angles to the B800 bacteriochlorins. In each $\alpha\beta$-apoprotein pair one histidine comes from the $\alpha$-apoprotein and one from the $\beta$-apoprotein. The bacteriochlorin rings of these Bchl*a* molecules are arranged in close proximity to each other. They are separated centre to centre by 9·5 Å within an $\alpha\beta$-apoprotein pair and by 8·8 Å to the closest Bchl molecule in the next $\alpha\beta$-apoprotein pair. The edge-to-edge spacing of these bacteriochlorin rings is, however, much closer (Fig. 9*b*). This ring of closely interacting Bchls is collectively responsible for the 850 nm absorption band (see Fig. 5) and they are called the B850 Bchls.

The Bchl molecules do not only consist of the bacteriochlorin rings, they also have phytol tails. The phytol chains have been traditionally thought of as a rather passive part of the molecule, just serving to make the overall pigment hydrophobic. Close inspection of the LH2 structure, however, reveals that the phytol chains are very important structural elements (Freer *et al.* 1996). Two examples serve to illustrate this point. The phytol chains from the B800 Bchls and the $\beta$-bound B850 Bchls fold around each other rather like two fingers clasping each other (Fig. 10*a*). The B800 phytol chain then passes across the outer face of the $\beta$-B850 making close van der Waals contacts with rings I and IV of the macrocycle. This interaction is clearly important for tying the B800 Bchls into the complex. The oxygen from the ester linkage between the phytol chain of the B850 Bchls and the ester on ring V of the bacteriochlorin of these two Bchls form a ring around $\beta$-Phe22, which is coloured purple in Fig. 10*b*. $\beta$-Phe22 is one of very few amino-acid side-chains that actually protrudes into the centre of the LH2 complex between the $\alpha$- and $\beta$-apoprotein $\alpha$-helices, where the space is almost fully occupied by the pigments alone. These interactions with the phytol chains appear to be the way in which the proteins are able to orientate the bacteriochlorin rings. Once the phytol tail has been locked into position

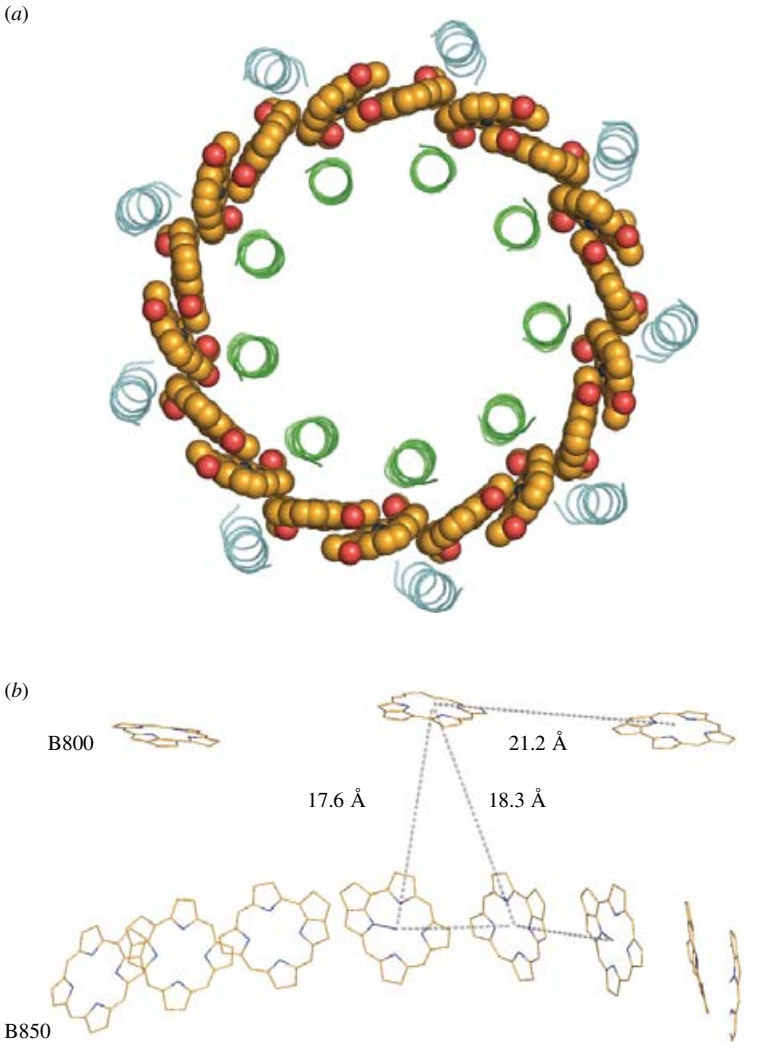


**Fig. 9.** The B850 Bchl molecules in the LH2 complex from *Rps. acidophila* viewed looking in a direction parallel to the direction of the transmembrane $\alpha$-helices. The BChls are sandwiched between the $\alpha$- and $\beta$-apoproteins, which are coloured green and cyan respectively. Key to Bchl atom colours: yellow/grey, carbon; green, magnesium; blue, nitrogen; red, oxygen. For clarity, the phytol chains have been removed from the Bchl molecules. (*b*) The relative separation of the B800 Bchls within their ring and their relative position and distance to the B850 Bchls.

then the orientation of the Bchl head group is also fixed. Therefore, since the Bchl*a* $Q_x$ and $Q_y$ transition dipoles lie in set directions within the molecular frame of the bacteriochlorin ring this then controls their relative positions. This is essential for efficient inter-pigment energy transfer during the LH process, since the relative orientation of the transition dipole moments of the different Bchls is a key determinant of the efficiency of energy transfer (this issue will be considered in depth below). Careful inspection of the B800 and B850 molecules in LH2 reveals that even through the planes of their bacteriochlorin rings are perpendicular to each other the relative orientations of their $Q_y$ transitions are rather parallel to each other, which is favourable for B800→B800 energy transfer (see Fig. 9*b*).

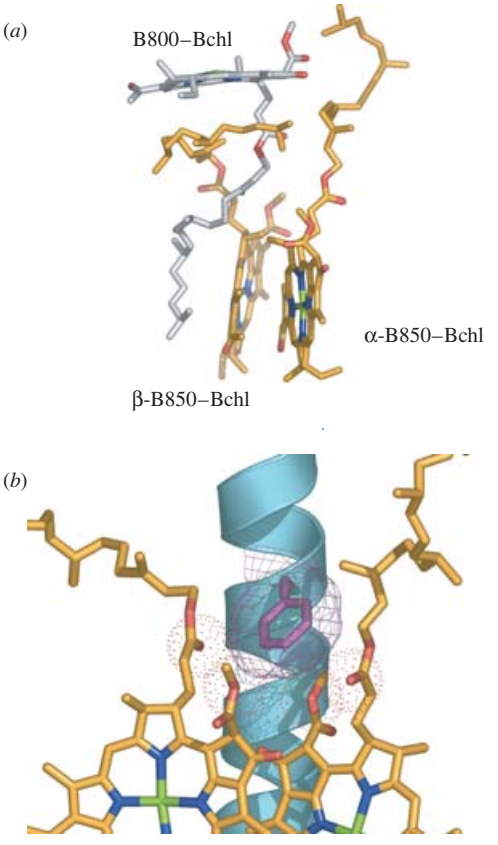


**Fig. 10.** The structural role of the phytol chains. (*a*) The mutual interactions of the phytol chains. Note that the phytol chains of the B800 Bchl*a* and $\beta$-bound B850 Bchl*a* interact strongly with each other. (*b*) van de Waals interactions between the $\beta$-Phe22 (purple) and the oxygen ester atoms of the B850 bchl molecules. Key to Bchl atom colours: yellow/grey, carbon; green, magnesium; blue, nitrogen; red, oxygen. The $\beta$-apoprotein is depicted as ribbon in cyan. (The figure was produced using PyMOL; DeLano, 2004.)

The original structural description of LH2 clearly identified the presence of a single, well-ordered Car molecule, rhodopin-glucoside. This Car has 11 conjugated double bonds, is in an all-*trans* configuration and when viewed down its long axis, is twisted to form about half a helix (Fig. 11*a*). Starting at the glucoside head group the Car is located in a hydrophilic pocket on the cytosolic side of the complex. The glucoside group is partially disordered, suggesting that it can take up to more than one conformation. This Car has an important structural role in LH2. It effectively 'bolts' adjacent $\alpha\beta$-apoprotein pairs together. Indeed in most species of purple bacteria in the absence of Cars the LH2 complexes fail to assemble (Hunter *et al.* 1994; Lang & Hunter, 1994). The Car passes in close contact to the edge of the bacteriochlorin ring of a B800 Bchl (closest contact 3·4 Å, see the left Bchl molecule drawn in wireframe in Fig. 11*b*). It then passes into the next $\alpha\beta$-apoprotein pair and runs over the face of the bacteriochlorin ring of the $\alpha$-bound B850 Bchl (Fig. 11*b*, *c*). In this case the closest contact is 3·7 Å. The improved 2·0 Å resolution structure of LH2 from *Rps. acidophila* has tentatively suggested the presence of a second rhodopin-glucoside molecule per $\alpha\beta$-apoprotein pair (Papiz *et al.* 2003). More recently, the Car–protein interactions in the LH2 complex of *Rps. acidophila* 10050 both

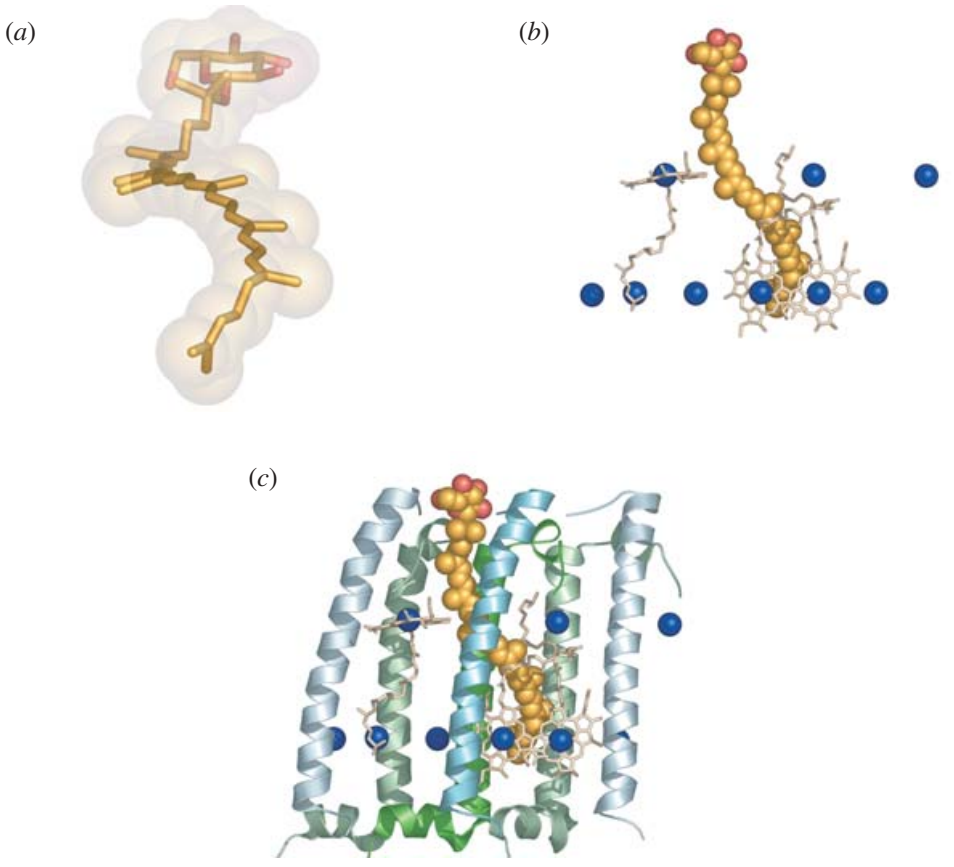


**Fig. 11.** The structure of the all-*trans* carotenoid rhodopin-glucoside in LH2 (*a*) Viewed along its long axis. (*b*) Interaction of the Car with the Bchl molecules viewed from outside of the pigment–protein complex. The $Mg^{+2}$ ions of the Bchl molecules from three $\alpha/\beta$-dimers are depicted as blue spheres. The B800-Bchl from the left-hand dimer and the B850-Bchl molecules from the central $\alpha/\beta$-dimer are shown in wireframe. (*c*) As (*b*) but with the apoproteins inserted. The $\alpha$-apoproteins are coloured in different shades of green, the $\beta$-apoproteins are coloured in different shades of cyan. (The figure was produced using PyMOL; DeLano, 2004.)

in 'free-in-solution' mixed micelles and in 3D crystals has been studied by Raman spectroscopy in resonance with the Car molecules (Gall *et al.* 2006). The results showed that the Car molecules when bound to their binding pockets show no significant differences when the LH2 complexes are 'free-in-solution' or packed in crystalline arrays and did not depend on the detergent type [*N*,*N*-dimethyldodecylamine-*N*-oxide (LDAO) *versus* n-octyl-$\beta$-D-glucopyranoside ($\beta$OG)]. Furthermore, there was no significant wavelength dependence observed in the Raman spectra using different excitation wavelengths, ranging from the 0–1 to the 0–0 components of the electronic absorption spectra of the LH2-bound Car molecules. This indicates that there is only one Car geometry in LH2 and thus only one Car molecule per $\alpha/\beta$-heterodimer. Therefore, these experiments strongly disagree with the interpretation of the 2·0 Å structure for the presence of a second double-*cis* Car molecule in LH2 complex from *Rps. acidophila*. They are, however, in accord with previous pigment analyses of the Bchl*a*:Car stoichiometry for these complexes, where it was concluded that one Car molecule was present per $\alpha/\beta$-apoprotein

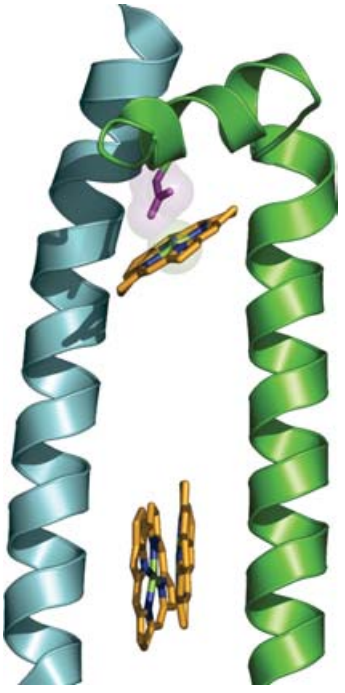

**Fig. 12.** The relative position of the Bchl molecules in the LH2 complex from *Rsp. molischianum* viewed looking in a direction perpendicular to the direction of the transmembrane $\alpha$-helices. The BChls are sandwiched between the $\alpha$- and $\beta$-apoproteins which are coloured green and cyan respectively. The central $Mg^{2+}$ atoms of the B800 Bchls are liganded to the protein *via* $\alpha$-Asp6 (purple). Key to Bchl atom colours: yellow/grey, carbon; green, magnesium; blue, nitrogen; red, oxygen. For clarity, the C- and N-terminal domains of the apoproteins and phytol chains have been omitted.

dimer (Arellano *et al.* 1998) and with the most recent crystallographic data on crystals of LH2 produced in the *meso* lipid phase, which have suggested that the putative RG2 molecule is actually a superposition of the electron density of LDAO and $\beta$OG detergent molecules at this site on the surface of the LH2 complex (Cherezov *et al.* 2006).

A high-resolution crystal structure of a LH2 complex from another species of purple bacteria, *Rhodospirillum* (*Rsp.*) *molischianum* (Giesberger, 1947), has also been described (Koepke *et al.* 1996). Interestingly this complex is an octamer rather than a nonamer. The overall folds of the $\alpha\beta$-apoproteins this complex are very similar to those found in the LH2 complex from *Rps. acidophila*. The most striking difference involves the B800 Bchls. In this case the central $Mg^{2+}$ atoms of the B800 Bchls are liganded to the protein via $\alpha$-Asp6. The result of this is that the bacteriochlorin rings of these B800 Bchls are rotated by 90° and lie at an angle of $\sim$20° to the plane of the lipid bilayer relative to the *Rps. acidophila* complex (Fig. 12). At this time nobody knows what structural features control whether the LH2 rings are 9-mers or 8-mers, or indeed whether these differences in ring size affect function. There has, however, been a recent molecular dynamics- based calculation on the influences of subunit structure on the oligomerization state of these two LH2 complexes (Janosi *et al.* 2005). The main conclusions of this were that the angles between adjacent $\alpha\beta$-apoproteins dimers in the rings were mainly controlled by surface contacts within their transmembrane domains. These ideas now need to be tested using site-directed mutagenesis.

## 2.2 Natural variants of peripheral antenna complexes

Most researchers who study purple photosynthetic bacteria work with a rather restricted number of species, such as *Rhodobacter* (*Rb.*) *sphaeroides*, *Rb. capsulatus, Rhodospirillum* (*Rsp.*) *rubrum, Rps. viridis, and Rps. acidophila*. These tend to be the ones that were historically easiest to grow and that are now the most genetically amenable. This only represents, however, a very small fraction of a total number of species of purple bacteria that have been described (Pfennig, 1967; Brunisholz & Zuber, 1992; Imhoff, 1995; Yurkov & Beatty, 1998; Glaeser & Overmann, 1999). Among this larger group are many bacteria which contain peripheral antenna complexes which have strikingly different NIR absorption spectra compared to the standard LH2 complex detailed above (see Fig. 13). Assuming that all these antenna complexes are constructed on the same modular principle, as that described for the LH2 complex from *Rps. acidophila*, the structural basis of this spectral variation is completely unknown.

If for example cells of *Rps. palustris* strain 2.6.1 (sometimes called strain FRENCH) are grown at low light intensity they synthesize a modified peripheral antenna complex (Fig. 13*a*) compared with the more standard LH2 complex (Fig. 13*b*), which they produce at higher light intensities (Hayashi *et al.* 1982; Evans *et al.* 1990). The *Rps. palustris* genome contains at least four different gene pairs that encode putative LH2 $\alpha\beta$-apoproteins (Tadros & Waterkamp, 1989; Tadros *et al.* 1993; Larimer *et al.* 2004). The gene expression pattern that produces the standard LH2 complex is different from that which produces the spectral variant (Evans *et al.* 1990; Tadros *et al.* 1993; Tharia *et al.* 1999; Hartigan *et al.* 2002). There is now a low-resolution crystal structure (7·5 Å) of this low-light complex (Hartigan *et al.* 2002). The structural model suggests that this complex is a $\alpha\beta$-octamer and that each of its $\alpha\beta$-apoprotein pairs binds an extra Bchl*a* relative to LH2 from *Rps. aciodophila*. Higher resolution data is needed to fully understand how this structural and spectral variation is achieved. But clearly one source of variation is to have multiple antenna apoprotein types. There could even be some complexes that have mixed apoprotein types within single complete rings and this then could in principle produce very different spectral forms.

A marine purple sulfur bacterium, *Chromatium* (*Chr.*) *purpuratum* (Imhoff & Trüper, 1980), produces a peripheral antenna complex that has a completely different NIR absorption spectrum (Fig. 13*g*). This complex has a single strong absorption band at 830 nm and a small shoulder at 800 nm (Cogdell *et al.* 1990). It contains Bchl*a*, an unusual Car, okenone (Fig. 2), and apparently two standard $\alpha\beta$-apoproteins, but nothing is yet known about their primary sequences. To date nobody has been able to produce a structural model of the B830 complex that can account for this absorption spectrum. It will be very interesting to see a structure of this complex and to try to understand the origin of its absorption spectrum.

Hopefully in the future high-resolution structures of several of these spectroscopic variants will be forthcoming and this will enable us to have a much deeper understanding of their structure–function relationships. It is generally assumed that these spectral variants help to equip the different species of purple bacteria to be effective competitors in their individual ecological niches. It will be very interesting indeed to be able to describe the detailed molecular mechanisms that underlie this.

## 2.3 RC–LH1 complexes

RC–LH1 'core' complexes were first visualized in EM pictures of membranes from *Rps. viridis* (Miller, 1979, 1982). This unusual, Bchl*b*-containing species only has LH1 complexes and RCs

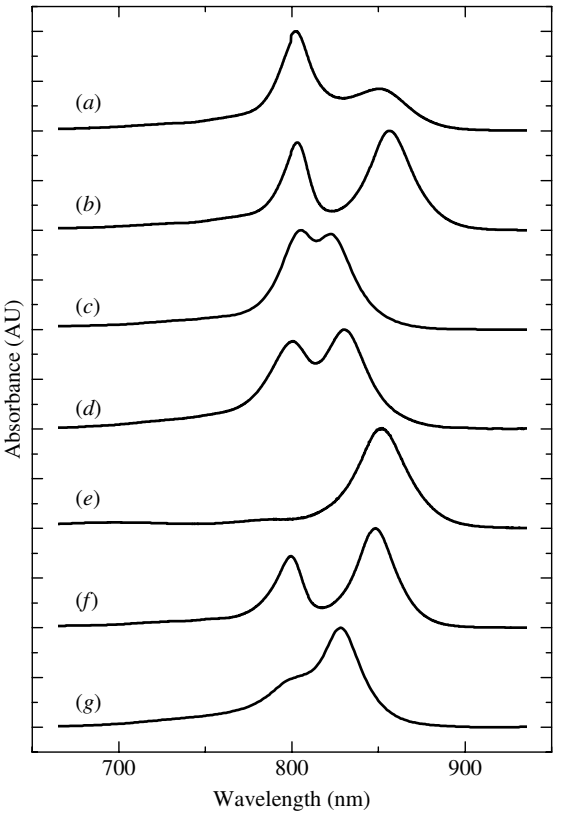


**Fig. 13.** The natural variation of Bchl*a* $Q_y$ transitions in peripheral LH complexes from a range of different species of purple bacteria observed at room temperature. (*a*) B800–850 from *Rps. palustris* 2.6.1 (low-light grown), (*b*) LH2 from *Rps. palustris* 2.6.1 (high-light grown), (*c*) LH3, or B800–820, from *Rps. acidiophila 7050* (low-light grown), (*d*) B798–B832 from *Erythromicrobium ramosum*, (*e*) LH2 from *Rb. sphaeroides* R26.1 that lacks B800–Bchl moleules, (*f*) LH2 from *Rb. sphaeroides* 2.4.1 and (*g*) the B830 complex from *Chr. puprar-atum*. All the complexes were isolated and purified in the presence of the detergent LDAO [0·1% (w/v)] except (*d*) and (*g*) which were purified in the presence of 0·9% (w/v) n-octyl-$\beta$-D-glucopyranoside.

(it lacks LH2). Moreover, the LH1 complexes form rather regular hexagonal arrays within the photosynthetic membranes (Jay *et al.* 1984; Stark *et al.* 1986); an example of this is shown in Fig. 14. These early pictures were interpreted to show that the LH1 complexes surrounded the RC and that the LH1 complexes were hexameric. Later somewhat similar EM pictures of 2D crystals of RC–LH1 'core' complexes from *Rhodobium marinum* (Meckenstock *et al.* 1992a, b, 1994) and *Rps. acidophila* (Gall, 1994) were also described and interpreted in a similar way (Fig. 15*a*).

The model became dogma and most workers in this area did not question it until in 1995 Karrasch *et al.* (1995) used electron crystallography and cryo-EM to study 2D crystals of the LH1 complex from *Rsp. rubrum*. These LH1 complexes were reconstituted from their individual components, i.e. purified $\alpha\beta$-apoproteins and Bchl*a*. Karrasch and co-workers were able to produce a 8·5 Å resolution projection map that showed that the LH1 complex was a circle. It was an $\alpha\beta$-16 mer with a 'hole' in the middle that was large enough to accommodate the RC (Fig. 15*b*). Interestingly they showed that at lower resolution the data appeared to have

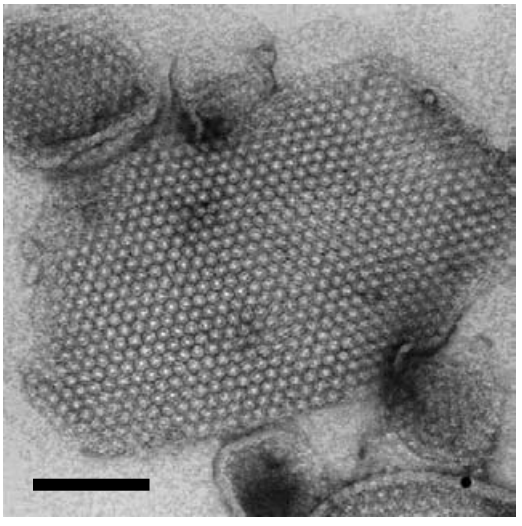

**Fig. 14.** A negatively stained electron micrograph of native membranes from *Rps. viridis*. The RC–LH1 'core' complexes are the 'light' particles which form an hexagonal array (bar, 100 nm). (Courtesy of S. Shimonaka and H. Hashimoto, Osaka City University.)

12-fold symmetry, but at higher resolution this broke down to reveal the 16-fold symmetrical structure.

Since this report there have been many other studies using AFM, cryo-EM, both on 2D crystals of RC–LH1 complexes or from membranes. There have been reports that the RC–LH1 complexes are circular (Gerken *et al.* 2003), square (Stahlberg *et al.* 1998), 'S'-shaped (Scheuring *et al.* 2004a, 2005; Siebert *et al.* 2004), elliptical (Scheuring *et al.* 2003; Fotiadis *et al.* 2004) or even just arcs (Bahatyrova *et al.* 2004b). Indeed this field has become, and indeed still is, very confused. In this review we present what we hope is a unified view of the structure of RC–LH1 complexes, and suggest some reasons for the current state of confusion. We will present this view first, before going into details of why, since this makes the later discussion much easier to understand.

First of all it now seems very clear that there are at least two distinct classes of RC–LH1 complexes. One class are monomeric, i.e. consist of one RC surrounded by one LH1 complex. Examples of this class are the RC–LH1 complexes from *Rsp. rubrum* and *Rps. palustris* (Gall, 1994; Karrasch *et al.* 1995). The second class are dimeric, i.e. consist of two RC–LH1 units. An example of this class is the RC–LH1 complex *Rb. sphaeroides* (Siebert *et al.* 2004). The other property of RC–LH1 complexes that needs to be appreciated is that, unlike the LH2 complexes, they are much less stable when they have been detergent-solubulized from their native membranes, and this is even truer in the absence of the RC. However, there are several reports where different species (*Rb. sphaeroides*, *Rsp. rubrum*, *Rps. viridis*) have been used which show that the LH1 structure is inherently rather flexible (Westerhuis *et al.* 2002; Scheuring, *et al.* 2003, 2004b; Bahatyrova *et al.* 2004b; Fotiadis *et al.* 2004) and this property has clearly been responsible for images showing odd shapes and even partial structures. There is one report for the RC–LH1 complex from *Rsp. rubrum* where the presence of the RC is believed not to influence the perfect circular nature of LH1 (Gerken *et al.* 2003). It is clear that much more conservative interpretation of the data in this area is needed. There is a further complication, especially in species such *Rb. sphaeroides*, which relates to a protein called PufX. When this protein is present in the RC–LH1

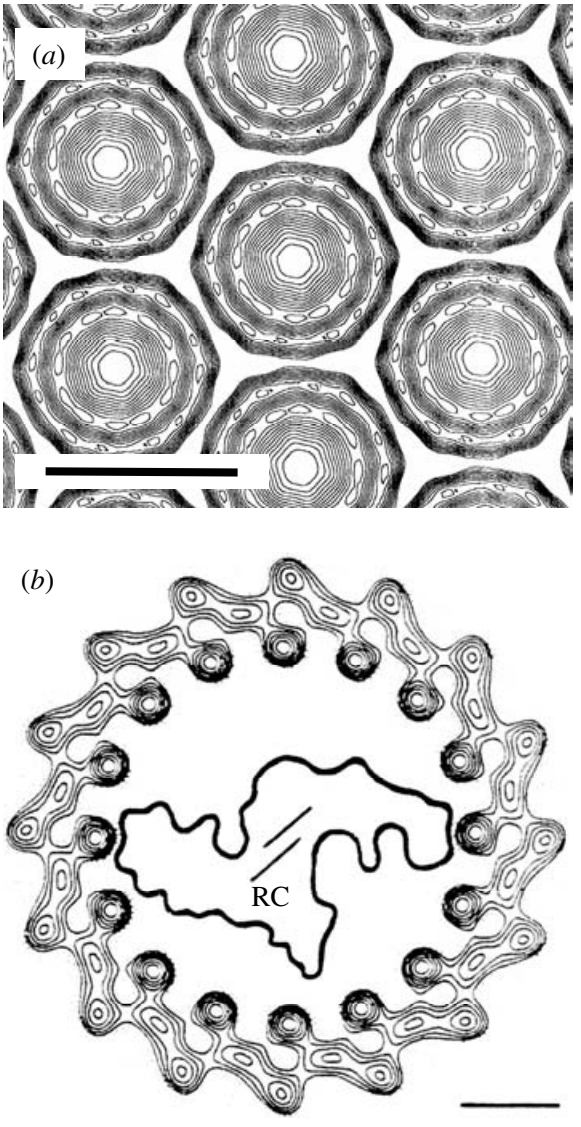


**Fig. 15.** (*a*) A 19 Å resolution projection map of negatively stained 2D crystals of RC–LH1 complexes from *Rps. acidophila* 7750. The map was created on the assuming six-fold symmetry of the LH1 ring (redrawn from Gall, 1994) (bar, 12 nm). (*b*) An 8·5 Å resolution projection map of 2D crystals of reconstituted LH1 complexes from *Rsp. rubrum*, showing that the hole in the centre is large enough to accommodate a RC complex. The electron density map is of sufficient quality that the relative positions of the 16-$\alpha/\beta$-dimers can be identified (bar, 20 Å). [Reprinted by permission of Macmillan Publishers Ltd; *EMBO Journal* (Karrasch *et al.* **14**, 631–638), © 1995].

complex they are dimeric. Whereas in a PufX$^-$ phenotype the RC–LH1 complex is monomeric (Siebert *et al.* 2004).

PufX first came to prominence in studies with *Rb. sphaeroides* and *Rb. capsulatus* (Donohue *et al.* 1988; Klug & Cohen, 1988). Mutants lacking PufX failed to grow photosynthetically (Farchaus & Oesterhelt, 1989; Lilburn & Beatty, 1992; Lilburn *et al.* 1992; Barz *et al.* 1995a, b; Recchia *et al.* 1998). Photosynthetic growth could be restored by a further deletion of the LH1 apoprotein

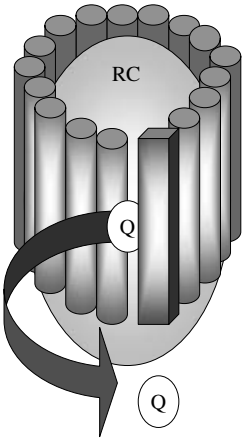


**Fig. 16.** A schematic model of the LH1 showing the PufX protein interrupting the ring of $\alpha/\beta$-dimers that surrounds the RC. In this model the gap created by PufX allows the migration of quinol (Q) through the LH1 ring into the photosynthetic membrane.

genes. It was suggested that the presence of PufX is required to allow a sufficiently rapid redox connection between the quinol reduced by the RC with the site of its oxidation on the cytochrome $b/c_1$ complex (Barz *et al.* 1995b). This connection is required for photosynthetic cyclic electron transport, which is a prerequisite for photosynthetic growth. The idea therefore grew up that PufX provides a portal to allow the quinol to escape through the LH1 helices (Cogdell *et al.* 1996; Parkes-Loach *et al.* 2001) (see Fig. 16 for a model). It has been proposed that PufX has a single transmembrane $\alpha$-helix, that the N-terminus of this helix is exposed at the cytoplasmic surface of the membrane and that it associates with the $\alpha$-apoprotein of the LH1 complex (Pugh *et al.* 1998; Recchia *et al.* 1998). PufX has also been suggested to have a role in *Rb. capsulatus* in the assembly of the RC–LH1 complex (Fulcher *et al.* 1998; Recchia *et al.* 1998). Some LH2$^-$ mutants of *Rb. sphaeroides* produce unusual tubular membranes (Hunter *et al.* 1988; Kiley *et al.* 1988; Sabaty *et al.* 1994). Membranes from the strain described by Sabaty *et al.* were negatively stained and imaged in the EM by Jungas *et al.* (1999). These authors interpreted their data as showing partially open, 'S'-shaped dimeric complexes, with a cytochrome $b/c_1$ complex sandwiched between the two RC–LH1 monomers. More recently Siebert *et al.* (2004) have shown that tubular membranes actually do not contain cytochrome $b/c_1$ complex. When PufX is present the RC–LH1 complex is a dimer, whether in the tubular membranes from LH2$^-$ mutants, or in the wild-type LH2$^+$ vesicular membranes, or in detergent-solubilized preparations (Frese *et al.* 2000, 2004; Bahatyrova *et al.* 2004a; Siebert *et al.* 2004; Qian *et al.* 2005). Recently, the structural functional consequences of the absence/presence of PufX in purified RC–LH1 complexes and membranes of *Rb. sphaeroides* were tested (Comayras *et al.* 2005a, b). It was concluded that patches of quinol-rich areas are preferentially located in the vicinity of the RC–LH1 complexes (Comayras *et al.* 2005a). These studies also showed that when PufX is absent the diffusion of ubiquinol from the monomeric RC, which is surrounded by a closed-ring of LH1 apoproteins, to the cytochrome $bc_1$ complex is about 2-fold slower, possibly suggesting an increased distance between the two complexes (Comayras *et al.* 2005b). These authors also showed that the $Q_B$ binding pocket in the PufX$^-$ mutant is modified and as a consequence RC function is impaired.

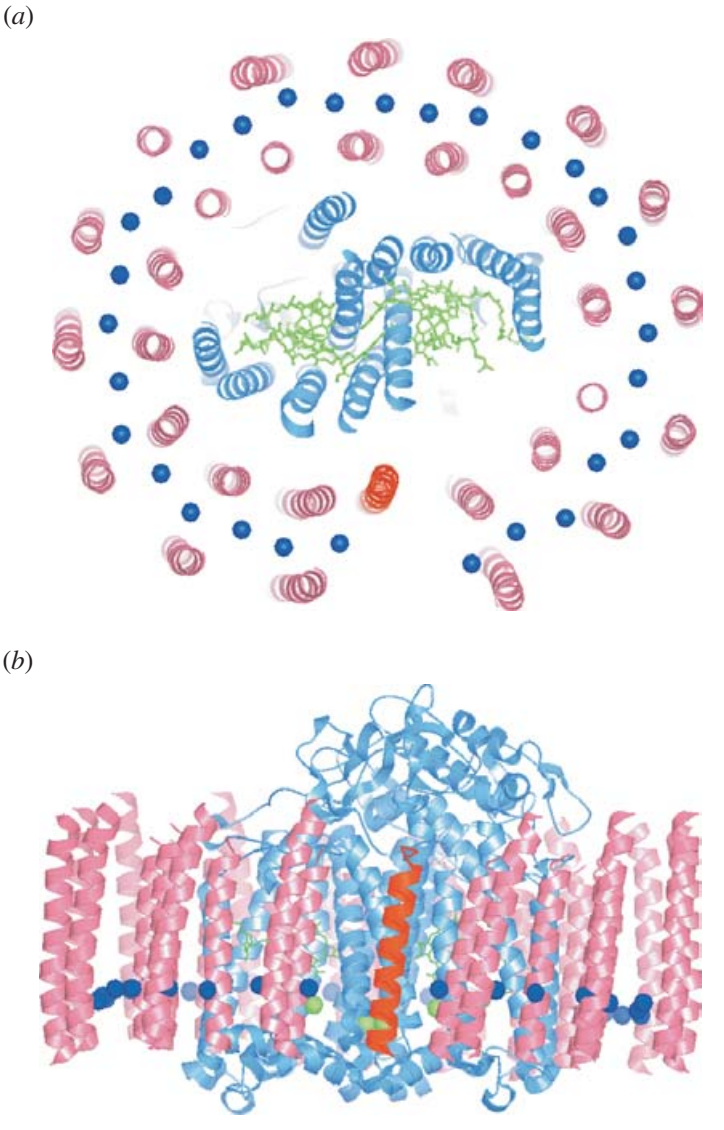


**Fig. 17.** The structure of the RC–LH1 complex from *Rps. palustris* at 4·8 Å resolution. (*a*) Looking down from the surface of the cytoplasm where the complex has been sectioned at the level of the ring of Bchls, which are shown in wireframe. (*b*) Side view showing the transmembrane $\alpha$-helices. The colour coding of the RC, LH1, and W are blue, purple and red respectively. The blue spheres represent the central $Mg^{2+}$ atoms of the LH Bchls. The bacteriochlorins of the RC are coloured green. (The figure was produced using PyMOL; DeLano, 2004.)

Before going on with the section we now present the 4·8 Å resolution crystal structure of the RC–LH1 complex from *Rps. palustris*. Although these crystals diffracted to 4·3 Å the data was only useable to 4·8 Å due to problems of twinning (Roszak *et al.* 2003). Unfortunately, at this rather low resolution, even though the general features of the structure can be visualized, the real molecular details remain obscure. A model of this RC–LH1 complex is shown in Fig. 17, both as a 'top' view, sectioned at the level of the ring of Bchls, and as a side view, showing the

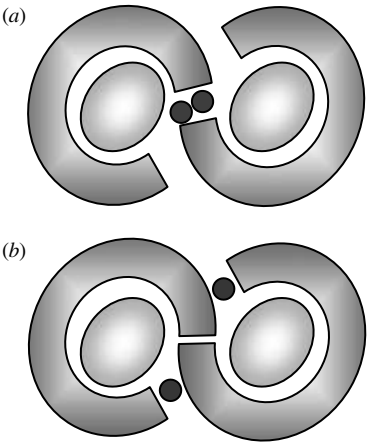


**Fig. 18.** The relative position of PufX within a dimeric RC–LH1 complex as proposed by (*a*) Scheuring and co-workers and by (*b*) the groups of Hunter and Bullough. The individual RC, LH1, and PufX are represented by an oval, an open-ring structure and a circle respectively.

transmembrane $\alpha$-helices. An elliptical LH1 complex encloses the RC. The outer dimension of the ellipse is $\sim$110 Å (measured from the centres of the opposite $\beta$-apoprotein $\alpha$-helices). The Bchl*a* molecules have been modelled into their overall electron density, but of course at this resolution their exact positions are not really defined. However doing this helps the viewer to understand the structure. The LH1 ellipse is interrupted by a protein we have called 'W'. W replaces an $\alpha\beta$-apoprotein pair and so the overall LH1 complex only contains 15 $\alpha\beta$ pairs. It has been suggested that 'W' is analogous to the PufX protein. Interestingly W is located next to the $Q_B$ binding site on the RC and effectively 'opens' the LH1 ring at this position. It is $Q_B$ that, when it is fully reduced, leaves the RC and delivers its reducing equivalents to the cytochrome $b/c_1$ complex and allows the cyclic electron transport to occur (Fig. 3). At this point in time very little is known about 'W' and it is coloured red in Fig. 17. Does it form a gate? Could this presumed gate open and close? These fascinating questions will only be answered when a higher resolution structure becomes available.

In the past 5 years or so there have been a series of papers describing the use of AFM to probe the structure of purple bacterial antenna complexes, both in reconstituted 2D arrays and *in vivo* (Scheuring *et al.* 2001, 2003; Bahatyrova *et al.* 2004b; Fotiadis *et al.* 2004; Frese *et al.* 2004). This data is especially interesting when the results from AFM are combined with those from parallel EM studies. Scheuring *et al.* used AFM to look at the structure and organization of the RC–LH1 (complexes) in membranes from *Rps. viridis* (Scheuring *et al.* 2003). They were able to show that these 'core' complexes were both monomeric and elliptical *in vivo* and that AFM can nanodissect out the RC. When the RC was removed the 'empty' LH1 complex became more circular. These workers have also looked at RC–LH1 complexes in 2D crystals from *Rb. sphaeroides* and membranes from *Rb. blastica* (Scheuring *et al.* 2005). In both cases the active RC–LH1 complexes are dimeric and they have interpreted their images as showing 'S'-shaped structures. This group favours the idea that PufX is located at that point in the LH1 structures where the two halves of the dimer come together, i.e. they are responsible for dimerization (Fig. 18*a*). The groups of Hunter and Bullough favour an alternative model (Fig. 18*b*). Based on rather similar data they agree that dimers only form in the presence of PufX, however this group favour dimers of

complete rings (Bahatyrova *et al.* 2004b). In their most recent studies (which has the highest resolution so far at 8·5 Å) on well-ordered 2D crystals of the RC–LH1 dimer from *Rb. sphaeroides* they have used both EM and AFM to investigate the structure of these core complexes (Qian *et al.* 2005). The two LH1 rings in the dimer interlace and PufX is located in the region where Scheuring and co-workers have a gap. Interestingly Qian *et al.* (2005) were able to overlay the X-ray crystal structure of the RC–LH1 complex from *Rps. palustris* (Roszak *et al.* 2003) onto their AFM image and get a remarkably good correlation, with 'W' in the same position as the PufX. The Hunter and Bullough groups reconcile the two sets of data by suggesting that the 'S'-shaped images seen in the EM reflect differential staining properties of the LH1 ring in the region of PufX, i.e they stain less well in this region. This then gives the appearance of a gap in the LH1 ring in the region of PufX. Recent crystallographic studies on crystals of the dimeric RC–LH1–PufX core complex from *Rb. sphaeroides*, which diffract to 12 Å, have a proposed LH1/RC stoichiometry of just over 13 $\alpha/\beta$-dimers (Abresch *et al.* 2005). This is very similar to that seen in *Rb. blastica* (Scheuring *et al.* 2005) and may suggest a gap in the LH1 ring. But this data would also fit with the interlocking model of Hunter and Bullough. Clearly further work is needed to clear up these different views.

## 3. Spectroscopy

### 3.1 Steady-state spectroscopy

A detailed understanding of the steady-state spectroscopic properties of the purple bacterial antenna complexes is an essential prerequisite for an in-depth discussion of which of the possible mechanisms of energy transfer, in which they are engaged, actually operate. In this section we will concentrate upon studies with LH2, where there is the best mixture of structural and functional information. This will be supplemented, as appropriate, with some additional information on LH1 complexes.

Two major types of factors control where a given Bchl*a*'s $Q_y$ absorption band will be located. The first is its site energy. The site energy gives the position of the $Q_y$ absorption that an independent Bchl*a* molecule in its binding site would have if it were free from any influence of any other Bchl*a* molecules. The second major factor results from Bchl*a*–Bchl*a* interactions. The main possible different interactions experienced by the Bchls, which alter the energy level of their $Q_y$ transitions, are summarized in Fig. 19.

Once the site energies of the Bchl*a* molecules in the ring of strongly interacting pigments have been 'set', then the final position of the $Q_y$ absorption band will (as described above) depend upon the details of these additional pigment–pigment interactions. The pigment–pigment interactions will be sensitive to (i) the size of the aggregate, (ii) the distances between the interacting pigments, (iii) the relative angles between the transition dipoles of the $Q_y$ transitions, (iv) the extent of static and dynamic disorder (see Section 5).

### 3.2 Factors which affect the position of the $Q_y$ absorption band of Bchl*a*

In principle it is possible to draw up a list of the potential ways in which site energies of Bchl*a* molecules can be modulated by their environment. Then, with reference to the structure of LH2, we can see which of these are actually employed by the natural system to tune the individual site energies.

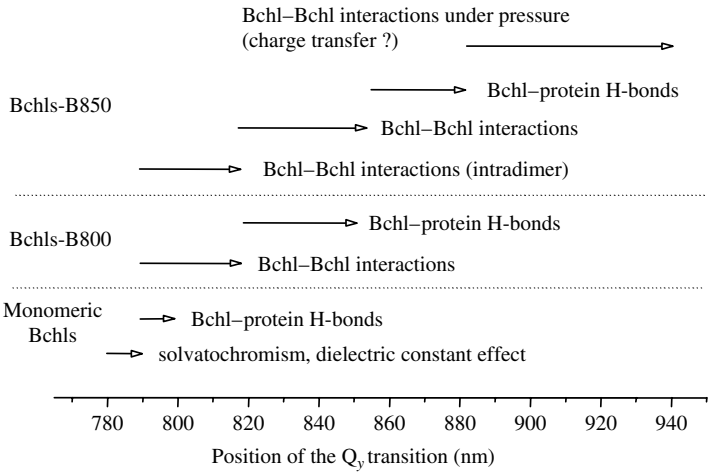


**Fig. 19.** An overview of the possible mechanisms involved in tuning the $Q_y$ electronic transitions of Bchl*a* in antenna complexes. (Redrawn from Robert *et al.* 2003.)

Most of the purple bacterial antenna and RC complexes studied so far have $Mg^{2+}$ as the central metal ion situated in the middle of the bacteriochlorin macrocycle. However, the central $Mg^{2+}$ ion can be replaced by $Zn^{2+}$ in the bacterium *Acidiphilium rubrum* (Wakao *et al.* 1996). This species was isolated from polluted, acidic lakes. Normally acid conditions will result in replacement of $Mg^{2+}$ with two hydrogen ions to produce bacteriopheophytin ($Q_y \sim 760$ nm). The $Zn^{2+}$ Bchl is more stable in acid conditions. Changes of the central metal ion can shift the absorption spectrum of Bchl*a* (Hartwich *et al.* 1998), however, this does not appear to be used by the bacteria to change site energies *in vivo*. There are probably two reasons why this is not used in the natural system. First, and most importantly, changing the central metal ion can dramatically reduce the excited singlet state lifetimes. If, for example, $Mg^{2+}$ is replaced with $Ni^{2+}$ then the lifetime of the first excited singlet state is reduced from 1–2 ns to a few ps (Musewald *et al.* 1998, 1999). This would be catastrophic for the efficiency of LH and therefore counterproductive. Second, $Mg^{2+}$ is put into the centre of the bacteriochlorin ring by a specific enzyme, $Mg^{2+}$ chelatase (Willows *et al.* 1996; Walker & Willows, 1997). It would be difficult to change the central metal ion without having a set of different enzymes each putting in a specific and different metal ion.

Usually the central $Mg^{2+}$ ion in Bchl*a* is five-coordinate, and a range of fifth ligands have been found including histidine, aspartate, $H_2O$, etc. (Deisenhofer *et al.* 1984, 1985; Allen *et al.* 1986; Tronrud *et al.* 1986; McDermott *et al.* 1995; Koepke *et al.* 1996; Prince *et al.* 1997; McLuskey *et al.* 2001; Papiz *et al.* 2003; Roszak *et al.* 2003). Changes of the fifth ligand can cause small shifts in the position of the $Q_y$ absorption band, but these effects are rather small and do not seem to be very important in the modulation of site energies.

If the proteinacceous binding site of a Bchl*a* molecule is thought of as the 'solvent' in which that Bchl*a* is 'dissolved', then it can be asked to what extent solvent polarity can shift the position of the $Q_y$ absorption band? If Bchl*a* is dissolved in a series of different organic solvents in which it remains monomeric, then typical shifts of the $Q_y$ band are of the order of 5 nm (Fig. 19). Unfortunately the detailed effects of the subtle changes in the polarity of the Bchl*a* binding sites in LH2 are presently very difficult to assess since there are not enough examples

'850 nm' MNQGKIWTVVNPAIGIPALLGSVTVIAILVHLAILSHTTWFPA**YW**QGGVKKAA
'820 nm' MNQGKIWTVVPPAFGLPLMLGAVAITALLVHAAVLTHTTWYAA**FL**QGGVKKAA

**Fig. 20.** Comparison of the primary amino-acid sequences of the $\alpha$-apoproteins of the 850 nm- and 820 nm-absorbing LH2 complexes from *Rps. acidophila*. Shown in bold are the $\alpha$-Tyr44 (Y) and $\alpha$-Trp45 (W) residues of the '850 nm' sequence from strain 10050 that are replaced by Phe (F) and Leu (L) in the 820 nm-absorbing complex from strain 7050.

with high-resolution crystal structures. It has been calculated (Eccles & Honig, 1983) that buried point charges, especially in a mainly hydrophobic environment, could induce large shifts in the $Q_y$ absorption band of Bchl*a*, i.e. tens of nm. The direction of the shift would depend upon the sign of the charge. However, for the LH2 complexes with crystal structures no buried charges are seen anywhere near the Bchl*a*s (McDermott *et al.* 1995; Koepke *et al.* 1996).

Careful inspection of the different groups of Bchl*a* molecules in the structure of LH2 from *Rps. acidophila* reveals that the bacteriochlorin macrocyles are distorted (Papiz *et al.* 2003). Resonance Raman studies, which can probe to a higher resolution than so far obtained in the crystal structures, has confirmed this and demonstrated that distorted macrocyles exist in both LH1 and LH2 complexes (Lapouge *et al.* 1999). Fajer and colleagues have used porphyrin models to investigate the effect of distortion of the macrocycle on their spectroscopic properties (Barkigia *et al.* 1988; Gudowska-Nowak *et al.* 1990). Steric hindrance from bulky side groups added on to the basic ring system can produce dramatic distortions, resulting in ruffling, saddling and propellering of the ring system (Barkigia *et al.* 1988). Such large distortions induce shifts in the absorption spectrum but even more dramatically cause major decreases in the lifetimes of the first excited singlet state (Gentemann *et al.* 1997). The distortion of the bacteriochlorin macrocycles seen in LH2 are much smaller than those seen in these synthetic models, and it is not clear how much they may contribute to the tuning of the Bchl*a* site energies in the antenna complexes. Clearly the positioning of large amino-acid side-chains around the bacteriochlorin rings could induce steric hindrance and thereby affect the site energy. This is another case where more structures of antenna complexes are needed before the importance of this possible effect can be evaluated.

It was noted several years ago that when certain strains of *Rps. acidophila* were grown under low-light intensities they switch to synthesize a new type of LH2 complex [now called LH3 or B800–820 (Cogdell *et al.* 1985)] which has its Bchl*a* $Q_y$ absorption bands at 800 and 820 nm rather than 800 and 850 nm (Cogdell *et al.* 1983; Heinemeyer & Schmidt, 1983; Bissig *et al.* 1988). The new apoproteins in the B800–820 complex were isolated and sequenced, and these compared with the sequences of the B800–850 apoproteins (Bissig *et al.* 1988; Brunisholz & Zuber, 1992). Two key residue changes were identified that correlated with the shift in the position of the $Q_y$ absorption band from 850 nm to 820 nm. These are indicated in Fig. 20. Residues $\alpha$-44 and $\alpha$-45 in the B800–850 apoproteins are always amino acids with the potential to hydrogen bond, i.e. Tyr and Trp. In the B800–820 complexes these residues are always replaced with non-hydrogen-bonding amino acids such as Phe and Leu. Resonance Raman (RR) spectroscopy can be used to investigate the hydrogen-bonding status of carbonyl groups present on the bacteriochlorin macrocycles when these carbonyls are in conjugation with the macrocycle, i.e. are in resonance with the conjugated system of the macrocycle (Lutz & Robert, 1988; Robert, 1996). Figure 21*a* illustrates the room-temperature Raman spectra of B800–850 and B800–820 in pre-resonance with the B850 and B820 Bchl molecules. The frequency of the

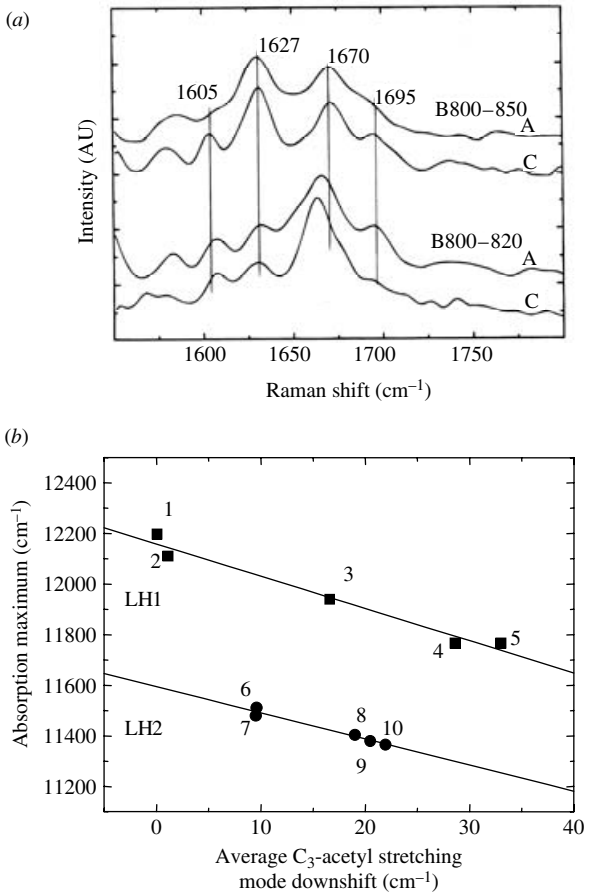


**Fig. 21.** (*a*) FT resonance Raman spectra in the carbonyl stretching region of the B800–850 (above) and B800–820 (below) complexes isolated from (A) *Rps. acidophila* and (C) *Rps. cryptolactis* ($\lambda_{ext} = 1064$ nm). (Redrawn with permission from Sturgis *et al.* 1995; ©1995 American Chemical Society.) (*b*) Relationship between the $Q_y$ absorption maximum and the down-shift of the $C_3$ acetyl stretching modes from the non-interacting frequency of 1660 $cm^{-1}$ in LH1 and LH2 complexes. The lines show linear regression fits to the two datasets. The data-points are: 1, *Rps. cryptolactis* B800–820; 2, *Rb. sphaeroides* B800–850 double mutant $\alpha$-Phe44, $\alpha$-Leu45; 3, *Rb. sphaeroides* B800–850 mutant $\alpha$-Leu45; 4, *Rb. sphaeroides* B800–850; 5, *Rv. gelatinosus* B800–850; 6, *Rb. sphaeroides* LH1 mutant $\beta$-Phe47; 7, *Rb. sphaeroides* LH1 mutant $\beta$-Tyr47; 8, *Rb. sphaeroides* LH1 wild-type $\beta$-Trp47; 9, *Rb. sphaeroides* LH1 mutant $\beta$-His47; 10, *Rb. sphaeroides* LH1 mutant $\alpha$-His43. (Adapted with permission from Sturgis & Robert, 1997; © 1997 American Chemical Society.)

carbonyl vibrational mode at 1627 $cm^{-1}$ in the B800–850 spectrum shows that the acetyl groupings are hydrogen bonded; these modes are degenerate in this particular complex but can be easily separated by spectral deconvolution in the LH2 from *Rb. sphaeroides* (Fowler *et al.* 1994; Sturgis *et al.* 1995). In the B800–820 complex the Raman vibrational modes of the carbonyls are shifted from $\sim$1620 $cm^{-1}$ to 1652 $cm^{-1}$ and 1660 $cm^{-1}$ (Sturgis *et al.* 1995) that indicates a lack of hydrogen bonds (Robert & Lutz, 1985; Lutz & Robert, 1988; Fowler *et al.* 1994). For comparison, the B800–850 and B800–820 complexes isolated from the related bacterium *Rps. cryptolactis* (Stadtwald-Demchick *et al.* 1990; Halloren *et al.* 1995) are also plotted in Fig. 21*a* and show a similar change in the carbonyl stretching modes between the 850 nm-absorbing and 820 nm-absorbing LH2 complexes. This idea that hydrogen bonding was

responsible for the shift from 850 nm to 820 nm was first tested in *Rb. sphaeroides* by site-directed mutagenesis (Fowler *et al.* 1992). The amino acids in *Rb. sphaeroides*, corresponding to $\alpha$-44 and $\alpha$-45 in the *Rps. acidophila* apoprotein, were changed from Tyr-Tyr to Phe-Phe. In the Phe-Phe double mutant the LH2 absorption spectrum was shifted from 850 nm to 820 nm. Moreover the RR spectrum of this mutated complex also showed that the key carbonyls were no longer hydrogen bonded (Fowler *et al.* 1994). Sturgis & Robert (1997) then demonstrated a consistent linear relationship, between the downshift in the Bchl*a* $C_3$ acetyl stretching mode and the red-shift in the $Q_y$ absorption maximum, in both LH1 and LH2 complexes (Fig. 21*b*). This linear relationship permitted them to estimate the contribution of H-bonding to the red shift observed in these complexes and the sensitivity of the absorption to changes in the immediate environment surrounding the $C_3$ acetyl group. Further investigation of changes in the Raman spectra caused by altering the excitation conditions revealed negligible changes in the positions of the methine bridge, the $C_3$ acetyl, and the $C_{13}$ keto stretching modes (see Fig. 2*a*). The lack of sensitivity of these bands to the resonance condition indicated that neither differences in distortion of the bacteriochorin ring nor the hydrogen-bonding network of these carbonyl groups are important in determining the inhomogeneous absorption bandwidth of the absorption spectrum of these complexes. From this, Sturgis and Robert suggested that the differences in coupling between the Bchl*a* molecules might be responsible for the static disorder, which results in inhomogeneous broadening of the absorption band as observed by previous hole burning studies (van der Laan *et al.* 1990; Reddy *et al.* 1991, 1992a, b). In addition, the hydrogen-bond network between the B850 Bchl*a* molecules and their binding sites in LH2, the position of the $Q_y$ absorption peak of the B850 Bchl*a*s is also sensitive to Car content (Gall *et al.* 2003a; Olsen *et al.* 2003).

When the crystal structure of the LH2 complex from *Rps. acidophila* was determined it was confirmed that in the B800–850 complex the acetyl carbonyl groups of the B850 bacteriochlorins were indeed hydrogen bonded to the key residues pinpointed by both amino-acid sequence studies and RR spectroscopy. More recently the crystal structure of the LH3 complex from *Rps. acidophila* strain 7050 has been determined (McLuskey *et al.* 2001). The overall structure of LH3, also called B800–820, is highly homologous with that of LH2. It is an $\alpha_9\beta_9$ non-americ ring and the apoprotein folds of the two structures can be almost exactly overlaid. The consequences of the different sequence of the apoproteins in LH3 at $\alpha$-44 and $\alpha$-45 are shown in Fig. 22. In this figure the $\alpha$- and $\beta$-bound bacteriochlorins of LH2 and LH3 are shown superimposed. The loss of the hydrogen-bonding residues in the LH3 structure is clearly seen. The result of this is that the acetyl groups, which were very nearly in plane with the bacteriochlorin rings in LH2, fixed into position by the hydrogen bonds, are now rotated out-of-plane in LH3 in the crystallographic model. In the case of the LH3 $\alpha$-bound Bchl*a* its acetyl group is hydrogen-bonded to Tyr at position $\alpha$-41 and this locks it into its new out-of-plane position. Since this acetyl group is now out of conjugation with the bacteriochlorin ring RR does not detect it. The acetyl group for the LH3 $\beta$-bound Bchl*a* is not hydrogen bonded and also rotates out-of-plane. When a carbonyl group is in plane with the conjugated system of the bacteriochlorin macrocycle it will add to the effective number of conjugated bonds and result in a red-shift of the $Q_y$ absorption. When it is out of plane the degree of conjugation is reduced and the $Q_y$ shifts to the blue. The effect has been treated theoretically by Fajer (Gudowska-Nowak *et al.* 1990) and Fig. 23 illustrates their work. This figure that is based on both theory and experiment with the Bchl*a* protein (Tronrud *et al.* 1986) from the green photosynthetic bacterium *Prosthecochloris aesturarii*, relates the rotation of the acetyl group to the change in the site energy

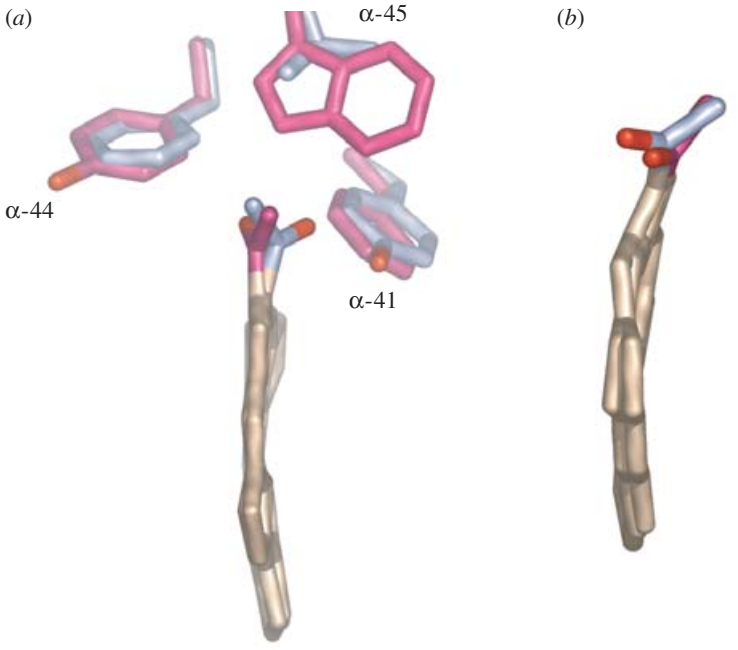


**Fig. 22.** A comparison of the (*a*) $\alpha$- and (*b*) $\beta$-bound B850–B820 bacteriochlorins in LH2 and LH3. For clarity only the macrocyles and $C_3$-acetyl groups are depicted. The amino-acid residues $\alpha$-41, $\alpha$-44 and $\alpha$-45 are overlaid in purple (LH2) and blue (LH3). The oxygen atoms are shown in red. (The figure was produced using PyMOL; DeLano, 2004.)

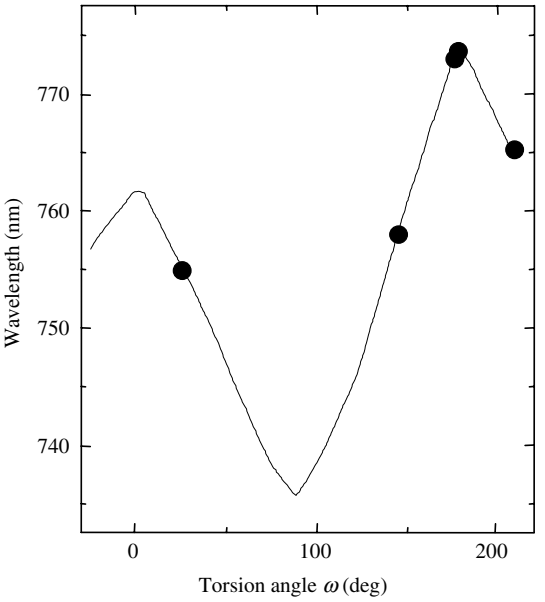


**Fig. 23.** The $Q_y$ excitation energy for Bchl*a* as a function of the torsion angle ($\omega$) of the acetyl group. The solid circles refer to the $\omega$ values assigned in the crystal structure of the water-soluble Bchl*a* protein from *Prosthecochloris aestuarii* (Tronrud *et al.* 1986) while the line represents the theoretical fit. (Adapted with permission from Gudowska-Nowak *et al.* 1990; © 1990 American Chemical Society.)

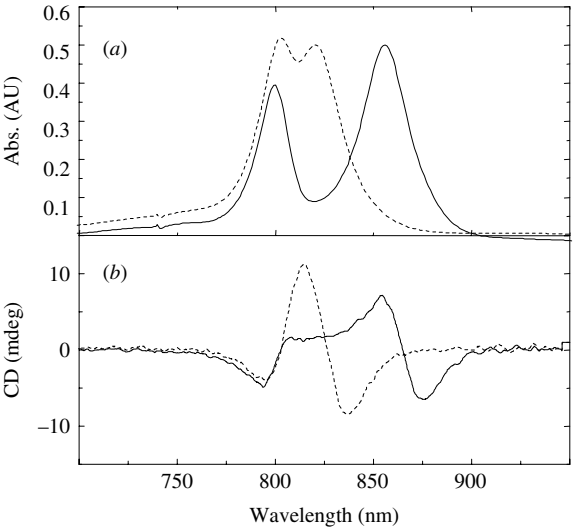


**Fig. 24.** The comparison of the room-temperature (*a*) $Q_y$–Bchl*a* absorption and (*b*) CD spectra of detergent-purified peripheral LH complexes from *Rps. acidophila*. The continuous and dotted lines represent the spectra from the LH2 (B800–850) and LH3 (B800–820) complexes, respectively. The spectra were normalized to the total Bchl*a* content.

of the Bchl*a* molecule. Using this graph as a calibration most of the shift in the $Q_y$ absorption band from 850 nm to 820 nm in going from LH2 to LH3 (see Fig. 24*a*) can be accounted for by rotation of the acetyl groups. However, it is still also possible that there is a direct effect of the hydrogen bond on the spectral position of the $Q_y$ band. But controlling the site energy of the Bchl*a* molecules by rotation of the acetyl groups is an attractive mechanism structurally. Relatively modest changes in amino-acid sequence can then result in quite significant spectral shifts.

Interestingly, the CD spectra of the LH2 and LH3 complexes from *Rps. acidophila* are very similar (Cogdell & Scheer, 1985) (see Fig. 24*b*). The two spectra are essentially identical except that the position of the positive/negative 'doublet' seen in the long wavelength absorption band is shifted by 30 nm in going from LH2 to LH3 (Fig. 24*b*). This is an important finding since the CD spectrum reflects the excitonic structure of the 850 nm and 820 nm absorption bands, and this reflects the overall structure of these two pigment groups. In other words the overall pigment–pigment interactions in these two pigment groups in the two complexes are very similar indeed. Indeed, within the resolution of the two crystal structures, the overall organization of the bacteriochlorin rings in LH2 and LH3 are, within the limits of detection of the current X-ray data, the same. The origin of the spectral properties of the B850 band will be discussed later in sections 5.3 and 5.4.

The effect of changing the strength of the interactions between the Bchl*a* molecules in the B850 ring can be probed by recording the absorption spectrum either as a function of temperature or pressure (Tars *et al.* 1994; Reddy *et al.* 1996; Wu *et al.* 1996, 1997a, 1998; Timpmann *et al.* 2001; Matsuzaki *et al.* 2001; Zazubovich *et al.* 2002b; Gall *et al.* 2003b; Braun *et al.* 2005; Urboniene *et al.* 2005). As the temperature is lowered from room temperature to $\sim$150 K the position of the 850 nm absorption band in LH2 from *Rps. acidophila* shifts to the red by 80 $cm^{-1}$. This is also accompanied by a narrowing of the absorption band. Freiberg and

colleagues demonstrated that as the pressure is increased the B850 absorption band in the LH2 complexes from *Rps. acidophila* and *Rb. sphaeroides* also shift to the red and is broadened (Tars *et al.* 1994; Timpmann *et al.* 2001). Absorption measurements were then combined with Raman spectroscopy under pressure in order to study the structure of the B850-binding sites (Gall *et al.* 2003b). In agreement with previous Raman spectra of the B875 absorption band collected under pressure (Sturgis *et al.* 1998), it was concluded that both the shift in peak position and spectral broadening of B850 can be explained broadly by solvatochromic effects and, in particular, to the modulation of the Bchl*a*–Bchl*a* interactions, induced by lowering the temperature or increasing the pressure.

The first attempts to calculate the absorption spectrum of the LH2 complex from *Rps. acidophila*, following the release of its structure, were carried out by Sauer *et al.* (1996). This is still an instructive study since it builds up the spectrum step by step, first using the pigments in an $\alpha\beta$-apoprotein dimer, then three dimers and then the whole complex. A good fit between theory and experiment in the B850 absorption band is only obtained when the full 18 strongly interacting BChls that contribute to the B850 band are included. The second major finding is that a simple model completely fails to account for the CD spectrum. The CD spectrum was only well fitted by theory comparatively recently (Georgakopoulou *et al.* 2002, 2004) and required the assumption that the site energies of the $\alpha$- and $\beta$-bound B850 Bchl*a* molecules are different and that the direction of the $Q_y$ transition moments of the individual Bchl*a* molecules are slightly rotated within the molecular frame of their bacteriochlorin rings relative to their orientations in free monomeric Bchl*a*.

Figure 24 compares the CD spectrum of the LH2 complex for *Rps. acidophila* with its absorption spectrum. Monomeric Bchl*a* in organic solvents such as 7:2 (v/v) acetone and methanol has a weak negative CD band in its long wavelength $Q_y$ absorption band centred at ~770 nm. When pigments, such as Bchl*a* come together to form exciton-coupled aggregates, such as dimers, the CD band in the $Q_y$ region is radically changed. Its magnitude is enhanced and it is transformed from a negative going signal to one with both positive and negative waves. The CD spectrum of this LH2 complex shows a small positive/negative signal at $\sim$800 nm and a stronger positive/negative signal in the 850 nm band. This CD spectrum was interpreted by assuming that the Bchl*a* molecules that absorb at 800 nm are largely monomeric whereas those that absorb at 850 nm are dimers (or maybe a larger exciton-coupled aggregate). These conclusions were reached several years before the structure of LH2 had been determined and were beautifully confirmed when the structure of LH2 appeared.

Once the structure of LH2 had been determined it was possible to try to calculate the absorption and CD spectra for the Bchl molecules (and the Car molecule) from first principles (Sauer *et al.* 1996; Alden *et al.* 1997; Dracheva *et al.* 1997; Hu *et al.* 1997, 2002; Krueger *et al.* 1998; Scholes *et al.* 1999; Mostovoy & Knoester, 2000; Sumi, 2000; Dahlbom *et al.* 2001; Jang *et al.*, 2001; Matsushita *et al.* 2001; Didraga & Knoester, 2002; Georgakopoulou *et al.* 2002, 2004). The results of these calculations have been independently described by several groups and have revealed important conclusions on the electronic structure of these antenna complexes. We are going to digress here to show how these calculations have been carried out. We hope that the following treatment will equip biologists with enough insight to allow them to at least follow the literature which has so far only been written by, and indeed targeted at, physicists and physical chemists who have studied quantum mechanics. Readers who are already experts in this area might wish to skip Section 5 after reading the next section on the regulation and assembly of the LH complexes.

## 4. Regulation of biosynthesis and assembly

The regulation and assembly of purple bacterial antenna complexes can be conveniently divided into two processes. The first is the regulation of the biosynthesis of the various components required to build an antenna complex, which are the apoproteins and the pigments. The second is the actual assembly of the antenna complexes from these individual components. There is quite a large body of information on the first of these two steps but almost nothing on the second.

The biosynthesis of the antenna apoproteins and their required pigments are controlled by a set of classical two-component regulatory systems (Swem *et al.* 2001). Basically there is an all or nothing switch that is controlled by oxygen tension (see Bauer, 1995; Young & Beatty, 2003). Once the oxygen tension falls below a critical level the biosynthetic processes are turned on. The extent of production of the antenna complexes is then regulated by light intensity (Bauer, 1995; Braatsch *et al.* 2002; Masuda & Bauer, 2002; Han *et al.* 2004; Jaubert *et al.* 2004). The lower the light intensity the more antenna complexes are made and the higher the LH2:LH1 ratio. Recently, an additional level of regulation has been described that involves bacterial phytochromes in photosynthetic purple bacteria (Giraud *et al.* 2002, 2004, 2005; Armitage & Hellingwerf, 2003; Jaubert *et al.* 2004; Kyndt *et al.* 2004; Evans *et al.* 2005). In this case not only the light intensity but also the colour of the incident radiation is critical. In the last few years there have been significant advances in the application of molecular genetics to investigate the control of the biosynthesis of the antenna complexes, which include DNA microarray technology (Pappas *et al.* 2004; Roh *et al.* 2004; Kaplan *et al.* 2005), the publication of genome sequences from a number of bacterial species (Haselkorn *et al.* 2001; MacKenzie *et al.* 2001; Larimer *et al.* 2004; Reslewic *et al.* 2005) (*Rsp. rubrum*; http://genome.ornl.gov/microbial/rrub/) and more coordinated experiments on the temporal and spatial development of the photosynthetic apparatus (Pugh *et al.* 1998; Koblizek *et al.* 2005). As a result there is beginning to be a more global picture of the changes in gene expression, which occur when the biosynthesis of the antenna complexes is induced, but these studies have only just begun.

### 4.1 Regulation

In general, cells of purple photosynthetic bacteria when exposed to elevated levels of molecular oxygen contain greatly reduced amounts of LH complexes. Lowering the oxygen tension results in the invagination of the cytoplasmic membrane together with the induction of the synthesis and assembly of the LH apparatus (Takemoto & Lascelles, 1973), which may make up over 50% of the total membrane protein content (Golecki *et al.* 1979; Drews & Golecki, 1995). Going from aerobic to anaerobic growth conditions is regulated by a nested sensing/signal-transduction system that is modulated by the presence of light (Sganga & Bauer, 1992; Eraso & Kaplan, 1994; Phillips-Jones & Hunter, 1994; Swem *et al.* 2001; Glaeser & Klug, 2005; Kaplan *et al.* 2005).

#### 4.1.1 Oxygen

The level of oxygen tension and the light intensity is sensed by an array of different proteins (e.g. AppA, CcoQ, FNRL and RegB) that in turn control the CrtJ, HvrA, IHF, and RegA effector proteins. These two-component regulatory systems then directly, or indirectly, control gene transcription and translation of the *bch*, *crt*, *puc*, *puf puh* and other operons (see Table 3) that

**Table 3.** *A summary of the operons that encode for the biosynthesis of the pigments and apoproteins of the light-harvesting (LH) and reaction centre (RC) complexes in photosynthetic purple bacteria*

| Operon | Gene product |
|---|---|
| *bch* | Bacteriochlorophyll biosynthetic enzymes |
| *crt* | Carotenoid biosynthetic enzymes |
| *puc* | Biosynthesis of the $\alpha$- and $\beta$-apoproteins of LH2 |
| *puf* | Biosynthesis of the $\alpha$- and $\beta$-apoproteins of LH1 and the M- and L-subunits of the RC |
| *puh* | Biosynthesis of the H-subunit of the RC |

encode the enzymes responsible for the biosynthesis of the pigments and apoproteins of the LH and RC complexes of photosynthetic purple bacteria.

Oxygen-dependent gene regulation in photosynthetic purple bacteria is regulated by three systems: AppA-PpsR/CrtJ, Prr/Reg proteins and FnrL (Khoroshilova *et al.* 1997; Gregor & Klug, 2002; Zeilstra-Ryalls & Kaplan, 2004). The FnrL regulator protein is believed to sense molecular oxygen *via* an oxygen-labile 4Fe-4S cluster and thus controls fumarate-nitrate regulation (Khoroshilova *et al.* 1997). The RegB/RegA, in *Rb. capsulatus* (Sganga & Bauer, 1992; Mosley *et al.* 1994) and the PrrB/ PrrA, in *Rb. sphaeroides* (Eraso & Kaplan, 1994, 1995; Phillips-Jones & Hunter, 1994) two-component systems modulate the oxygen-dependent expression of the genes that encode for the photosynthetic apparatus. These systems consist of a membrane-associated PrrB/RegB histidine kinase and its partner, the DNA-binding PrrA/RegA response regulator. At low oxygen concentration PrrB/RegB undergoes autophosporylation and transfers the phospho group to the PrrA/RegA regulator (Oh & Kaplan, 2000). PrrA/RegA then 'turns on' the transcription of several operons linked to the biosynthesis of the photosynthetic apparatus (Eraso & Kaplan, 1996; Du *et al.* 1998; Bowman *et al.* 1999). Furthermore, it has been recently suggested that regulation of gene expression under the ultimate control of oxygen tension is more global than previously considered and that the $cbb_3$ oxidase activity is more intertwined with the Prr/Reg regulatory system (Oh & Kaplan, 2001; Oh *et al.* 2004; Kaplan *et al.* 2005).

Redox regulated gene repression also occurs at high oxygen tension. The PpsR/CrtJ proteins (in *Rb. sphaeroides* and *Rb. capsulatus* respectively) repress the photosynthetic gene clusters at high oxygen tension. The PpsR/CrtJ regulatory system acts on the *bch*, *crt* and *puc* operons. For more in-depth discussions of these regulatory systems the interested reader should consult the reviews by Bauer (1995) and Young & Beatty (2003).

### 4.1.2 Light

It has been known for many years that the light regime can regulate both the amount of photosynthetic system and the spectral properties of LH2 complexes (e.g. the synthesis of B800-820 complexes of *Rps. acidophila* and the 'low-light' form of B800–850 complexes of *Rps. palustris*) as well as their relative abundance in the PSU (see Section 2.2).

Very recently it has been described that this regulation occurs both via classical two-component regulatory systems and by a range of bacterial phytochromes. We now know that photosynthetic purple bacteria exhibit a range of responses to light that are, in part, regulated by photoreceptor proteins (Giraud *et al.* 2002, 2005; Gomelsky & Klug, 2002; Braatsch & Klug, 2004; Han *et al.* 2004; Kyndt *et al.* 2004; Anderson *et al.* 2005; Evans *et al.* 2005). Three

such responses are the 'blue light' perception in bacteria (classical) (Braatsch & Klug, 2004), phototaxis (bacteriophytochrome) (Sistrom, 1978; Glaeser & Overmann, 1999; Armitage & Hellingwerf, 2003), and regulation of the gene expression of the type of LH2 complex (bacteriophytochrome) (Giraud *et al.* 2002, 2005; Evans *et al.* 2005). In the following two sub-sections we shall describe the current state of understanding of AppA-mediated 'blue light' perception and the roles assumed by bacteriophytochromes (BphPs).

#### 4.1.2.1 AppA: blue-light-mediated regulation

There are three types of photoreceptor proteins that use flavin molecules as the chromophore in blue-light-mediated regulation: cryptochromes (Lin, 2000), the LOV (light, oxygen, voltage) subset of PAS (Per–Arnt–Sim) domain (Taylor & Zhulin, 1999; Losi, 2004) and the BLUF [blue light sensing using FAD (flavin adenine dinucleotide)] photoreceptor domain of AppA (Gomelsky & Klug, 2002; Han *et al.* 2004; Anderson *et al.* 2005). AppA is transcriptional antirepressor known to participate in the redox-dependent control of photosynthesis gene expression in photosynthetic purple bacteria (Masuda & Bauer, 2002). For example, in *Rb. sphaeroides*, the photosynthetic apparatus is produced at low oxygen tension and low light intensity, whereas under aerobic and highlight conditions, formation of photosynthetic complexes is inhibited by the transcriptional repressor PpsR. Under conditions of low oxygen tension and low light intensity, PpsR is complexed with AppA, which allows transcription to proceed. Blue light disrupts the interaction of AppA to PpsR thereby initiating its anti-repression function, thus restoring the PpsR binding activity to the promoter region of photosynthesis genes such as the *puc* operon (Braatsch *et al.* 2002, 2004; Gomelsky & Klug, 2002; Han *et al.* 2004). The following paragraph gives a short summary of the latest developments from studies of the mechanism of action of AppA.

The FAD co-factor of AppA is essential for the blue light-dependent sensory transduction of this response (Braatsch *et al.* 2002). AppA was the first example of a protein with dual sensing capabilities that integrates both redox and light signals. This field is particularly rapidly advancing. For example, in *Rb. sphaeroides*, the X-ray structure of the dark state of the BLUF domain of AppA has just been determined to 2·3 Å resolution (Anderson *et al.* 2005). The structure of the BLUF domain of AppA has revealed that its overall topology (but not its primary sequence) and hydrogen-bond network is very similar to that of a LOV domain. Also, when compared with LOV/PAS domains the BLUF domain contains a large number of conserved amino-acid residues in the flavin-binding pocket. The first ultra-fast measurements of the photocycle of AppA have been undertaken recently (Gauden *et al.* 2005). It was concluded from these measurements that the signalling state of the BLUF domain is formed directly from the FAD singlet excited state. Futhermore, recent studies have suggested that the BLUF domain does not undergo major structural changes upon illumination and that the different structural transitions in the complete AppA are dominated by inter-domain reorganizations (Laan *et al.* 2006).

#### 4.1.2.2 Bacteriophytochromes (BphPs)

BphPs were recognized in bacterial genomic sequences and in particular have now been found to be functionally involved in light-mediated regulation in photosynthetic and non-photosynthetic bacteria (Hughes *et al.* 1997; Davis *et al.* 1999; Giraud *et al.* 2002, 2004, 2005; Armitage & Hellingwerf, 2003; Karniol & Vierstra, 2003; Jaubert *et al.* 2004; Kyndt *et al.* 2004; Evans *et al.*

2005). BphPs sense light in the red(r)/far-red(fr) region of the spectrum. Light then switches these proteins between two quasi-stable forms called Pr and Pfr. One form is the so-called active form, and this controls subsequent gene expression. In photosynthetic bacteria, BphPs have various roles in the regulation of, Car synthesis (Davis *et al.* 1999), chalcone synthase ( Jiang *et al.* 1999), LH complex biosynthesis (Giraud *et al.* 2002), and phototaxis (Armitage & Hellingwerf, 2003; Kyndt *et al.* 2004). In these bacteria the chromophore involved is biliverdin, a linear tetrapyrrole synthesized directly from haem by the enzyme haem oxygenase (Bhoo *et al.* 2001).

At present, mainly due to the published genome sequences rather than by functional analyses, *BphP* genes have been identified in the following photosynthetic bacteria: *Rb. sphaeroides, Rps. palustris*, *Rsp. rubrum*, *Rsp. centenum*, *Chr. tepidum* and *Bradyrhizobium* ORS278 (Jiang *et al.* 1999; Giraud *et al.* 2002; Kyndt *et al.* 2004, 2005). All the *BphP* gene products contain a phytochrome domain that can potentially bind biliverdin. They differ in their C- and N-terminal regions. Like plant phytochromes, the BphPs in *Rsp. centenum* and *Rsp. rubrum* have histidine kinase-like C-terminal domains that are related to two-component sensor kinase/response regulatory systems (Stock *et al.* 2000). In contrast, the C-terminal ends of the BphPs from *Rb. sphaeroides* and *Chr. tepidum* is replaced by a diguanylate cyclase/phosphodiesterase domain. The BphPs from *Chr. tepidum* and *Rsp. centenum* also have extensions to their N-terminal region that incorporate a photoactive yellow protein (PYP) domain (a specialized PAS domain) that is associated with phototaxis (Armitage & Hellingwerf, 2003; Braatsch & Klug, 2004; Kyndt *et al.* 2004, 2005). It is clear, therefore, that in different bacteria the types of BphP expressed can have very different functions. To date, the most studied BphP system in anaerobic photosynthetic purple bacteria is that of *Rps. palustris*.

There are six BphPs in the genome of *Rps. palustris* strain CGA009 although it is believed that only four of them are involved in the regulation of photosynthesis due to their proximity to photosynthetic gene clusters (Larimer *et al.* 2004). At this point it is useful to state again that *Rps. palustris* contains four functional copies of the *pucBA* genes (i.e. *pucBAa*, *pucBAb*, *pucBAd* and *pucBAe*) that encode different LH2 $\alpha$- and $\beta$-apoproteins. The *pucAc* gene, in the *pucBAc* gene pair, has a frameshift and is therefore a non-functional pesudogene (Larimer *et al.* 2004). The different functional *pucBA* genes encode slightly different $\alpha$- and $\beta$-apoproteins. The major difference between the $\alpha$-apoproteins is that the $\alpha_d$-apoprotein does not have the hydrogen-bonding Tyr and Trp residues that are important for the 'normal' 850 nm $Q_y$-Bchl*a* NIR absorption band (see Section 3.2). If the $\alpha$- and $\beta$-apoproteins (the gene products from *pucBAa*, *-b*, *-d* and *-e*) are synthesized in approximately equal stoichiometry then a 'normal' B800–850 LH2 complex is produced (see Fig. 13*b*). However, when the $\alpha_d$-apoproteins make up the majority of LH2 $\alpha$-apoproteins then an atypical LH2 is synthesized, where the relative intensity of the 850 nm-absorpbing $Q_y$-Bchl*a* transition is greatly reduced (Evans *et al.* 1990; Tadros *et al.* 1993; Tharia *et al.* 1999) (see Fig. 13*a*). This unusual LH2 complex is synthesized under 'low-light' conditions (see Section 2.2) and presumably is somehow regulated by the light regime. Recently, the groups of Vermeglio and Papiz investigated this process with respect to the type of BphP used. Unfortunately these two studies used different *Rps. palustris* strains (Giraud *et al.* 2002, 2004, 2005; Evans *et al.* 2005). The *RpBphP1* gene (*rpa1537*; Larimer *et al.* 2004) controls the synthesis of the LH1 'core' complexes by acting on the *pufAB* genes (Giraud *et al.* 2002). Unlike all the other RpBphPs, RpBphP1 does not have a histidine kinase C-terminal domain and is thus incapable of participating in a classical phosphorelay-ordered mechanism. Instead the C-terminal domain has an S-box (also called PAS; see Kyndt *et al.* 2004; Evans *et al.* 2005) domain that is believed to be involved in direct protein–protein recognition (Giraud *et al.*

2002). Giraud and co-workers suggested that BrBphP1 in its Pr form antagonizes the repressive activity of the redox-sensitive PpsR1 and that both proteins belong to the same light-mediated regulatory system (Giraud *et al.* 2004; Jaubert *et al.* 2004). They suggested that BrBphP1 acts as the sensor and that PpsR1 is its regulatory element. The *RpBphP2* (*rpa3015*) and *RpBphP3* (*rpa3016*) genes are located next to each other directly upstream from the *pucBAd* genes, that encode the $\alpha/\beta$-apoproteins responsible for the 'low-light' form of LH2 (Evans *et al.* 2005; Giraud *et al.* 2005). Both RpBphP2 and RpBphP3 auto-phosphorylate in their dark-adapted Pr forms and transfer their phosphate to a common response regulator Rpa3017. The light-induced isomerization of biliverdin in RpBphP3 converts the Pr form to an active form absorbing at shorter wavelength around 645 nm, designated as Pnr for near-red. This unusual light-switch in wild-type cells grown under semi-aerobic conditions is only activated by a narrow window of incident wavelengths between 680 nm and 730 nm. This is concomitant with the synthesis of the 'low-light' LH2 complexes. Deletion mutants of RpBphP2 and RpBphP3 are no longer able to produce the 'low-light' LH2 complexes. Thus Giraud *et al.* (2005) concluded that RpBphP2 and RpBphP3 directly modulate the expression of the *pucBAd* genes. The *RpBphP4* (*rpa1490*) gene product is immediately downstream of pucABe but does not bind biliverdin and is therefore not a light sensor. However, it may still function as a histidine kinase (Evans *et al.* 2005).

### 4.1.3 From the RC to the mature PSU

There have been many studies aimed at determining the time-course of the insertion of the different components of the PSU into the CM.

It has been well documented that under aerobic conditions cells of *Rb. sphaeroides* do actually synthesize very low levels of Bchl*a* and small amounts of the RC H- and M-apoproteins (Chory *et al.* 1984). When the cells grow anaerobically the PSU develops. Very recently, the development of the photosynthetic apparatus in *Rb. sphaeroides* has been monitored using a coordinated approach where near infra-red fast repetition rate (IRFRR) fluorescence measurements, absorption spectroscopy, electron microscopy and pigment analyses were correlated with each other (Koblizek *et al.* 2005). The result of these measurements elegantly demonstrated a sequential development of the PSU during transition from aerobic to anaerobic culture conditions. The sequence was as follows (i) inactivated RC–LH1–PufX 'core' complexes were produced, (ii) this was followed by activation of electron transport, (iii) and finally the LH2 complexes assemble and this stimulated CM invagination producing a fully matured, vesicular, ICM.

## 4.2 Assembly

The problem of trying to determine the molecular mechanisms involved in assembling the antenna complexes in the photosynthetic membrane has been approached in two ways. Using an *in vivo* approach it has been possible to study how changes in the primary sequences of the apoproteins influence antenna assembly using site-directed mutagenesis. This approach takes advantage of the cell's natural assembly processes and the *de facto* provision of the required pigments (and lipids). Alternatively it has been possible to reconstitute LH1 complexes *in vitro* from their individual components and therefore to study the assembly process in a test tube (Ghosh *et al.* 1988; Davis *et al.* 1995; Karrasch *et al.* 1995; Lapouge *et al.* 2000). This field was

excellently reviewed in 1995 by Loach & Parkes-Loach (1995). We shall therefore mainly concentrate here on progress since 1995.

### 4.2.1 LH1

The *in vivo* studies on the assembly of LH1 have largely been carried out in *Rb. capsulatus* and *Rb. sphaeroides*. These studies have been most informative when they have concentrated on either the putative Bchl*a* binding site [$\alpha$-(Gly)Ala28-X-X-X-His32] or key residues at the N- and C-terminii. For example, it was shown that in both these species $\alpha$-His32 is absolutely required for the formation of a stable LH1 (Bylina *et al.* 1988; Olsen *et al.* 1997). Similarly, in *Rb. sphaeroides*, the related His residue on the $\beta$-apoprotein was also important but not absolutely critical for the LH1 assembly since mutations to Asn and Gln also formed viable antenna complexes (Olsen *et al.* 1997). In *Rb. sphaeroides* site-directed mutagenesis studies demonstrated that the $\alpha$-Trp43 and $\beta$-Trp47 residues, which are situated nearer the C-terminal, are important in maintaining the correct hydrogen-bond network to the Bchl*a* molecules and by inference the native tertiary structure (Olsen *et al.* 1994, 1997; Sturgis & Robert, 1997) (see Fig. 21*b*). All of these studies show that the correct ligation of Bchl*a* to the apoproteins, which is partially meditated by the Bchl-apoprotein hydrogen-bonding network (see Section 2), is vital for *in vivo* LH1 assembly. The removal of the C-termius from the $\alpha$-apoprotein inhibits LH1 formation completely (McGlynn *et al.* 1996).

Using *Rb. capsulatus* as a model system, it was shown that specific $\alpha$-apoprotein residues near the N-terminus (Richter *et al.* 1991) are important for $\alpha$-apoprotein insertion into the membrane ($\alpha$-Trp8) and for correct interaction with the $\beta$-apoprotein at the membrane interface ($\alpha$-Pro13). This led to a structural model of LH1 assembly based on electrostatic charge interactions between the $\alpha$- and $\beta$-apoproteins (see Drews, 1996). In contrast to this electrostatic model it was proposed in 1994 that the largest part of the driving force for antenna assembly comes from hydrophobic interactions between the neighbouring apoproteins (Sturgis & Robert, 1994). The latter model was based on evidence from *in vitro* studies prior to the elucidation of the structure of the LH2 complex from *Rsp. molischianum* (Koepke *et al.* 1996). The apoproteins of this particular LH2 complex have remarkable homologies with the primary sequences of LH1 apoproteins (Zuber & Cogdell, 1995). The structure of the LH2 complex from *Rsp. molischianum* showed that although direct contacts between the $\alpha$- and $\beta$-apoproteins are located at the N- and C-terminal regions, little (if any) interaction of an electrostatic nature can be seen. This has been taken as strong evidence for hydrophobic interactions being the major driving force during LH1 assembly. Both of these models, however, do not take into account the role of pigment–pigment and pigment–protein interactions.

The 8·5 Å resolution projection map of the 2D crystal of the LH1 complex from *Rsp. rubrum* (Karrasch *et al.* 1995) (since it was a reconstituted complex) is a clear demonstration of the successful *in vitro* assembly of LH1 complexes from their individual components, i.e. purified $\alpha\beta$-apoprotein dimers and Bchl*a* (in this case in the absence of Car molecules). Reconstitution is achieved by the removal of excess detergent. The peak position of the $Q_y$ transition of Bchl*a* in the fully reconstituted LH1 complex, which is at 873 nm, depends on the 'correct' interactions of the $\alpha/\beta$-apoprotein dimers in the 'ring' (e.g. Ghosh *et al.* 1988; Loach & Parkes-Loach, 1995; Westerhuis *et al.* 1999). Once purified, native Car-less LH1 complexes can be dissociated in the presence of the detergent $\beta$OG. Addition of excess detergent leads to an 820 nm-absorbing species called B820, which are mainly $\alpha/\beta$-apoprotein dimers (Sturgis &

Robert, 1994; Loach & Parkes-Loach, 1995). If the $\beta$OG concentration is further increased the B820 complex itself dissociates into a 777 nm-absorbing form (Ghosh *et al.* 1988; Parkes-Loach *et al.* 1988). The B777 spectral form is actually composed of a mixture of monomeric apoproteins each non-covalently attached to a Bchl*a* molecule (Sturgis & Robert, 1994). This stepwise dissociation process from B873 to B777 *via* B820 is completely reversible (Ghosh *et al.* 1988). The minimal structural elements of the apoproteins required for B820 formation were determined using studies of modified apoproteins where different parts of the C- and N-terminii were removed by limited proteolysis, or substituted with non-native amino-acid terminal sequences (Kehoe *et al.* 1998; Meadows *et al.* 1998; Arluison *et al.* 2002). The reaction order for the formation of the *Rsp. rubrum* LH1 complex from B777 was established using a combination of non-denaturing polyacrylamide gel electrophoresis in the presence of $\beta$OG, and spectroscopic and biochemical characterization of the different polypeptide bands in the gels (Arluison *et al.* 2002). It was concluded that it was impossible for the $\alpha$-B777 complex to form $\alpha_2$-homodimers but that B820 complexes can be formed from $\beta_2$-dimers. However, only $\alpha/\beta$-heterodimeric B820 complexes were able to further aggregate into B873 complexes.

The reversibility of the LH1 dissociation process was used to estimate the thermodynamic parameters associated with the formation of B820 (namely two Bchls bound to a single $\alpha/\beta$-apoprotein heterodimer) and revealed the presence of higher-order intermediate states (Visschers *et al.* 1992; Sturgis & Robert, 1994; Pandit *et al.* 2001, 2003; Vegh & Robert, 2002). These were tetrameters of $\alpha/\beta$-apoproteins and their aggregates. The long-term stability of the tetrameric and higher-order states enabled them to be characterized (Vegh & Robert, 2002; Westerhuis *et al.* 2002; Pandit *et al.* 2003).

In 2004 the groups of Robert and Loach independently concluded (as suggested previously by the *in vivo* studies) that the N-terminal region was also structurally important in the assembly of the *in vitro* LH1 complex and plays a dominant role in the dimerization of individual peptides into $\alpha/\beta$-dimers (Arluison *et al.* 2004; Parkes-Loach *et al.* 2004). The reason the LH1 $\alpha$-apoprotein does not form homodimeric B820 complexes was attributed to steric clashes between their amino-acid residues. No such steric hindrance is present in LH1 $\beta$-apoprotein.

The notion of 'hydrophobic pockets' (Arluison *et al.* 2004) was introduced to explain why a conserved tryptophan residue ($\alpha$-Try5 in *Rsp. rubrum*) close to the N-terminal cytoplasmic interface has key hydrophobic interactions with a number of neighbouring amino-acid residues on both apoproteins ($\alpha$-Ile4, $\alpha$-Pro10, $\alpha$-Leu14, $\beta$-Leu8 and $\beta$-Ala16), including the conserved $\beta$-His20 which is found in all LH $\beta$-apoproteins (Zuber & Cogdell, 1995). This interaction is believed to create a hydrophobic pocket, with a possible hydrogen-bond between $\alpha$-Try5 and $\beta$-His20, which maintains the stability of the $\alpha/\beta$-dimer during LH1 assembly (Arluison *et al.* 2004). Indeed, related mutagenesis studies on the equivalent conserved '$\beta$-His20' residue ($\beta$-His21 in *Rb. sphaeroides*) in LH2 indicated that it was also vital in stabilizing this complex (Crielaard *et al.* 1994; Visschers *et al.* 1994).

The inclusion of Cars into the *in vitro* reconstitution mixture shifts the equilibrium in favour of the intact LH1 complex (Davis *et al.* 1995; Fiedor *et al.* 2004; Fiedor & Scheer, 2005).

### 4.2.2 LH2

Unlike LH1, Car molecules are generally considered essential for the *in vivo* assembly of the LH2 complex (Lang & Hunter, 1994). This then initially inhibited studies on the *in vitro*

assembly of LH2 since previous work using LH1 has shown that in the presence of Car you could not easily see assembly intermediates (see Davis *et al.* 1995; Loach & Parkes-Loach, 1995). However, since the LH2 from *Rsp. molischianum* has many characteristics of an LH1 complex (Germeroth *et al.* 1993; Visschers *et al.* 1995; Zuber & Cogdell, 1995; Koepke *et al.* 1996) it has been the subject of reconstitution experiments (Todd *et al.* 1998). Similar intermediate forms such as B820 have been described. There is however room for a lot more work with this particular complex, since the fine details of its reconstitution have not been well characterized.

The purple sulphur bacteria are able to assemble a $Car^-$ LH2 complex (Krikunova *et al.* 2002) however virtually no *in vitro* reconstitution experiments have been carried out on these complexes (Toropygina *et al.* 2003). What features allow these species to assemble $Car^-$ LH2 complexes are unknown.

*In vivo* studies in *Rb. sphaeroides* have shown that partial removal of the N-terminus can produce an LH2 complex devoid of B800 Bchl*a* molecules (Koolhaas *et al.* 1998) and alterations at the C-terminus result in the formation of 'rings' (McGlynn *et al.* 1996; Todd *et al.* 1999; Braun *et al.* 2002). As in the case of LH1, the conserved His residues ($\alpha$-His20 and $\beta$-His21) in the transmembrane domain are absolutely required for Bchl*a* binding and antennae assembly (Olsen *et al.* 1997). In related studies Hu and co-workers investigated a range of LH2 mutants of *Rb. capsulatus* and concluded, at least in part, that the overall geometry of the LH apoproteins influence the observed LH2 and LH1-like absorption properties (Hu *et al.* 1998). To further investigate how the overall geometry affects antennae structure Olsen and co-workers swapped the C-terminal amino-acid sequence of the LH2 $\alpha$-apoprotein of *Rb. sphaeroides* for the corresponding residues from LH1 of the same bacterium and the LH2 complex from *Rsp. molischianum* (Olsen *et al.* 2003). The domain-swapped mutants were found to have 'rings' of near identical size to that of native LH2 complexes. This indicates that during *in vivo* assembly factors other than the C-terminii must influence LH ring size since the original antennae were of different dimensions (8,9 or 16 $\alpha/\beta$-dimers).

Braun and co-workers recently revisited the role of the central hydrophobic amino-acid residues during LH2 assembly (Braun *et al.* 2002, 2003; Kwa *et al.* 2004). These authors replaced the native sequences of the $\alpha$- and $\beta$-apoproteins in the transmembrane helical region with 'simplified' sequences consisting of 14 amino-acid residues made up from only alanines and leucines, although the conserved His ligands to the B850 Bchls were not mutated (Braun *et al.* 2002). Only bacteria containing the 'simplified' mutations in the transmembrane region in both the $\alpha$- and the $\beta$-apoproteins failed to assemble antenna complexes. It was concluded that a relatively few strategically placed residues are required to stabilize the transmembrane region, to allow Bchl*a* binding, and to assemble intact antenna complexes. These studies also showed that the disruption of the hydrogen-bond between the $\alpha$-Ser27 residue and the $C_{13}$-keto of the $\beta$-B850 Bchl*a* molecule reduces the thermal stability of the LH2 complex but does not appear to significantly alter its spectral properties (Braun *et al.* 2003; Kwa *et al.* 2004). It would be interesting to investigate more thoroughly the relationship between antenna stability and the structural role of the hydrogen-bond network in the transmembrane helical region and how this relates to the overall assembly process.

Although there have been several studies which have been able to pinpoint key residues and regions of the antenna apoproteins that are required for successful assembly, we are still only at the beginning of trying to really understand the molecular details of how this process is controlled *in situ* in the PS membrane.

## 5. Frenkel excitons

### 5.1 General

A starting point to understand the fundamental properties of the optically excited states of the purple bacterial pigment-protein complexes is provided by the formalism of Frenkel excitons (Frenkel, 1931a, b; Knox, 1963; Davydov, 1971). As a first approximation each molecule can be described as a two level system consisting of a ground state and a single electronically excited state separated by an excitation energy $E_0$. A state $|n\rangle$ (see the Appendix for a fuller explanation of the mathematical nomenclature used here) represents molecule $n$ in the electronically excited state and all other molecules $1, 2, \ldots, n-1, n+1, \ldots, N$ in the ground state. The states $|1\rangle$ to $|n\rangle$ feature the same excitation energy $E_0$ which is localized on an individual molecule. The energy transfer between Bchl*a* pigments requires that the molecules interact. This interaction, $V$, between the electronically excited states of the Bchl*a* pigments can be described by the Hamiltonian

$$H = \underbrace{\sum_{n=1}^{N} E_0 |n\rangle\langle n|}_{\text{diagonal elements}} + \underbrace{\sum_{n=1}^{N}\sum_{m\neq n} V_{nm} |n\rangle\langle m|}_{\text{off-diagonal elements}}, \tag{1}$$

where $V_{nm}$ denotes the matrix element $\langle n|V|m\rangle$ (see Appendix) of the interaction between molecules in excited states located on molecule $n$ and $m$. If the Hamiltonian is represented as a matrix the first term refers to the diagonal elements of the matrix whereas the second term refers to the off-diagonal elements of the matrix. Due to the interaction the wavefunctions of the individual pigments are not eigenfunctions of the Hamiltonian [Eq. (1)]. Instead, the excited states are linear combinations of the localized wavefunctions, so-called Frenkel excitons (Frenkel, 1931a, b; Knox, 1963; Davydov, 1971),

$$|k\rangle = \frac{1}{\sqrt{N}} \sum_{n=1}^{N} e^{i2\pi k\frac{n}{N}} |n\rangle \quad (k = 0, \ldots, N-1). \tag{2}$$

The initial degeneracy of the localized excited states (all states have the same energy) is lifted by the interaction, $V$, and results in a manifold of energy levels – the exciton band. For this ideal system where all molecules are equivalent the exciton wavefunctions have equal amplitudes on each pigment and the excitation is fully delocalized over all $N$ pigments. The two sets of states $|n\rangle$ and $|k\rangle$ represent the extreme cases for the description of the excited states either as fully localized or as fully delocalized, respectively. Mathematically the $|n\rangle$ and $|k\rangle$ state representations are Fourier transforms with respect to each other, which also means that each $n$-state can be expressed as a linear combination of $k$-states where each $k$-state contributes equally. The $n$-states can be regarded as being fully delocalized in $k$-space, whereas the $k$-states are fully delocalized in $n$-space.

However, in the case of LH2 there are various deviations from this situation that break the perfect symmetry and tend to localise the excitation energy on a smaller part of the aggregate. For example local variations in the protein environment of the binding sites give rise to static disorder in the site-energies of the pigments, represented by a random shift $\Delta E_n$ with respect to the average transition energy $E_0$. Alternatively, any other deviations from perfect symmetry which result in a variation of the pigment–pigment interactions are represented by $\Delta V_{nm}$. In the

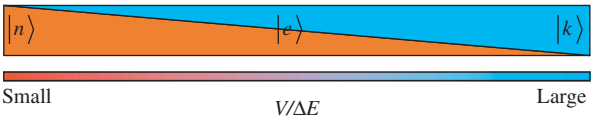


**Fig. 25.** A visualization of the notion of a fully localized or fully delocalized excited state $|e\rangle$. Only if $V/\Delta E$ is small with respect to 1 (left) the state $|e\rangle$ is appropriately described in terms of a localized state $|n\rangle$. On the other hand, if $V/\Delta E$ is large with respect to 1 (right) the state $|e\rangle$ is appropriately described in terms of a delocalized state$|k\rangle$. For an intermediate situation the state $|e\rangle$ can be expressed by Eq. (4) [or Eq. (5)] and is neither fully localized nor fully delocalized.

simplest approximation of the Coulomb interaction between the electrons of neighboring pigments, the Bchl*a* molecules may be described as interacting point-dipoles having specific mutual orientations and center to center distances. In such a simple model three main factors determine the electronic structure and the resulting spectroscopic properties of the LH2 complex (i) the transition energy or site-energy of each pigment (ii) the strength of the electronic interaction between the pigments and (iii) the direction and magnitude of the transition dipole moments. These can be combined into the following Hamiltonian

$$H = \sum_{n=1}^{N} (E_0 + \Delta E_n)|n\rangle\langle n| + \sum_{n=1}^{N}\sum_{m\neq n} (V_{nm} + \Delta V_{nm})|n\rangle\langle m|. \tag{3}$$

Since the disorder in the energies $\Delta E_n$ affects the diagonal elements of the Hamiltonian this is commonly refered to as diagonal disorder. For the same reason the variations in the interaction strength are refered to as off-diagonal disorder. Whether the site representation, $|n\rangle$, or the exciton representation, $|k\rangle$, is more appropriate for the description of the electronically excited states depends on the relative magnitudes of $V$ and $\Delta E$ with respect to each other. Commonly, one distinguishes two limiting cases. In the regime of weak coupling, $|V/\Delta E| \ll 1$, the interaction between the transition dipoles is much smaller than the difference in site energies of the pigments and the description of the excitations in terms of the localized states $|n\rangle$ is a good approximation. In the other extreme, the strong coupling limit, $|V/\Delta E| \gg 1$, the interaction is much larger than the difference in site energies of the pigments and the Frenkel exciton states $|k\rangle$ provide a good starting point for the description of the excited states. Strictly speaking neither the *n*-states nor the *k*-states provide an exact description of a disordered system. The 'true' eigenstates $|e\rangle$ are linear combinations of the basis states and can be either expressed in the $|n\rangle$

$$|e\rangle = \sum_n a_n|n\rangle \quad \text{with} \quad \sum_n |a_n|^2 = 1 \tag{4}$$

or the $|k\rangle$ representation

$$|e\rangle = \sum_k b_k|k\rangle \quad \text{with} \quad \sum_k |b_k|^2 = 1. \tag{5}$$

This is illustrated in Fig. 25. If the system is closer to the weak-coupling limit, Fig. 25, left-hand side, it is best to use the site representation, $|n\rangle$, because one of the coefficients $a_n$ in Eq. (4) dominates and the transfer of energy between the pigments can be visualized as an diffusive hopping process (incoherent energy transfer). Although the interaction mechanism does not have to be necessarily of the well-known Förster type (dipole–dipole) this is usually called the

Förster limit. If the system is closer to the strong-coupling limit, Fig. 25 right-hand side, it is advantageous to use the exciton representation, $|k\rangle$, since only very few of the coefficients $b_k$ contribute significantly to the sum, Eq. (5), and the transfer of excitation energy occurs in a wavelike manner (coherent energy transfer). Since the $k$-states can be thought of as a 'wave' an eigenstate corresponding to a superposition of $k$-states is usually called a wavepacket. If the interaction strength and the site-energy differences are similar in magnitude, the energy transfer is expected to be intermediate between the extremes of incoherent (hopping) and coherent (wavelike) energy transfer.

Another process that tends to localise the excitation energy is dynamic disorder or exciton-phonon interactions. The protein environment is not static but it undergoes dynamic fluctuations, for example low-frequency oscillations of the protein backbone (phonons) that lead to time-dependent variations in the site energies and interactions of the pigments. So far, the concepts detailed above are only valid for temperatures close to absolute zero, where the interactions of excitons with phonons are small (Fig. 26*a*). Raising the temperature, and thereby increasing the exciton–phonon interactions, will lead to a growing scattering rate among the exciton states resulting in a change of shape of the wavepacket over time. Since the width of the wavepacket in k-space is inversely proportional to the extension of the excitation in real space an increase in width of the wavepacket will be associated with a decrease in the localization of the excitation in real space (Fig. 26*b*, *c*). As soon as the width of the wavepacket in $k$-space is sufficiently large, such that the corresponding spatial extension of the excitation in real space approaches the average interpigment distance, the excitation becomes fully localized on an individual Bchl*a* and the transition from coherent wavelike energy transfer to incoherent hopping occurs (Fig. 26*d*). It should be noted that the situation where incoherent energy transfer occurs is the equivalent to what is called a Frenkel exciton in solid-state physics. Apparently, this is related to but different from the Frenkel excitons, $|k\rangle$ introduced earlier in this review.

### 5.2 B800

It is commonly accepted that the electronic excitations of the B800 pigments of LH2 are best described in the weak coupling limit (Sauer *et al.* 1996; Alden *et al.* 1997; Mukai *et al.* 1999; Sundström *et al.* 1999; Yang *et al.* 2001; Hu *et al.* 2002). Experimental values for the orientation and distances of the pigments can be deduced from the crystal structure and the dipolar coupling between neighbouring B800 Bchl*a* molecules has been estimated to be $\sim 24\ \mathrm{cm}^{-1}$. The variation in site energies has been estimated from the inhomogeneously broadened ensemble spectrum to be $\sim 180\ \mathrm{cm}^{-1}$. This yields a $|V/\Delta E|$ ratio of $\sim 0{\cdot}1$ that is clearly in the weak coupling regime and a strong localization of excitation on the individual Bchl*a* is expected (see below for experimental verification of this).

### 5.3 B850

In order to describe the spectroscopic properties of the B850 ring, two parameters are important: the site energies of the individual B850 pigments and their intermolecular interactions. Although the intermolecular interactions between the B850 pigments can be calculated from the structure parameters of the $C_9$ symmetric ring it is not possible *a priori* to calculate the site energies of the B850 $\alpha$- and $\beta$-Bchl*a* molecules. The simplest approach to calculate the

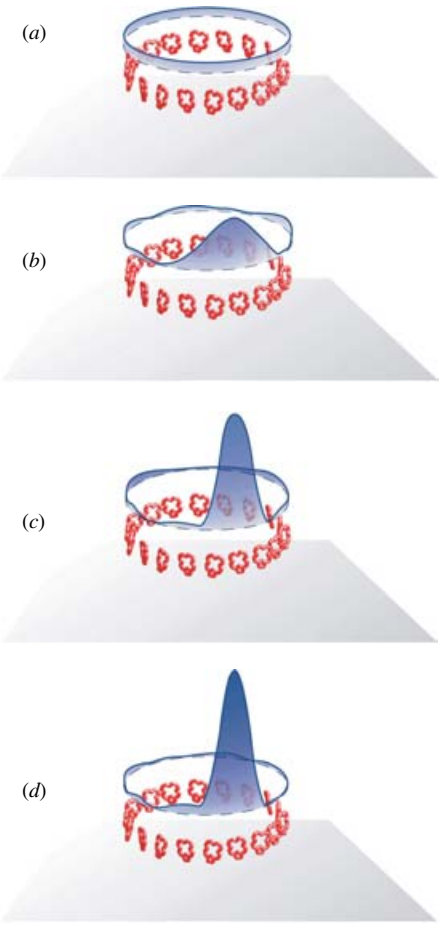


**Fig. 26.** For a perfectly symmetric B850 ring (geometry and site energies), initially the excitation energy is fully delocalized over all 18 BChl*a* molecules. Any deviation from this situation tends to localize the excitation energy on a few BChl*a* molecules and the wavefunction of the excited state is given by a linear combination of exciton states (wavepacket). The figure shows from top to bottom the probability density (full line with respect to the dashed line) to find the excitation energy at the position of a distinct Bchl*a* molecule for a pure exciton state, and for wavepackets that result from the superposition of the lowest five, the lowest seven, and the lowest fifteen exciton states, respectively. For illustration purposes this function has been centred arbitrarily on one of the BChl*a* molecules; it is actually determined by the deviation from the perfect symmetry of the system. In the native system the localization of the excitation energy as sketched here from top to bottom takes place on an ultrafast timescale of some hundred femtoseconds.

interactions is to use the point-dipole approximation (Sumi, 1999; Hu *et al.* 2002). Model calculations for a perfectly symmetric LH2 ring have estimated the intermolecular interaction strength for the B850 molecules to be $V \approx 300\ \mathrm{cm}^{-1}$ (Sauer *et al.* 1996). However, since the closest distance between the pigments is rather small compared with the size of the Bchl*a* molecules, the validity of this approximation must be questioned, and therefore other theoretical approaches have been employed as well. For example, a point-monopole approach (Sauer *et al.* 1996) and the transition density cube method (Krueger *et al.* 1998) were applied to include a spatial distribution of the electric charges. Quantum-chemical calculations have been used to take into account exchange interactions (Alden *et al.* 1997; Scholes *et al.* 1999). All of

**Table 4.** *An overview of the intra- and inter-B850 interaction strengths determined for the most widely studied LH2 complexes. The values were obtained using a variety of different approaches*

| | Type of pigment interaction | | | |
|---|---|---|---|---|
| Species | Intra | Inter | Reference | Method |
| *Rps. acidophila* | 273 | 291 | Sauer *et al.* (1996) | Point-monopole calculations |
| | 250 | 230 | Ketelaars *et al.* (2001) | Single-molecule experiments |
| | 280 | – | Koolhaas *et al.* (1998) | Circular dichroism experiments |
| | 322 | 288 | Sundström *et al.* (1999) | Dipole–dipole approximation |
| | 320 | 255 | Scholes & Fleming (2000) | *ab initio* density cube method |
| | 238 | 213 | Krueger *et al.* (1998) | *ab initio* density cube method |
| | 320 | 255 | Scholes *et al.* (1999) | CIS Gaussian 94 |
| | 394 | 317 | Alden *et al.* (1997) | Quantum mechanical force field for $\pi$-electrons (QCFF/PI) |
| | 622 | 562 | Linnanto *et al.* (1999) | Intermediate neglect of differential overlap parametirised for spectroscopy (INDO/S) |
| | 771 | 612 | Linnanto *et al.* (1999) | Intermediate neglect of differential overlap parametrized for spectroscopy (INDO/S) (dielectric medium) |
| | 540 | 380 | Mukai *et al.* (1999) | Dipole–dipole approximation |
| | 320 | – | Wu & Small (1998) | Dipole–dipole approximation |
| | 340 | 320 | Dahlbom *et al.* (2001) | Dipole–dipole approximation |
| | 410 | 310 | Pullerits *et al.* (1997) | Dipole–dipole approximation |
| | 367 | 284 | Scholes *et al.* (1999) | Dipole–dipole approximation |
| | 300 | 233 | Koolhaas *et al.* (1998) | Absorption and circular dichroism experiments |
| *Rps. molischianum* | 339 | 336 | Sundström *et al.* (1999) | Dipole–dipole approximation |
| | 806 | 377 | Hu *et al.* (1997); Cory *et al.* (1998) | Semi-empirical INDO/S effective Hamiltonian |
| | 408 | 366 | Tretiak *et al.* (2000b) | Collective electronic oscillator approach |
| | 363 | 320 | Tretiak *et al.* (2000a) | Collective electronic oscillator |
| | 258 | 210 | Tretiak *et al.* (2000a) | Collective electronic oscillator (dielectric medium) |
| *Rb. sphaeroides* | 412 | 317 | Chachisvilis *et al.* (1997) | Transient absorption experiments |
| | 230 | 110 | Jimenez *et al.* (1996) | Fluorescence up-conversion experiments |
| | 300 | 233 | Koolhaas *et al.* (1998) | Circular dichroism experiments |
| | 360 | 244 | Trinkunas & Freiberg (2006) | Polarized fluorescence excitation spectroscopy |

these different approaches produce similar values for the strength of the pigment–pigment interactions. The general consensus is that the interaction strength is in the order of 250–400 $cm^{-1}$. Table 4 provides an overview of the various B850 interaction strengths obtained by different approaches that are discussed in the literature. The magnitude of the diagonal disorder $\Delta E$ can be estimated from the inhomogeneous width of the B850 absorption lines, which is caused by static disorder and slow fluctuations of the local environment, to be $\Delta E \approx 200\ cm^{-1}$. These numbers (for $V$ and $\Delta E$) suggest that for the B850 molecules the excitonic interactions have to be taken into account and that the excitation energy is

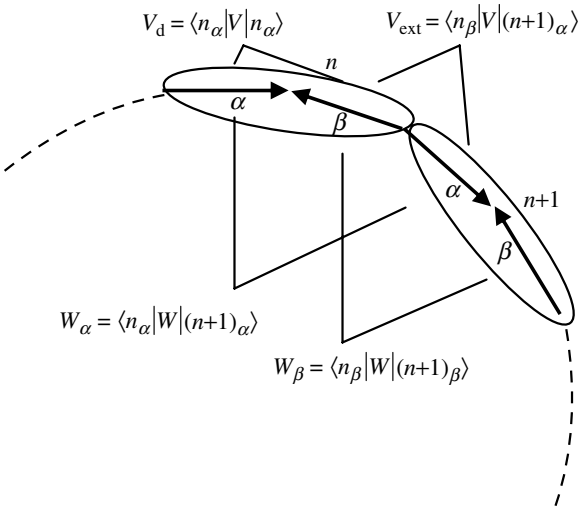


**Fig. 27.** A schematic sketch of the transition–dipole moments for the $\alpha$- and $\beta$-bound Bchl*a* molecules in adjacent dimers ($n$ and $n+1$) in the B850 ring of LH2 from *Rps. acidophila*. The strongest contributions to the interaction are the intradimer (nearest neighbour) interaction $V_d$, the interdimer (nearest neighbour) interaction $V_{ext}$, the $\alpha$-next-nearest-neighbour interaction $W_\alpha$, and the $\beta$-next-nearest-neighbour interaction $W_\beta$ respectively.

delocalized among the pigments. The details of the exciton manifold of the B850 assembly of LH2 has been subject of numerous studies (Sauer *et al.* 1996; Alden *et al.* 1997; Ha *et al.* 1997; Krueger *et al.* 1998; Scholes *et al.* 1999; Mostovoy & Knoester, 2000; Sumi, 2000; Dahlbom *et al.* 2001; Jang *et al.* 2001; Matsushita *et al.* 2001; Didraga & Knoester, 2002; Hu *et al.* 2002). For the purposes of the present discussion we only want to provide an insight into the general features of the B850 excited states and calculate the exciton states for an unperturbed B850 ring using Eq. (3) with $\Delta E_n = 0$ and $\Delta V_{nm} = 0$, *e.g.* with no diagonal and off-diagonal disorder. The LH2 complex from *Rps. acidophila* consists of $N = 9$ dimers, each of two Bchl*a* molecules bound to the $\alpha$- and $\beta$-polypeptides as the basic building block. In the following we label the dimers by $n$ and denote the two molecules within a dimer by the subscripts $\alpha$ and $\beta$, having site energies $E_\alpha$ and $E_\beta$. If for the interaction only contributions from adjacent dimers are considered, the Hamiltonian for the set of $N$ dimers is

$$
\begin{aligned}
H = & \sum_{n=1}^{N} \left( E_\alpha |n_\alpha\rangle\langle n_\alpha| + E_\beta |n_\beta\rangle\langle n_\beta| \right) \\
& + \sum_{n}^{N} \left( V_d \left( |n_\alpha\rangle\langle n_\beta| + |n_\beta\rangle\langle n_\alpha| + V_{ext} \left( |n_\beta\rangle\langle (n+1)_\alpha| + |(n+1)_\alpha\rangle\langle n_\beta| \right) \right) \right) \\
& + \sum_{n}^{N} \left( W_\alpha \left( |n_\alpha\rangle\langle (n+1)_\alpha| + |(n+1)_\alpha\rangle\langle n_\alpha| \right) + W_\beta \left( |n_\beta\rangle\langle (n+1)_\beta| + |(n+1)_\beta\rangle\langle n_\beta| \right) \right). \qquad (6)
\end{aligned}
$$

The contributions to the interaction are the nearest-neighbour intradimer interaction $V_{\alpha\beta,nn} = \langle n_\alpha | V | n_\beta \rangle = V_d$, the nearest-neighbour interdimer interaction $V_{ext} = \langle n_\beta | V | (n+1)_\alpha \rangle$, the $\alpha$ next-nearest-neighbour interaction $W_\alpha = \langle n_\alpha | W | (n+1)_\alpha \rangle$, and the $\beta$ next-nearest-neighbour interaction $W_\beta = \langle n_\beta | W | (n+1)_\beta \rangle$, as illustrated in Fig. 27. For the simplest case

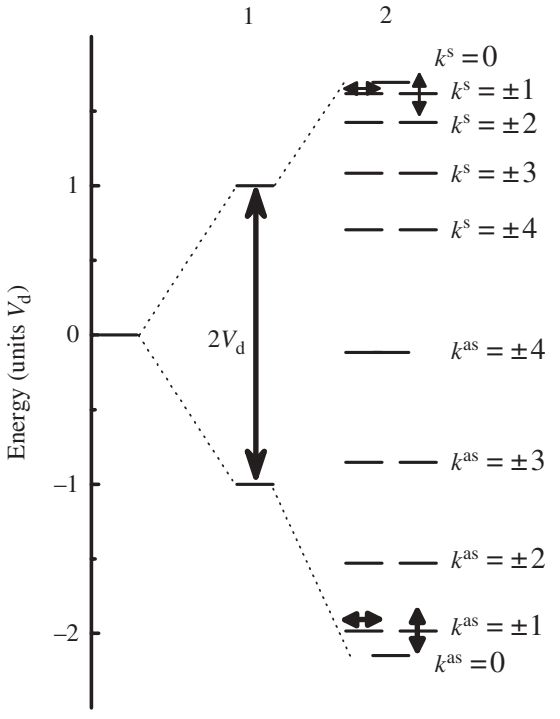


**Fig. 28.** A schematic representation of the energy level scheme of the excited state manifold of a dimer (manifold 1) and of the B850 ring of LH2 (manifold 2). The mutual orthogonal orientation of the transition moments of the $k^j = \pm 1$ degenerate pairs is indicated by the arrows. The interaction within the dimer $V_d$ (intradimer) leads to the splitting into the two Davydov components ($j = $ s, as), the degeneracy of which is lifted by the interdimer interactions. For a more detailed description see the Appendix.

where $E_\alpha = E_\beta = E_0$ and $W_\alpha = W_\beta = W_0$ the eigenstates of this Hamiltonian are given by

$$|k^j\rangle = \frac{1}{\sqrt{N}} \sum_{n=1}^{N} e^{i2\pi k \frac{n}{N}} \left| n^j_{\alpha\beta} \right\rangle \quad (j = \mathrm{s}, \mathrm{as}), \tag{7}$$

where $|n^j_{\alpha\beta}\rangle$ are the symmetric ($j = $ s) and antisymmetric ($j = $ as) dimer states (see Appendix). The energies of the exciton states can be expressed as follows

$$E^j_k = E_0 + 2W_0 \cos k^j \frac{2\pi}{N} \pm \sqrt{V_d^2 + V_{ext}^2 + 2V_d V_{ext} \cos k^j \frac{2\pi}{N}}, \tag{8}$$

where $j = $ s refers to the ' + ' and $j = $ as to the ' − ' sign. The quantum number $k^j$ of each exciton state in the manifold extends from $k^j = 0, \pm 1, \ldots,$ to $\pm(N-1)/2$ if $N$ is odd and from $k^j = 0, \pm 1, \ldots,$ to $\pm N/2$ if $N$ is even. A full treatment of this exciton system including the conditions where $E_\alpha \neq E_\beta$ and $W_\alpha \neq W_\beta$ can be found in (Matsushita *et al.* 2001). The resulting energy levels of the exciton manifold are depicted in Fig. 28. This figure shows how the structure of the exciton manifold develops as one goes from a single dimer to a system of $N$ interacting dimers. The exciton states are separated in lower (as) and upper (s) branches. This reflects the interactions within a dimer and is commonly known as Davydov splitting (Davydov, 1948; Wolf, 1967; Robinson, 1970; Silbey, 1976; Burland & Zewail, 1979) (see Fig. 28,

manifold 1). Each branch in section 2 of Fig. 28 consists of eight pairwise degenerate states, labelled by $k^j = \pm 1, \pm 2, \pm 3, \pm 4$, and one nondegenerate state $k^j = 0$. As a result of the strong interaction within the B850 ring the initial degeneracy of the excited states of the 18 B850 Bchl*a* molecules is lifted and the energy of the 18 exciton eigenstates is spread over a band with a width of $\sim 1200\ \mathrm{cm}^{-1}$.

For the optical transitions between the ground state and any given exciton state one has to calculate the resultant transition–dipole moment according to

$$\begin{aligned}\vec{M}(k^j) = \langle g|\vec{D}|k^j\rangle &= \left\langle g\left|\vec{D}\frac{1}{\sqrt{N}}\sum_{n=1}^{N} e^{i2\pi k^j \frac{n}{N}}\right|n^j_{\alpha\beta}\right\rangle \\ &= \frac{1}{\sqrt{N}}\sum_{n=1}^{N} e^{i2\pi k^j \frac{n}{N}} \underbrace{\langle g|\vec{D}|n^j_{\alpha\beta}\rangle}_{\vec{m}(n^j_{\alpha\beta})} = \frac{1}{\sqrt{N}}\sum_{n=1}^{N} e^{i2\pi k^j \frac{n}{N}}\vec{m}(n^j_{\alpha\beta}),\end{aligned} \tag{9}$$

where $\vec{D}$ is the transition–dipole moment operator and $\vec{m}(n^j_{\alpha\beta})$ refers to the transition–dipole moment of the respective dimer wavefunction. To obtain a non-zero result for the summation a constructive interference of the individual transition–dipole moments $\vec{m}(n^j_{\alpha\beta})$ is required. (This is explained more fully in the Appendix.) Consequently, both the magnitude and the mutual arrangement of the individual transition–dipole moments have a crucial influence on the resulting selection rules for the optical transitions. Due to the circular arrangement of the pigments in LH2 only the exciton states $k^j = 0, \pm 1$ have a non-vanishing transition–dipole moment. The $k^j = 0$ transitions can be excited with light polarized parallel to the $C_9$-symmetry axis of the ring whereas transitons to the $k^j = \pm 1$ states can be excited with light of mutually orthogonal polarization within the plane of the ring, (see the effect that this has on the single-molecule spectroscopy described below). Since the individual transition–dipole moments of the B850 pigments are oriented mainly in the plane of the ring rather little of the total oscillator strength is associated with the $k^j = 0$ states. Due to the head-to-tail arrangement of the transition–dipole moments within an individual dimer nearly all the oscillator strength is concentrated in the lower exciton manifold ($j = \mathrm{as}$) which results in a strong electronic transition from the $k^{\mathrm{as}} = \pm 1$ states (seen *in vivo* as the strong NIR absorption band at $\sim 860$ nm). The upper exciton components $k^{\mathrm{s}} = \pm 1$ carry less than 3% of the total oscillator strength and give rise to very weak absorptions up to $\sim 790$ nm (Sauer *et al.* 1996).

Random diagonal disorder, caused by stochastic variations in the protein environment, introduces the term $\Delta E_n$ into Eq. (3). The main effects on the exciton manifold are, a mixing of the different exciton levels, a modification of the energy separation of the exciton levels and lifting their pair-wise degeneracy, and a redistribution of oscillator strength to nearby states, including the $k = 0$ state. The random off-diagonal disorder described by the term $\Delta V$ in Eq. (3), is caused by the variations in the dipolar coupling between the Bchl*a* pigments and originates from fluctuations in the orientations and positions of the individual transition dipole moments. The influence of these various types of disorder on the B850 exciton states have been analysed intensively. Since the effects of random off-diagonal disorder are experimentally indistinguishable from those of random diagonal disorder (Fidder *et al.* 1991) many studies have focused on the latter type of disorder (Sauer *et al.* 1996; Alden *et al.* 1997; Jang *et al.* 2001). More recently, however, studies have also included combinations of random diagonal and correlated off-diagonal disorder (Dempster *et al.* 2001) as well as combinations of random on- and off-diagonal

disorder and correlated on- and off-diagonal disorder on the B850 exciton states (Jang *et al.* 2001). Predictions based on these models differ with respect to subtle details in the spectra such as the extent and distribution of the energy separation between the $k = \pm 1$ states and the intensity ratio of the respective transitions.

In LH2 the phonon frequencies are in the order of some ten wavenumbers peaking at $\sim 30\ \mathrm{cm}^{-1}$ (Reddy *et al.* 1987; Small, 1995; Wu *et al.* 1996; Hofmann *et al.* 2005) that corresponds to a dephasing time of $\sim 1$ ps. In contrast, the summed nearest-neighbour transition–dipole interactions are in the order of several hundred wavenumbers. This means that the excitation energy between adjacent pigments is transferred coherently on a time scale of less than $\sim 0{\cdot}1$ ps. Consequently, the phonons appear to the excitons as being static and dynamic disorder can be reasonably modelled by static fluctuations of the site energies of the B850 pigments (Sumi, 2000, 2001).

### 5.4 B850 delocalization

The degree of delocalization of excitonic excitations in molecular aggregates has always been a matter of hot debate. In 1D aggregates, like the LH2 complex, the delocalization of the exciton can be described in terms of the number of molecules that share the excitation. Estimates for the number of B850 Bchl*a* molecules over which the excitation is coherently delocalized range from 2 to essentially the whole ring (Leegwater, 1996; Leupold *et al.* 1996; Pullerits *et al.* 1996; Meier *et al.* 1997; Ray & Makri, 1999; van Oijen *et al.* 1999b; Zhao *et al.* 1999). One reason for these discrepancies is that several expressions for the delocalization length have been introduced into the literature. One measure defines the exciton delocalization length as inverse participation ratio associated with the distribution of the entries of the exciton density matrix (Meier *et al.* 1997). Other groups have defined the delocalization length as the full-width half maximum of the autocorrelation distribution for site $n$ of the exciton density matrix averaged over the contributions from all other sites in the aggregate (Kuhn & Sundström, 1997). The most widely used measure for the delocalization length, however, is the inverse participation ratio given by

$$\frac{1}{P} = \frac{\left(\sum_n |a_n|^2\right)^2}{\sum_n |a_n|^4}, \tag{10}$$

where $a_n$ is the coefficient of the excited state wave function $|e\rangle$ at the site $n$ (Thouless, 1974; Fidder *et al.* 1991). This equation yields the correct values in both limits of completely delocalized and localized states. A detailed comparison of the different measures of the exciton delocalization in LH2 can be found in Dahlbom *et al.* (2001). Another, and more important reason, for the discrepancies in the extent of the exciton delocalization results from the fact that different experimental techniques yield *per se* different delocalization sizes. For example, single-molecule excitation spectroscopy monitors the exciton wavefunction when it is 'born'. In contrast, time-resolved and steady-state methods will give different results if the exciton delocalization length is time dependent. Another complication comes when the excitation pulse is ultrashort and therefore spectrally broad. Under these conditions the excitation pulse creates a coherent superposition of a number of exciton states, i.e. an excitonic wave packet. Because of interference, the wave packet may have a major part of its amplitude in a very localized region of the aggregate. Then that coherence between exciton states is rapidly destroyed due to dephasing and exciton relaxation.

Other problems in determining the delocalization length can result from the consequences of the methods applied. In a model calculation for 1D aggregates Knoester and co-workers showed that the experimental value obtained for the delocalization length derived from pump-probe experiments provides a useful measure only if the energy level spacing between the exciton states is more than $10^4$ times larger than the homogeneous linewidth (Bakalis & Knoester, 1999). Otherwise the experimentally obtained values for the delocalization length levels off and is determined by the homogeneous broadening of the absorption bands. These authors showed that it is impossible with the pump-probe method to determine a delocalization length that is longer than a saturation value that is given by Bakalis & Knoester (1999),

$$N_{\mathrm{sat}} = \sqrt{3\pi^2 \frac{V}{\Gamma_{\mathrm{hom}}}} - 1, \tag{11}$$

where $V$ denotes the interaction strength and $\Gamma_{\mathrm{hom}}$ the homogeneous linewidth. Taking into account the inhomogeneous linebroadening as well, makes this effect even more severe since for an ensemble $\Gamma_{\mathrm{hom}}$ in Eq. (11) has to be substituted by $\Gamma_{\mathrm{inhom}}$, the inhomogeneous linewidth (see also the discussion of inter- and intracomplex heterogeneity in Section 7.2.2.2). Applying this idea to the B850 ring and using $V = 250\ \mathrm{cm}^{-1}$ and $\Gamma_{\mathrm{inhom}} = 200\ \mathrm{cm}^{-1}$ for the inhomogeneous linewidth, respectively, yields a saturation value for the delocalization length of the B850 exciton of $\sim 5$ molecules, in agreement with the values reported in the pump-probe literature (Pullerits *et al.* 1996; Novoderezhkin *et al.* 1999). However, as clearly shown in Bakalis & Knoester (1999) this value may be determined by the method rather than by the 'true' delocalization length.

## 6. Energy-transfer pathways: experimental results

### 6.1 Theoretical background

In the life sciences the transfer of excitation energy between a donor, D, and an acceptor molecule, A, is usually described by Förster's weak interaction, energy-transfer mechanism. However, Förster energy transfer is only a very special case of a much more general theoretical picture. We will outline this more basic theoretical framework here and try to highlight the main features that characterize any energy-transfer process which occurs between discrete molecules. This is actually required for a description of many of the energy-transfer steps encountered in the purple bacterial antenna system, because, in these cases, the classical Förster mechanism is not applicable. Indeed, it mainly fails to account for the measured rates of energy transfer.

In Fig. 29 the energy transfer between a donor and an acceptor is depicted. Initially the donor is in the electronically excited state $\tilde{\mathrm{D}}$ and the acceptor is in the electronic ground state A. This state is denoted $|\tilde{\mathrm{D}}\mathrm{A}\rangle$. Energy transfer from $\tilde{\mathrm{D}}$ to A requires that these molecules interact. As a result of this interaction, $V$, between the molecules the excitation energy can be transferred to the acceptor resulting in the final state $|\mathrm{D}\tilde{\mathrm{A}}\rangle$, corresponding to the donor in the ground state and to the acceptor in the excited state.

If the interaction between the molecules is relatively weak, i.e. the individual molecules can still be thought of as essentially independent entities, then a description in terms of two molecules plus an interaction is justified and the system can be treated by pertubation theory – a well-developed method of quantum mechanics. For the situation as shown above, where the final states of the donor as well the excited states of the acceptor are given by continous manifolds

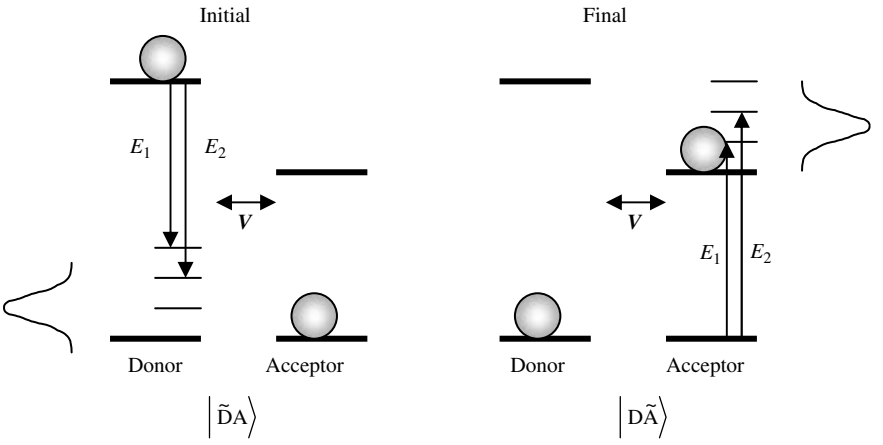


**Fig. 29.** Excitation-energy transfer between a donor and an acceptor molecule connected by an interaction $V$. For an explanation see the main body of the text.

(for example by electronic states connected to vibrational or librational states) pertubation theory allows us to calculate the energy-transfer rate using Fermi's Golden Rule, which we show here in a simplified form below. We will now describe the main features of this equation which we hope will allow the biologist to at least get a qualitative picture of the important factors that affect the rate of the process of energy transfer.

$$k_{\mathrm{DA}} = \frac{2\pi}{\hbar} \int \mathrm{d}E \underbrace{\left|\langle \mathrm{D}\tilde{\mathrm{A}}| V |\tilde{\mathrm{D}}\mathrm{A}\rangle\right|^2}_{\mathrm{A}} \underbrace{\rho(E)}_{\mathrm{B}} \underbrace{\delta(E_f - E_i)}_{\mathrm{C}}. \tag{12}$$

Term A in this expression describes that the system is initially in state $|\tilde{\mathrm{D}}\mathrm{A}\rangle$ and then induced by the interaction $V$ that it develops into state $\langle \mathrm{D}\tilde{\mathrm{A}}|$. A strict definition of the mathematically correct meaning of the symbols $|\rangle$ and $\langle|$ is beyond the scope of this review; however we have provided a short summary of this in the Appendix. The transfer of energy between the donor and the acceptor can occur at different energies, as indicated in Fig. 29 for two different energies $E_1$ and $E_2$. For any one energy $E$ the probability of energy transfer is proportional to the density of initial (in the donor) and final (in the acceptor) states at that energy. Therefore one has to know the number of possible states at each particular energy and this is taken into account by the density of states $\rho(E)$, term B. The term $C$, in the above expression, is a so-called delta function, which ensures energy conservation is maintained for each particular energy-transfer process. Finally the product of these terms is integrated over all possible energies at which energy transfer can occur.

In order to find an expression for the interaction $V$ a molecular picture is required where the electrostatic interactions of the charges and induced dipole moments between the donor and acceptor are taken into account. The conventional way to do this is to take only the leading term of the electrostatic interaction (the dipole–dipole interaction) between the donor and the acceptor molecules into account. This approximation is justified if the size of the optically active part of the donor and acceptor molecules, $d$, is small with respect to the distance between them, $r$, Fig. 30. Usually due to a lack of knowledge of the real densities of states there is a problem. This can be overcome by referring to the emission spectrum of the donor and the absorption

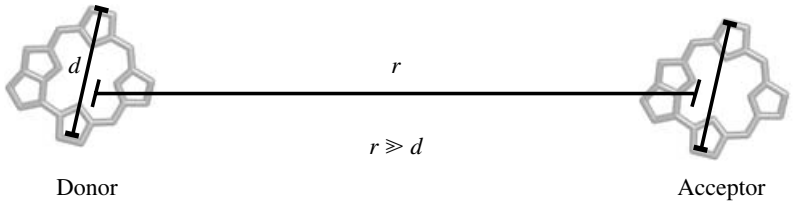


**Fig. 30.** Illustration of two uncharged molecules of spatial extension *d* separated by a distance *r*. If $r \gg d$ holds the electrostatic interaction between the two molecules can be reduced to the dipole–dipole interaction.

spectrum of the acceptor. The assumption is that the density of states will be reflected by the area under these two spectra. These considerations, both the dipole–dipole approximation for the interaction and the use of the spectra for the density of states, now lead to the well-known Förster energy-transfer equation. It is worth noting that the same formalism, i.e. perturbation theory, yields the Dexter energy-transfer mechanism if, instead of the dipole–dipole interaction, an electronic exchange interaction is introduced into Fermi's Golden Rule. An important consequence of the Förster approach is that excitation-energy transfer is only permitted between optically allowed states (more precisely dipole-allowed electronic states).

It is clear, however, that the fundamental pre-requisite of Förster energy transfer, i.e. that the size of the optically active part of the molecules has to be small with respect to their mutual distance, $r \gg d$, is, for example, not fulfilled for the B850 assembly of LH2 (Fig. 31*a*). Consequently, this approximation breaks down for the B850 ring and the Förster approach fails. In the case of the energy-transfer step from a B800 Bchl*a* molecule to the B850 ring the acceptor states are excitons and these extend over a large part of the ring. In other words the size of the acceptor ensemble is large with respect to the intermolecular distances between the B800 molecule and the B850 ring. A more sophisticated approach is also needed to characterize this energy-transfer process because of the following complication. The closest distance between a B800 Bchl*a* molecule and a B850 Bchla molecule is $\sim$18 Å whereas the largest distance between such molecules is $\sim$60 Å (see Fig. 31*b*). This means that the interaction of the B800 Bchl*a* molecule with its closest B850 Bchl*a* neighbour is $\sim$40 times stronger compared with its interaction with the most remote one (see Fig. 31*b*). The donor B800 molecule is therefore unable to 'feel' the full transition–dipole moment of an exciton state because of these differential strengths of interactions with the different B850 molecules in the ring. This means that the interactions between the donor and acceptors have to be summed locally (Sumi, 1999). A direct consequence of this is that both optically allowed and forbidden states can participate in this energy-transfer process which is in striking contrast to the Förster mechanism.

Other approaches to describe the excitation energy transfer in the antenna system that have been discussed in the literature include (i) generalized Förster resonance energy transfer (Scholes *et al.* 2001), (ii) multichromophoric Förster resonance energy transfer (Jang *et al.* 2004) as well as, (iii) Red-field theory (Chernyak & Mukamel, 1996; Zhang *et al.* 1998; van Grondelle & Novoderezhkin, 2006).

### 6.2 'Follow the excitation energy'

The process of energy transfer in purple bacterial antenna complexes [B800→B800, B800→B850, B850→B850, LH2→LH1 (B850→B875) and LH1→RC] has been well reviewed

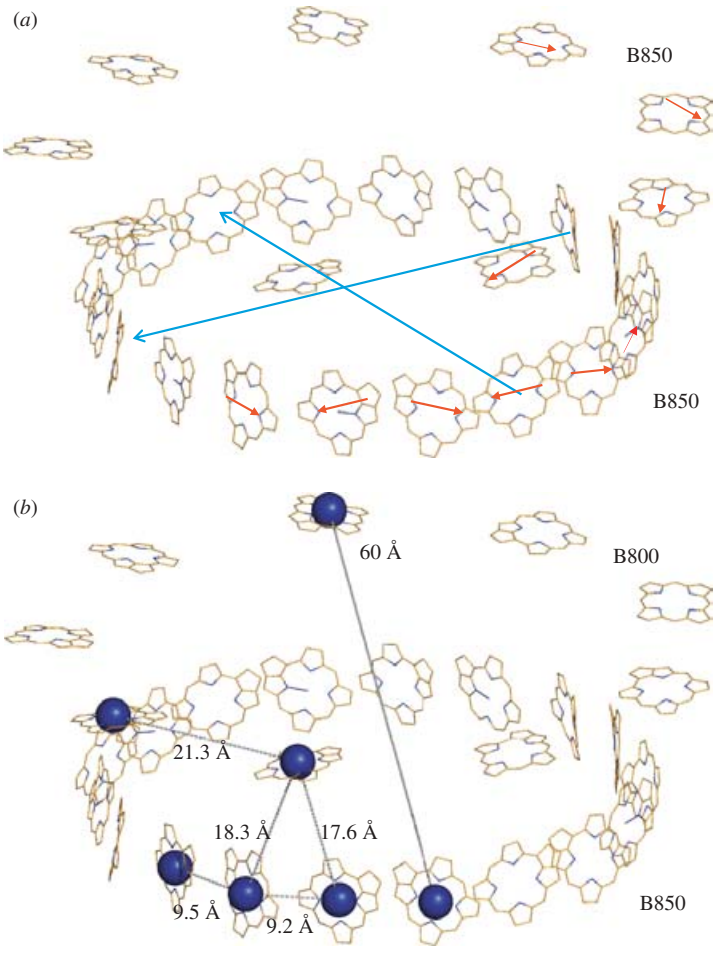


**Fig. 31.** Relation between Bchl–Bchl distance and the transition dipole moments in LH2. (*a*) The transition–dipole moments of some of the individual Bchl*a* molecules are indicated by the small red arrows. The major transition–dipole moments of the B850 exciton are depicted by the large double-headed blue arrows. (*b*) The range of distances between a B800 and B850 Bchl*a* molecules in the LH2 from *Rps. acidophila*.

in the following articles (Sundström & van Grondelle, 1995; Pullerits & Sundström, 1996; Sundström *et al.* 1999; Robert *et al.* 2003). In the following subsections we shall discuss these energy-transfer rates in turn, as well as Car→Bchl energy transfer.

### 6.2.1 Bchl*a*→Bchl*a* energy transfer

#### 6.2.1.1 *B800→B800*

When an LH2 B800 Bchl*a* molecule is excited by an ultrashort laser flash the $Q_y$ absorption band of that Bchl*a* molecule bleaches (for an example see Bergström *et al.* 1988) B800→B800 singlet-singlet energy transfer can then occur, but it is rather difficult to measure since when two adjacent B800 Bchl*a* molecules exchange energy there is no net change in absorption, the two B800 Bchl*a* molecules being spectroscopically identical. It is, however, possible to monitor

this energy transfer process by making use of the fact that the different B800 molecules in LH2 are arranged at different angles relative to each other (see Fig. 9*b*). The laser excitation pulses are polarized and so if the B800 bleaching is also analysed with respect to polarization (i.e. with the measuring beam polarized either parallel or perpendicular to the excitation pulse) then the polarization ratio ($P$) of this bleaching can be measured *vs.* time [i.e. $P=(\Delta A_v-\Delta A_H)/(\Delta A_v+\Delta A_H)$, where $A_v$ and $A_H$ are the vertical and horizontal polarized absorption intensities respectively] (Bergström *et al.* 1988; Kennis *et al.* 1997b). The decay of this ratio from the theoretical maximum of 0·4, for randomly ordered LH2 complexes in solution, to a minimum value of 0·05 will then reflect B800→B800 energy transfer. In LH2 complexes from *Rps. acidophila* it takes 0·9 ps for this polarization ratio to decay to half its initial value. This then implies B800→B800 energy 'hopping' times of ∼1·5 ps. These times have been detected using both this anisotropy decay and three-pulse echo shift peak (3PEPS) studies (Hess *et al.* 1993; Kennis *et al.* 1997b; Salverda *et al.* 2000), although slightly faster times have also been proposed (Ma *et al.* 1997). This data is hard to determine accurately because the population of the B800 excited singlet states is rapidly depleted during the measurement due to B800→B850 energy transfer, which competes with the B800→B800 transfer. This has the effect of making the polarization ratio data increasingly noisy with time, since the size of the B800* signal quickly gets smaller over the time-course of the depolarization measurements.

#### 6.2.1.2 B800→B850

The singlet–singlet energy transfer from B800 to B850 in LH2 is part of the energy transfer pathway to the RC. This has been measured extensively by many groups using LH2 complexes from both *Rb. sphaeroides* (including mutant LH2 complexes) and *Rps. acidophila* (Sundström *et al.* 1986; Freiberg *et al.* 1988; Shreve *et al.* 1991; Hess *et al.* 1993, 1994; Monshouwer *et al.* 1995; Fowler *et al.* 1997; Kennis *et al.* 1997b; Ma *et al.* 1997; Pullerits *et al.* 1997). In LH2 complexes from *Rps. acidophila* the time constant for this energy-transfer step is 0·8–0·9 ps at room temperature (Hess *et al.* 1993; Kennis *et al.* 1997b). Like most of the energy-transfer steps in LH2 this reaction is very largely temperature independent and only slows down to 1·8–2·4 ps at low (1·4–10 K) temperature (Kennis *et al.* 1997a; Reddy *et al.* 1993). Since the publication of the structure of LH2 from *Rps. acidophila* several groups have attempted to use Förster theory to calculate the rate of this energy-transfer reaction, see Sundström *et al.* (1999) and references therein. For example, Krueger and co-workers investigated the role of the carotenoid molecule in mediating B800 to B850 energy transfer and proposed that the presence of mixed Bchl*a* and Car excited states could partly account for the discrepancies between experimental data and Förster theory (Krueger *et al.* 1999). Unfortunately, in every case the calculated values are too slow and this is because it is actually inappropriate to use the Förster theory for this transfer. Perhaps the best experimental proof of the inadequacies of Förster theory comes from experiments in which the B800 Bchl*a* molecules in LH2 from *Rps. acidophila* have been replaced with a range of different Bchl*a* derivatives as well as chlorophyll *a* (Herek *et al.* 2000). This exchange procedure was developed by Scheer (Bandilla *et al.* 1998) and involves the use of an unusual oligosaccharidic detergent called Triton–BG10 (Union Carbide). When the LH2 complexes are dissolved in this detergent a mild acid treatment of pH 4·5 removes the B800–Bchl*a* molecules. Other pigments can then be selectively reconstituted in the vacant B800 binding sites when the pH is raised to 8·0. In this way the absorption of the 'B800' pigments can be shifted gradually all the way down to 670 nm. A classical Förster treatment of this situation would predict a dramatic

**Table 5.** *$Q_y$ absorption maxima of the (bacterio)chlorins occupying the B800 site in native and reconstituted LH2 complexes in* Rps. acidophila *and the time constants for B800→B850 energy transfer at room temperature (redrawn from Herek et al. 2000)*

| B800 site | $\lambda_{max}^{abs}$ (nm) | $\tau$ (ps) |
|---|---|---|
| Native LH2 | | |
| BChl | 800 | 0·9 ± 0·1 |
| (B)Chl-B800 reconstituted complexes | | |
| BChl | 800 | 0·9 ± 0·1 |
| BChlgg | 800 | 0·8 ± 0·1 |
| 132-OH-BChl | 800 | 0·8 ± 0·1 |
| Zn-Bphe | 794 | 0·8 ± 0·1 |
| 3-vinyl-BChl | 765 | 1·4 ± 0·2 |
| $3_1$-OH-BChl | 753 | 1·8 ± 0·2 |
| 3-acetyl-Chl | 694 | 4·4 ± 0·5 |
| Chl | 670 | 8·3 ± 0·5 |

decrease in the energy-transfer rate due to a drastic reduction in the spectral overlap between the emission of the donor B800 molecules and the absorption of the acceptor B850 molecules. Table 5 shows the experimental result of measuring both the position of the $Q_y$ absorption reconstituted pigments and the rate of energy transfer to B850. Even with Chl*a* in the B800 binding site the rate only decreases $<$10-fold (to 8·3 ps). In an attempt to understand the origins of these energy-transfer rates second-order perturbation theory has been applied (Kimura & Kakitani, 2003).

#### 6.2.1.3 B850→B850

Once the electronic excitation reaches the B850 ring the resultant excited state is rapidly depolarized. When this depolarization is monitored in absorption the polarization ratio is already low, $\sim$0·1, by 80 fs following a laser flash (Kennis *et al.* 1997b). If the depolarization is followed in emission, using the fluorescence up-conversion method, then the main depolarization time is $\sim$50 fs (Jimenez *et al.* 1996). However, unlike in the case of B800→B800 energy transfer where the participating Bchl molecules can be mainly considered to be monomeric, this depolarization is the result of a completely different process. As described above in sections 5.3 and 5.4, the correct electronic description of B850 has to take account of the strong excitonic coupling between the individual B850 Bchl molecules. This means that when the B850 ring is excited a collective excited state is produced. In other words an excitonic wave packet is created. Initially the amplitude of this wave packet will be delocalized over many Bchls, then due to various types of disorder it will lose its coherence and become more localized. This process results in the measured depolarization. The resulting more localized excitonic state can then migrate around the ring on a very fast timescale.

Rapid energy migration around the B850 ring (i.e. fast compared to the decay of the excited singlet state) is functionally important in the photosynthetic membrane. The direct consequence of this is that energy is available for transfer out of the 'ring' with equal efficiency from each Bchl*a* molecule. This then means that 'ring' to 'ring' transfers, whether LH2→LH2 or LH2→LH1, will be efficient irrespective of the overall intramembrane architecture, so long as the different antenna 'rings' are arranged sufficiently close to each other. In other words there

are no *a priori* requirements for highly regular arrangements of the antenna complexes in order to maintain a highly efficient LH system, and therefore overall performance is expected to be rather tolerant with respect to the precise organization of the antenna complexes in the membrane. For a more comprehensive and in-depth review dealing with the factors that influence B800→B850 energy transfer the reader should consult the excellent review by Scholes & Fleming (2000).

#### 6.2.1.4 B850→*B875*

In native photosynthetic membranes, especially in the case of membranes from *Rb. sphaeroides* and *Rps. acidophila*, the rate of singlet–singlet energy transfer from LH2→LH1 has been time resolved and is rather temperature independent (Sundström *et al.* 1986; van Grondelle *et al.* 1987, 1994; Zhang *et al.* 1992b; Hess *et al.* 1995; Nagarajan & Parson, 1997). It takes between 2–5 ps for this energy transfer to occur (Hess *et al.* 1995).

This data, however, now needs to be critically re-evaluated. Several recent AFM investigations of the organization of antenna complexes in photosynthetic membranes have shown very clearly that there is a large degree of heterogeneity in their supramolecular arrangement (Scheuring *et al.* 2003, 2004b; Bahatyrova *et al.* 2004b; Fotiadis *et al.* 2004; Frese *et al.* 2004). This is evident for the LH2/LH1 organization both within any given membrane and, more especially, from species to species (see, e.g. Deinum *et al.* 1991; Trissl, 1996; Scheuring *et al.* 2004b). This means that there must be many different rates for the LH2→LH1 energy-transfer step depending upon which exact area of the membrane is being interrogated. The results obtained so far, therefore, represent a crude average of the real situation since no attempt has been made to take account of this heterogeneity. A resolution of this situation will require the development of methods to repeat these measurements on restricted small domains of single membranes where the precise architecture has also been determined. Interestingly, there has been one theoretical attempt to try to calculate how the overall efficiency of photosynthetic LH in this system depends upon detailed architecture (Hu *et al.* 2002). Two limiting cases were investigated, one where rows of dimeric RC–LH1 complexes were separated by areas of LH2 complexes and one where monomeric RC–LH1 complexes were each completely surrounded by LH2 complexes. The calculated difference in overall efficiency was only 6–8%, i.e. rather small. It will be important to see how closely these calculations compare with real experimental data, when it becomes available.

#### 6.2.1.5 B875→*RC*

Photosynthetic LH can be thought of as 'successful' when the absorbed energy is finally delivered to and 'trapped' by the RC. Here in the RC the electronic energy is used to drive the primary redox reaction. A detailed discussion on the structure, spectroscopy and function of RCs is outside the scope of this review but the reader may wish to consult the review by Hoff & Deisenhofer (1997). It takes 20–50 ps for the energy in the B875 'ring' of the LH1 complex to be transferred to the RC (Sundström *et al.* 1986; Visscher *et al.* 1989; Zhang *et al.* 1992a; Beekman *et al.* 1994; Freiberg *et al.* 1996). This final step is the slowest of all the energy-transfer steps discussed so far because it takes place over the longest distance, i.e. ∼40 Å.

This distance is important. It is essential that electron transfer from any LH1 Bchl*a* molecule to the oxidized Bchl*a*s of the RC never occurs. If one Bchl*a* cation is created in the LH1 ring, e.g. by chemical oxidation with potassium ferricyanide (Law & Cogdell, 1998), then the lifetime of the excited singlet state in the 'ring' is drastically quenched so that LH1 can no longer act as

a light-harvester. Electron transfer, however, has a very strong distance dependence so at a separation of ~40 Å electron transfer will not occur during the lifetime of the potentially dangerous oxidized Bchl*a*s in the RC (Moser *et al.* 2003). This separation between the RC and LH1 Bchl*a*s therefore acts rather like a 'cordon sanitaire' ensuring that this harmful electron-transfer reaction never takes place. An energy-transfer rate of 20–50 ps still beats the 1–2 ns singlet excited state lifetime of LH1 by more than enough to ensure very efficient LH. The separation between the RC and the LH1 Bchl*a*s, therefore, does not compromise the overall efficiency of LH. Although beyond the remit of this present review it is never the less interesting to note that similar antenna chlorophyll no-fly-zones are present in the RCs of photosystems I and II (see Fromme *et al.* 2006 for a comparison of their structures). Thus, this particular design constraint appears to be universal for photosynthetic systems irrespective of their overall architecture.

### 6.2.2 Car↔Bchl*a* energy transfer

Car engage in energy transfer with the Bchl*a*s in the antenna complexes in both directions (Cogdell & Frank, 1987; Frank & Cogdell, 1996). At the level of singlet-singlet energy transfer they donate energy to the Bchl*a*s and thereby act as accessory LH pigments. This, therefore, allows photosynthesis to harvest light over a wider spectral range while at the level of triplet–triplet energy transfer they accept energy from the Bchls. This triplet–triplet exchange reaction is the essential function of the Car in bacterial photosynthesis. In the absence of Car over-excitation of Bchls will result in the production of Bchl triplets. These triplets can last for 10's of μs, which is long enough to allow a biomolecular collision reaction with oxygen to occur that leads to the production of singlet oxygen. Singlet oxygen is a very powerful and dangerous oxidizing agent and is lethal to cells in which it is produced (Foote, 1976). The triplet–triplet exchange reaction between the Bchl*a* triplet and the Car, in both LH2 and LH1, stops this harmful reaction from taking place. In the antenna complexes Car triplets are produced from the Bchl*a* triplets in a few ns (Monger *et al.* 1976; Bittl *et al.* 2001). This reaction then out-competes the potential bimolecular collision reaction with oxygen by ~3 orders of magnitude and so very effectively detoxifies these Bchl*a* triplets. There are two essential prerequisites for a Car to be successful in this protective reaction. First, the energy level of it first excited triplet state must be below that of the first excited triplet state Bchl*a*. Second, the energy level of this triplet state must also be below that of singlet oxygen, so that it in turn cannot sensitize the production of singlet oxygen itself. Both these criteria are fulfilled for Car with more than eight conjugated double bonds (Foote & Denny, 1968; Foote *et al.* 1970; Foote, 1976; Krinsky, 1978).

The triplet–triplet energy-transfer reaction takes place via an electron exchange mechanism (Dexter, 1953). This mechanism requires that the molecules involved come into van der Waals contact with each other, a structural requirement that is clearly satisfied in LH2 (see Fig. 11).

At first glance Car are unlikely molecules to have been selected by evolution as accessory LH pigments. Their excited singlet states, which are involved in the LH process, have very short lifetimes, on the order of ~100 fs and a few ps respectively. Consequently this means that there is very little time for productive energy transfer to occur and for it to be able to out-compete the rapid decay channels that naturally deplete the Car excited singlet states. Productive energy transfer is only possible from the Car because they are packaged so closely to the Bchls in the antenna complexes.

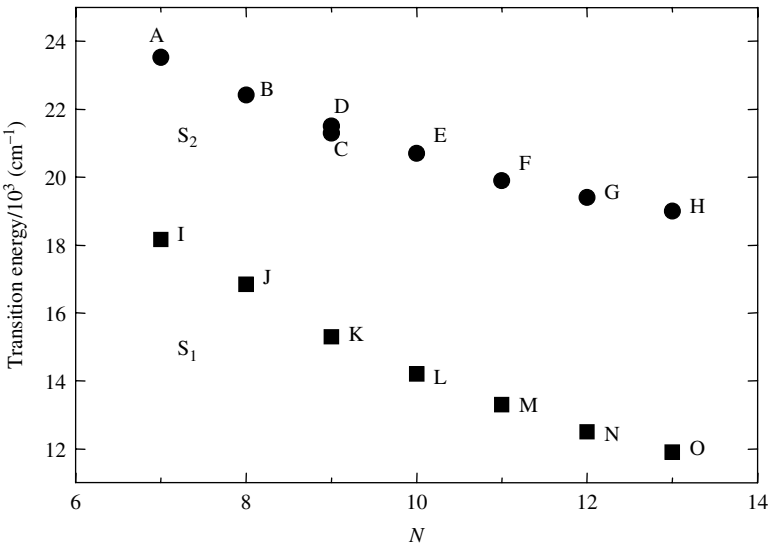


**Fig. 32.** The energy gap between carotenoid $S_1$ and $S_2$ states as a function of conjugation length. Data-points A (heptaene), B (octaene), D (nonaene), I (heptaene) and J (octatene) were measured by Frank *et al.* (2002). Data-point E (spheroidene) was measured by Polivka *et al.* (2002). Data-points C (neurosporene), K (neurosporene) and L (spheroidene) were measured by Fujii *et al.* (1998). The data-points F (lycopene), M (lycopene), N (anhydrorhodovibrin) and O (spirilloxanthin) were measured by Fujii *et al.* (2001). All the measurements were made in *n*-hexane at 293 K, 295 K or RT.

Carotenoid photochemistry is very complicated and has been recently exhaustively reviewed elsewhere (Hu *et al.* 2002; Hashimoto *et al.* 2004; Polivka & Sundström, 2004). We will therefore only provide a simplified overview here and just point out some of the more detailed issues that remain to be clarified. Car with more than six conjugated double bonds are strong absorbers of visible radiation. Unusually, however, these absorptions reflect the transition from the ground state to their second excited singlet state because it is the lowest one photon allowed excited singlet state. This $S_2$ state has $B_u$ symmetry ($^1Bu^+$). Their lowest excited singlet state, called $S_1$, has $A_g$ symmetry ($^2A_g^-$) and can only be populated by either a two-photon event or by internal conversion from $S_2$. The theoretical basis for understanding Car photochemistry has been provided by detailed calculations on polyenes carried out by Tavan & Schulten (1986). They showed in their work that the exact energy levels of the $S_2$ and $S_1$ states, and the energy gap between them, depends upon the number of conjugated double bonds and has since been confirmed by experimentation (Fig. 32). Tavan and Schulten explained why, for reasons of conservation of angular momentum, transitions only occur between states of different parity (i.e. g or u; Ag→Bu or Bu→Ag). A transition between Ag→Bg would also be forbidden despite the fact that the states have different symmetry. The ground state of Car has Ag symmetry and therefore the lowest energy one-photon-induced transition goes to $S_2$ not $S_1$.

A study of the LH role of Car that clearly illustrated the basic reactions involved was carried out by McPherson *et al.* (2001). This work compared the decay kinetics of the $S_2$ and $S_1$ states of the Car, rhodopsin–glucoside (11-conjugted double bonds) in both organic solvents and in the LH2 complex from *Rps. acidophila*. Using fluorescence up-conversion to monitor the decay kinetics of the $S_2$ state it was shown that the lifetime of $S_2$ was reduced from $124 \pm 8$ fs in

benzylalchohol to $57 \pm 2$ fs in the LH2 complex. This shortening of the $S_2$ lifetime is a consequence of the opening of an additional decay channel for the $S_2$ decay due to the singlet–singlet energy transfer from rhodopin-glucoside to Bchl in LH2. Comparison of these lifetimes then gives an energy-transfer efficiency of 51%. In contrast the lifetime of the $S_1$ state of rhodopin-glucoside, monitored by recording the $S_1$–$S_n$ absorption band at 580 nm, showed only a very small change in going from organic solvent to the LH2 complex ($4{\cdot}1 \pm 0{\cdot}1$ ps in benzyl alcohol to $3{\cdot}7 \pm 0{\cdot}1$ ps in LH2). In this case $S_1$ was not being very efficiently utilized for energy transfer to the Bchls (only 5%). The overall energy-transfer efficiency calculated from these kinetic measurements agreed very well with that determined from the fluorescence excitation spectrum of LH2 (i.e. 56%). In the LH2 from *Rb. sphaeroides*, which has Car with either 9- or 10-conjugated double bonds, however, the efficiency of the singlet-singlet energy transfer from the Car to the Bchl*a* is much higher. Depending upon which Car is present it can be very nearly 100% (Cogdell *et al.* 1981). The extra efficiency is achieved because now the $S_1$ state can also be utilized (Koyama *et al.* 1996). This can be clearly seen as a strong reduction in the Car's $S_1$ lifetime in the LH2 complex compared to it in organic solvent [e.g. for neurosporene ($n = 9$) the $S_1$ lifetime in organic solvents such as acetone is $\sim$21 ps while in LH2 this is reduced to $\sim$2 ps (Zhang *et al.* 2000)]. The reason for the drop-off of efficiency at 11-conjugated double bonds for harvesting the $S_1$ state is not yet clear. Both the B800 and the B850 Bchl*a* in LH2 accept energy from the Car (MacPherson *et al.* 2001).

So far we have presented a consistent basic picture of how Car participate in LH. Potentially the energy transfer can take place from $S_2$ or $S_2$ and $S_1$. If it only takes place from $S_2$ then the overall efficiency is limited to 50–60%. If the energy from $S_1$ can also be harvested then efficiencies up to nearly 100% are possible. The 'real' situation, however, appears to be much more complex. In their original theoretical description of polyene excited singlet states Tavan & Schulten (1986) predicted the presence of additional low-lying excited singlet states located between the $S_2$ and $S_1$ states. Experiments carried out with both RR spectroscopy and flash photolysis with sub-10 fs excitation pulses have been interpreted as providing evidence for the involvement of these extra excited singlet states (Cerullo *et al.* 2002; Fujii *et al.* 2004; Koyama *et al.* 2004; Nakamura *et al.* 2004; Nishimura *et al.* 2004; Polli *et al.* 2004; Rondonuwu *et al.* 2004) (see Fig. 33). However, some of this evidence is contradictory and how, or indeed whether, these possible 'new' states participate in LH is not yet clear (Christensen, 1999; Kukura *et al.* 2004; Polivka & Sundström, 2004) (see Polivka & Sundström, 2004 for a detailed discussion of this).

Until recently it was dogma that Car could not be directly excited to their triplet state following one photon excitation (Cogdell & Frank, 1987; Frank & Cogdell, 1993). However in the LH1 complex for *Rsp. rubrum* direct excitation of its carotenoid, spirilloxanthin, does produce a triplet on the ps timescale. This phenomenon has been investigated using laser flash photolysis. Another, as yet undesignated excited state, called S* has been identified (Gardinaru *et al.* 2001). S* is formed directly from $S_2$ (Fig. 33), in competition with $S_1$, and is then the direct precursor of the triplet states (Cars have a very subtle photochemistry) and can also contribute to energy flow to the Bchls in the LH complexes (Papagiannakis *et al.* 2002, 2003; Wohlleben *et al.* 2003). The polyenes studied by Tavan & Schulten (1986) in their theoretical investigation are highly symmetric. In Cars the addition of methyl groups already distorts their symmetry. This is then compounded in LH2 where the tightly bound Car is further perturbed by interaction with the protein and the Bchls so that it is twisted into half a helix, when viewed down the long axis of the molecule (see Fig. 11). It is not clear how these deviations from the perfect polyene symmetry

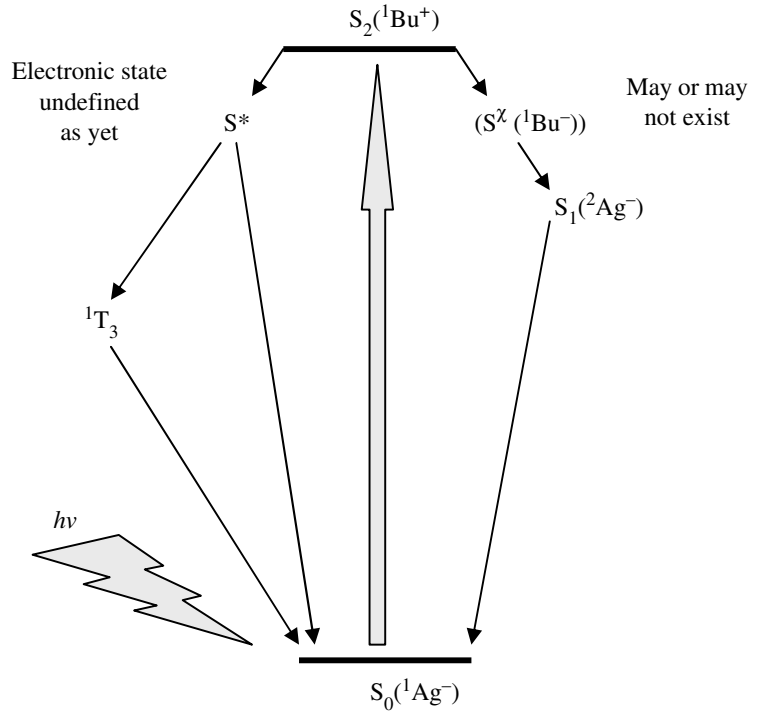


**Fig. 33.** A current model of the different excited states of a carotenoid, which can be formed following a one photon excitation of the ground state ($S_0$).

might 'allow' additional photochemical reactions to occur that would be 'forbidden' for the planar polyenes. There is a real need for the work of Tavan & Schulten (1986) to be extended to Cars and for the photochemical consequences of progressive losses of symmetry, such as those seen in the purple bacterial antenna complexes, to be explored.

Car to Bchl*a* singlet–singlet energy transfer cannot be described in terms of the Förster theory. The molecules involved are clearly too close to each other and interact strongly. There have been several attempts to calculate the rate of these energy transfers and these have been well discussed by Xu *et al.* (2002). It is sufficient to say here that major elements required to give a strong enough interaction between the Car and the Bchl to approach the experimentally determined rates involves Columbic coupling (Hu *et al.* 2002) as initially proposed by Nagae *et al.* (1993).

## 7. Single-molecule spectroscopy

### 7.1 Introduction to single-molecule spectroscopy

The introduction of single-molecule spectroscopy (Moerner & Kador, 1989; Orrit & Bernard, 1990) has allowed a qualitatively new approach to gain insights into the electronic structure of heterogeneous samples. The intriguing feature of this technique is that it provides information free from averaging over spatial inhomogeneities and it became immediately obvious that single-molecule spectroscopy can reveal spectroscopic details that are normally obscured by the

ensembled average in bulk experiments (Moerner & Basch, 1993; Orrit *et al.* 1993; Basche *et al.* 1997; Plakhotnik *et al.* 1997; Xie & Trautman, 1998; Rigler *et al.* 2001; Zander *et al.* 2002; Böhmer & Enderlein, 2003; Kulzer & Orrit, 2004). Besides the possibility to determine the whole distribution of parameters rather than only their average values, as is common for conventional spectroscopic techniques, it also allows the observation of dynamic processes usually obscured in an ensemble. A single molecule that undergoes a temporal development between different states is at any time in a distinct and well-defined state, so that in principle the whole sequence of steps can be studied. This allows in particular the identification of short-lived intermediate states that might be essential for understanding the process under study. In order to obtain this data from similar experiments on an ensemble of molecules would require a temporal synchronization of all the molecules. This is often very difficult if not impossible to accomplish.

The application of single-molecule detection techniques to biology and biochemistry has led to a revolution in this field. Fascinating experiments have become possible and conformational changes of complex biomolecular structures can now be followed, such as the observation of single enzymatic turnovers (Lu *et al.* 1998), following the Brownian motion of individual lipid molecules in biomembranes (Schmidt *et al.* 1996), recording the movement of an individual myosin head along an actin filament upon hydrolysis of a single ATP molecule (Kitamura *et al.* 1999), or monitoring molecular rotations of the F1-ATPase (Kinosita, 1999).

However, under ambient conditions photobleaching of the probe molecules usually limits the observation time to some tens of seconds. This can be avoided by working at cryogenic temperatures where photobleaching plays a negligible role. This then offers the opportunity to determine the electronic eigenstates of an individual system, i.e. to perform single-molecule *spectroscopy* rather than single-molecule *detection*. We will now present below an overview of the results of a series of single-molecule experiments on individual LH2 complexes and highlight the extra insights that these have revealed.

## 7.2 Single-molecule spectroscopy on LH2

### 7.2.1 Overview

Generally, information about the parameters that determine the description of the electronic structure of LH complexes can be obtained by optical spectroscopy. The great difficulty encountered when determining the various parameters that play a role in the description of the electronic structure of LH complexes and the process of energy transfer, is the fact that the optical absorption lines are inhomogeneously broadened as a result of heterogeneity in the ensemble of absorbing pigments. To avoid the difficulties arising from the heterogeneity of these types of systems single-molecule spectroscopic techniques have been applied to study LH2 (Bopp *et al.* 1997, 1999; van Oijen *et al.* 1998, 1999b; Tietz *et al.* 1999; Wrachtrup *et al.* 2002; Hofmann *et al.* 2003a; Rutkauskas *et al.* 2005). The fluorescence-excitation spectra of several individual LH2 complexes are shown in Fig. 34. The upper trace shows, for comparison, the fluorescence-excitation spectrum taken from a bulk sample (dashed line) together with the spectrum that results from the summation of the spectra of 19 individual LH2 complexes (solid line). The two spectra are in excellent agreement and both feature two broad structure-less bands around 800 nm and 860 nm corresponding to the absorption of the B800 and B850 pigments of the complex. By measuring the fluorescence-excitation spectra of the individual complexes,

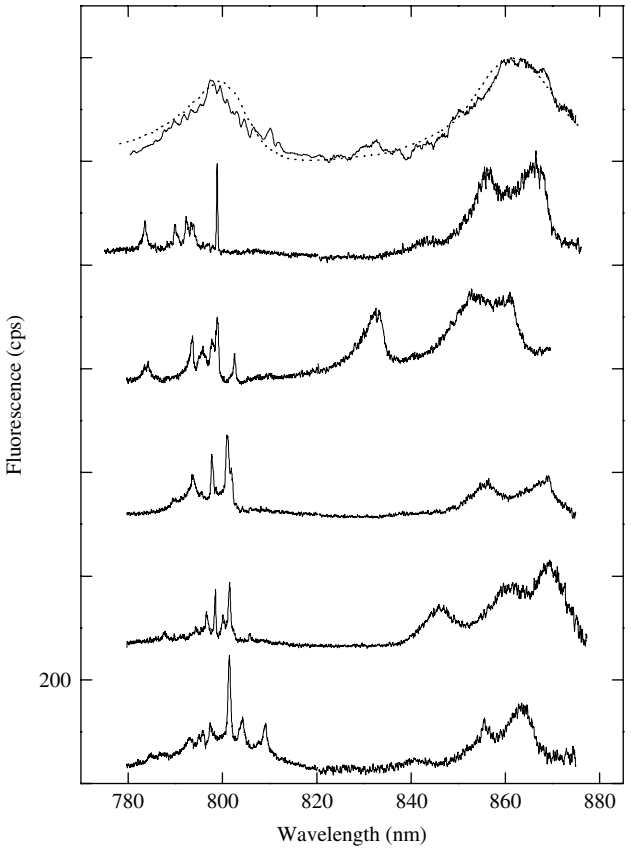


**Fig. 34.** Fluorescence-excitation spectra of LH2 complexes of *Rps. acidophila*. The top traces show the comparison between an ensemble spectrum (dashed line) and the sum of spectra recorded from nineteen individual complexes (solid line). For each complex this included six individual spectra that were obtained at different excitation polarizations. The lower five traces display spectra from single LH2 complexes. All spectra were measured at 1·2 K at 20 W/cm$^2$ with LH2 dissolved in a PVA buffer solution. (Redrawn from Ketelaars *et al.* 2001.)

remarkable features become visible which are obscured in the ensemble average. In particular, a striking difference between the B800 and B850 bands becomes evident: the spectra around 800 nm show a distribution of narrow absorption bands, whereas in the B850 spectral region 2–3 broad bands are present. To understand the striking differences between the two absorption bands it is useful to consider the intermolecular interaction strength $V$ between neighbouring Bchl*a* molecules in a ring and their spread in transition energies $\Delta E_n$.

### 7.2.2 B800

#### 7.2.2.1 General

Unambiguous experimental evidence that the excitonic coupling $V/\Delta E$ (see Section 5.1 above) is significantly smaller among the B800 Bchl*a* molecules as compared to the B850 Bchl*a* molecules comes from experiments that have been performed on individual pigment–protein complexes (van Oijen *et al.* 1998, 2000). Recording the fluorescence-excitation spectrum in the region of the B800 band produces a pattern of spectral bands that can be assigned to absorptions

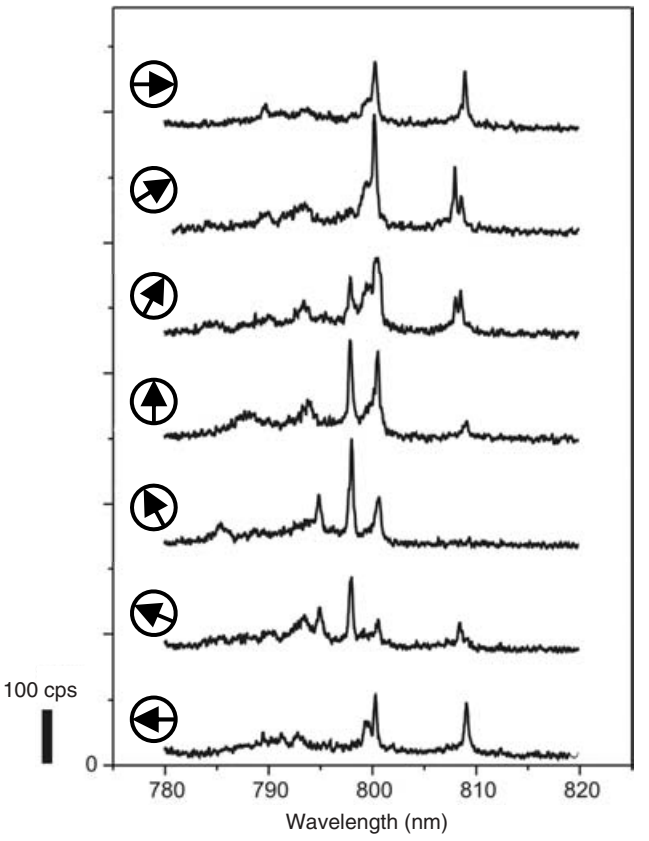


**Fig. 35.** The dependence of the B800 fluorescence-excitation spectrum of a single LH2 complex from *Rps. acidophila* on the polarization of the incident radiation. The polarization vector has been changed in steps of 30° from one spectrum to the next. The vertical scale is valid for the lowest trace, all others are displaced for clarity. (Redrawn from van Oijen *et al.* 1999a.)

from individual B800 Bchl*a* molecules, which are separated in their spectral positions due to differences in each of their local protein environments (inhomogeneous broadening). It has been found that the intensities of these absorption lines vary dramatically upon changing the polarization of the excitation light (Fig. 35) (van Oijen *et al.* 1999a). This would be expected if the excitations are largely localized on the individual Bchl*a* pigments, because their transition–dipole moments are arranged in a circular manner in the LH2 structure (see Fig. 31) and, as a result of this, they all have different orientations with respect to the polarization vector of the exciting light.

#### 7.2.2.2 Intra- and Intercomplex disorder of site energies

Comparing the fluorescence-excitation spectra in the B800 region from individual LH2 complexes reveals significant variations in the spectral distribution of the individual resonances between different LH2 complexes, as well as for the spectral mean of each line pattern (defined below) (see Fig. 36). The spread of the individual absorption bands directly reflects the distribution in site energies of the individual B800 Bchl*a* molecules (diagonal disorder). Single-molecule spectroscopy, therefore, offers a unique opportunity to obtain statistical information

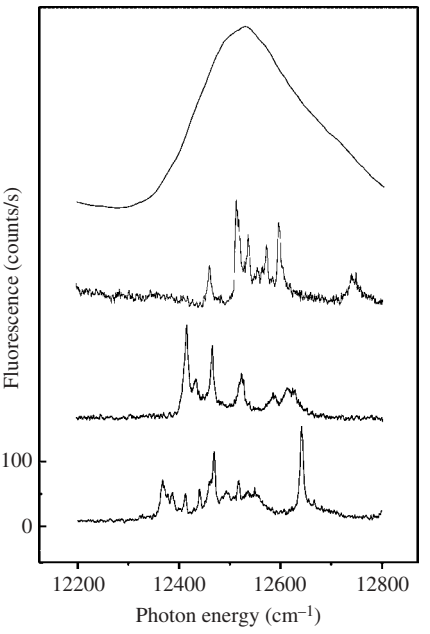


**Fig. 36.** Fluorescence-excitation spectra of the B800 band from *Rps. acidophila* for an ensemble of LH2 complexes (upper trace) and for three individual LH2 complexes (lower trace) illustrating the intra- and intercomplex spectral heterogeneity that contributes to the ensemble spectrum. (Adapted from van Oijen *et al.* 2000.)

about the distribution of the B800 transition energies within an individual complex (intra-complex disorder) as well as, by comparison between several complexes the variation of the transitions energies between different complexes (intercomplex disorder) (van Oijen *et al.* 2000). In order to find a suitable way to measure the *inter*complex heterogeneity we have introduced a term that we have called the spectral mean value, $\bar{\nu}$, of the fluorescence-excitation spectrum of a single LH2 complex by

$$\overline{\nu} = \frac{\sum_i I(i) \cdot \nu(i)}{\sum_i I(i)}, \tag{13}$$

where $I(i)$ denotes the fluorescence intensity at data-point $i$, $\nu(i)$ the spectral position corresponding to data-point $i$, and the sum integrates over all data-points of the spectrum. A histogram of $\bar{\nu}$, obtained from the fluorescence-excitation spectra of 46 complexes, is shown in Fig. 37*a* and has a width of about $\sim$120 cm$^{-1}$. The *intra*complex heterogeneity, or diagonal disorder, can be extracted from this data by calculating the standard deviations $\sigma_\nu$ of the intensity distributions in the individual spectra

$$\sigma_\nu = [\overline{\nu^2} - \bar{\nu}^2]^{\frac{1}{2}}, \tag{14}$$

where $\overline{\nu^2}$ is given by

$$\overline{\nu^2} = \frac{\sum_i I(i) \cdot [\nu(i)]^2}{\sum_i I(i)}. \tag{15}$$

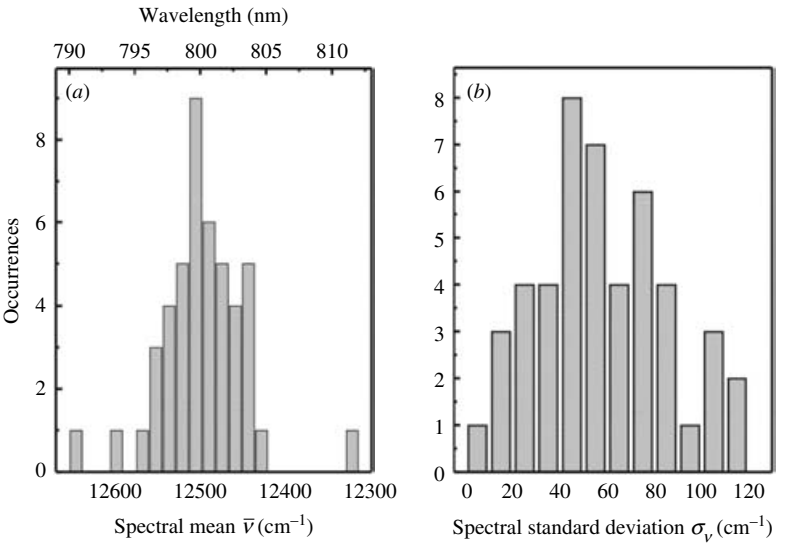


**Fig. 37.** (*a*) Distribution of the spectral mean of the B800 fluorescence-excitation spectrum for 46 LH2 complexes featuring the amount of intercomplex heterogeneity. (*b*) Distribution of the standard deviations for the spread of absorption lines in the individual fluorescence-excitation spectra for the same 46 LH2 complexes. (From van Oijen *et al.* 2000.)

The result of this is shown in Fig. 37*b*. The distribution for $\sigma_\nu$ is centred at a value of $\sim$55 cm$^{-1}$. The full width at half maximum (FWHM) of the distribution of site energies is obtained by multiplying this value by a factor of 2·36. This yields for the FWHM of the diagonal disorder a value of 130 cm$^{-1}$. Clearly, an ensemble spectrum (i.e. the conventional absorption spectrum) reflects the convolution of both contributions to the overall heterogeneity. From this data we calculate that the B800 band has a total inhomogeneous linewidth of $\sim$180 cm$^{-1}$, which is in good agreement with results from the bulk spectra of LH2 of *Rps. acidophila* taken at 1·2 K (van Oijen *et al.* 2000). It is worth pointing out here that only the intracomplex type of disorder is of relevance for the delocalization of the excitation energy.

#### 7.2.2.3 Electron-phonon coupling

Typically, the spectrum of the first electronically excited state of an organic molecule embedded in a matrix gives rise to a homogeneously broadened zero-phonon line (ZPL) accompanied by a relatively broad phonon-side band (PSB) (Rebane, 1970). The ZPL results from the pure electronic transition, whereas the PSB corresponds to an electronic transition in combination with the simultaneous excitation of a vibration of the host. In order to distinguish the intramolecular vibrations of the molecules from those of the host, in which they are embedded, the latter are commonly referred to as phonons, an expression that has been adapted from solid-state physics. The distribution of the intensity between the ZPL and the PSB, i.e. the profile of the electronic spectrum, is determined by the electron-phonon coupling strength, and provides information about the strength of the interaction of the probe molecule with its local surrounding, here between a B800 Bchl*a* molecule and its protein environment.

The experimental problem that arises when attempting to measure such a profile of the electronic spectrum of an individual B800 absorption is that the spectra are subjected to

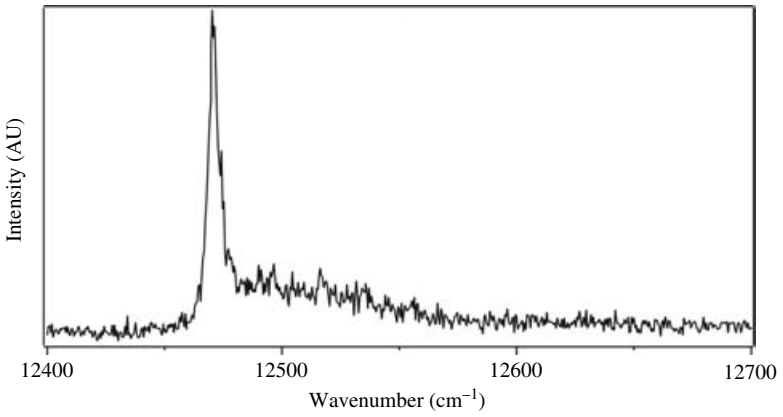


**Fig. 38.** Recurrent motif in the B800 spectra from individual LH2 complexes of *Rsp. molischianum* after a multivariate statistical analysis of the data. (From Hofmann *et al.* 2005.)

temporal fluctuations (spectral diffusion) due to structural fluctuations in the local environment of the probe molecule. This results in temporal averaging of the signal and the subtle details of the PSB are, therefore, washed out. In order to extract the information about the electron-phonon coupling from the B800 fluorescence-excitation spectra Hofmann *et al.* (2005) recorded thousands of B800 spectra from the same LH2 complex in rapid succession and employed a multivariate statistical analysis (MSA) pattern recognition approach. Such algorithms have been used for the comparison of amino-acid sequences of proteins from different species or for the reconstruction of the 3D structure of large biological macromolecules from two-dimensional projections obtained by single particle cryo-EM. For more details about the algorithm the reader is referred to van Heel *et al.* (2000). The statistical analysis of such a stack of B800 spectra from an individual LH2 complex from *Rsp. molischianum* uncovered a narrow peak accompanied by a weak broad shoulder on its high-energy side. This picture was revealed as a recurrent motif for the individual B800 absorptions. An example is shown in Fig. 38. The sharp feature has been assigned to the ZPL of the pure electronic transition of an individual Bchl*a* molecule and the broad feature to the associated PSB. The electron-phonon coupling is usually described by the Huang–Rhys factor, $S$, defined as $e^{-s} = I_{ZPL}/(I_{ZPL} + I_{PSB})$, where $I_{ZPL}(I_{PSB})$ refers to the integrated intensity of the ZPL (PSB) respectively (Orrit *et al.* 1993). For the B800 molecules in *Rsp. molischianum* Hofmann *et al.* found a value of 0·44 for the Huang–Rhys factor which reflects a weak electron-phonon coupling.

#### 7.2.2.4 B800→B800 energy transfer revisited

In the weak coupling limit, where $V/\Delta E < 1$ excitations may be assumed to be completely localized on individual pigments and energy transfer between B800 pigments is commonly described by Förster theory (Joo *et al.* 1996; Kennis *et al.* 1997b). In this description the corresponding energy-transfer rate is determined by the overlap of the fluorescence spectrum of the donor and the absorption spectrum of the acceptor. However, since extremely narrow zero-phonon lines are distributed throughout the complete B800 absorption it is clear that the spectral overlap of neighbouring B800 pigments is in fact very small, and in most cases negligible. The first doubts about whether the Förster mechanism is really suitable to describe the energy transfer among the B800 Bchl*a* were raised in 1996 from comparisons of model calculations

with data from spectral hole burning and time-resolved experiments. Kolaczkowski *et al.* (1994) derived an analytical expression for the energy-transfer rate between pigments in the case of strong inhomogeneous broadening, as a function of the electron-phonon coupling strength, and the energy difference in site energies. Using this expression, Wu *et al.* (1996) showed that the Förster-overlap integral may indeed become very small when the electron-phonon coupling is weak.

The currently available single molecule data now allows us to examine these predictions in great detail. From an analysis of the B800 spectra from 46 individual LH2 complexes from *Rps. acidophila* we have estimated that the average difference in site energy between neighbouring B800 Bchl*a* molecules is of the order of 30–60 $cm^{-1}$ (van Oijen *et al.* 2000). According to the formalism developed by Wu *et al.* under these conditions Förster-type energy transfer would occur with a transfer time of 10–30 ps. These numbers are in stark disagreement with conclusions from both hole-burning (de Caro *et al.* 1994) and direct time-resolved measurements (Kennis *et al.* 1997a), which show that energy transfer among the individual B800 pigments is in fact much faster (as described in Section 6.2.1.2 above). The time-resolved depolarization measurements which have been used to measure the B800–B800 hopping rate are fully consistent with the hole-burning measurements and in good agreement with the typical homogeneous linewidths in the single-molecule spectra of the B800 band. In summary, we conclude that a Förster-type approach is not an appropriate way to describe the energy transfer that takes place within the B800 band in LH2.

Moreover, the spectral information obtained with the single LH2 complexes allows a more general consideration of the validity of the assumption that $V/\Delta E \ll 1$ for the B800 Bchl*a* molecules. In the point-dipole approximation $V$ can be calculated by

$$V = \frac{1}{4\pi\varepsilon_0}\left(\frac{\vec{\mu}_1 \cdot \vec{\mu}_2}{r^3} - 3\frac{(\vec{\mu}_1 \cdot \vec{r})(\vec{\mu}_2 \cdot \vec{r})}{r^5}\right), \tag{16}$$

where $\vec{\mu}_i$ is the transition dipole moment of molecule $i$ and $\vec{r}$ is the intermolecular distance vector. Using $|\vec{\mu}| = 2{\cdot}046 \times 10^{-29}$ Cm (corresponding to 6·13 Debye and a transition strength of $|\vec{\mu}^2| = 37{\cdot}6$ Debye$^2$) (Sauer *et al.* 1966) $|\vec{r}| = 2{\cdot}13$ nm, and the known geometry for the arrangement of the B800 molecules, one finds an interaction strength of $-24$ $cm^{-1}$. As pointed out above, from the single complex spectra, the average difference in site energy between adjacent B800 molecules was estimated to be in the order of 30–60 $cm^{-1}$. This yields $V/\Delta E \approx 0{\cdot}2$–1 for the B800 pigments which suggests that some B800 Bchl*a* molecules have a small excitonic coupling with their neighbours which leads to a slight delocalization of the excited state over 2–3 pigments. We have tested and verified this point of view by examining the polarization-dependent measurements shown in Fig. 35 in more detail. When combining all the polarization-dependent spectra of a single LH2 complex, nine absorption lines should be observed, corresponding to completely localized excitations on each of the nine individual Bchl*a* molecules present in LH2. However, typically in these combined spectra only 6–7 absorption lines were found, thereby supporting the idea that the excited state is slightly delocalized over 2 or 3 neighbouring Bchl*a* molecules in the B800 manifold, with a concomitant redistribution of oscillator strength. This effect arises from occasional (near)-degeneracy of the site energies of adjacent B800 pigments.

This interpretation has been further substantiated in a detailed study of the B800 band of LH2 from *Rsp. molischianum* (Hofmann *et al.* 2003b). The general idea of this approach was as

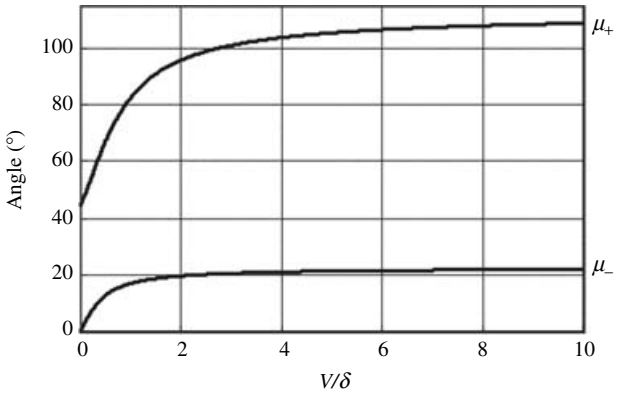


**Fig. 39.** The dependence of the orientation of the transition–dipole moments $\vec{\mu}_+$ (upper curve) and $\vec{\mu}_-$ (lower curve) on the ratio $V/\delta$. The orientations of the initial transition moments $\vec{\mu}_1$ and $\vec{\mu}_2$ were set to 0° and 45° and provide the reference frame. (From Hofmann *et al.* 2003b.)

follows. The geometrical structure of the B800 ring in the LH2 complex of *Rsp. molischianum* yields an interchromophore distance of 22 Å. If the electronic excitation of the B800 ring would be strictly localized on a single Bchl*a* chromophore the mutual angles between the transition–dipole moments of the individual Bchl*a* chromophores would then be equal to multiples of 45° (i.e. 360°/8). However, coupling between two adjacent molecules will lead to eigenstates that are different from those of the uncoupled chromophores and consequently to a change in the orientation of the transition–dipole moments. For the sake of brevity the following discussion will be restricted to two adjacent Bchl*a* molecules with excitation energies $E_1$ and $E_2$ ($E_1 > E_2$). For the resulting energies and eigenstates of the coupled system one finds

$$E_\pm = \tfrac{1}{2}(E_1 + E_2) \pm \tfrac{1}{2}\sqrt{\delta^2 + 4V^2}, \tag{17}$$

$$\left.\begin{aligned} |\Psi_+\rangle &= \cos\frac{\Theta}{2}|1\rangle + \sin\frac{\Theta}{2}|2\rangle, \\ |\Psi_-\rangle &= -\sin\frac{\Theta}{2}|1\rangle + \cos\frac{\Theta}{2}|2\rangle, \end{aligned}\right\} \tag{18}$$

where $\tan\Theta = 2V/\delta$, $\delta = E_1 - E_2$, and $|i\rangle$ denotes the excited state localized on molecule $i$. The transition–dipole moments of the eigenstates are then

$$\left.\begin{aligned} \vec{\mu}_+ &= \vec{\mu}_1\cos\frac{\Theta}{2} + \vec{\mu}_2\sin\frac{\Theta}{2}, \\ \vec{\mu}_- &= -\vec{\mu}_1\sin\frac{\Theta}{2} + \vec{\mu}_2\cos\frac{\Theta}{2}, \end{aligned}\right\} \tag{19}$$

where $|\vec{\mu}_i|$ denotes the transition–dipole moment of an individual Bchl*a* molecule in the B800 ring. From Eq. (19) the orientations of the transition–dipole moments of the B800 Bchl*a* molecules have been calculated as a function of $V/\delta$, see Fig. 39. The orientations of the initial transition moments, $\vec{\mu}_1$ and $\vec{\mu}_2$, corresponding to $V/\delta = 0$, were set to 0° and 45°.

As $V/\delta$ increases the orientations of the transition moments $\vec{\mu}_+$ and $\vec{\mu}_-$ change gradually with respect to their initial orientations and level off at angles of 22·5° and 112·5° (corresponding to $180^\circ - 112{\cdot}5^\circ = 67{\cdot}5^\circ$) for values of $V/\delta$ larger than $\sim 6$. In order to determine the orientations of the transition–dipole moments experimentally the excitation laser was swept throught the B800 spectral region and a sequence of spectra were recorded in rapid succession. The polarization of the incident radiation was rotated by 1·8° between each successive scan. Fig. 40*a* shows a part of the B800 fluorescence-excitation spectral data taken from an individual LH2 complex from *Rsp. molischianum*. The horizontal axis gives the wavenumber, the vertical axis the angle of the polarization of the incident light, and the intensity is colour coded. In Fig. 40*b* the fluorescence-excitation spectrum is presented that results from the summation of all the traces in Fig. 40*a*. In Fig. 40*c* the fluorescence intensity is displayed as a function of the polarization of the incident radiation for the two absorption lines indicated by the boxed regions in Fig. 40*a*. The observed variation in intensity has been fitted by a $\cos^2$ dependence (full and dashed line respectively). From the difference of the phases in the two traces the mutual angle between the transition–dipole moments related to these two absorption lines has been determined to be 91°. This procedure has been applied to 88 absorption lines from 24 individual LH2 complexes in order to find the statistical distribution of the mutual orientations of the transition–dipole moments within each complex. The histogram in Fig. 40*d* shows the result of this. The distribution covers nearly the whole range between 0° and 90° with slight preferences for the values around 0°, 20°, 45°, and 70°.

As a result of these experiments it was concluded that the observation of mutual orientations of transition–dipole moments different from 0°, 45° and 90°, provides direct evidence for an electronic coupling between the individual Bchl*a* molecules in the B800 assembly in the weak to intermediate range. Moreover, the actual strength of the electronic coupling between adjacent molecules is distributed over a range of values as a result of the difference in site energies of adjacent molecules.

In the above description of the dynamic properties of the excited states of the B800 ring we have ignored energy transfer to the B850 ring, a process that of course competes with relaxation within the excited state manifold of B800. The energy gap between B800 and B850 is $\sim 750\ \mathrm{cm}^{-1}$, i.e. much larger than typical phonon frequencies. It is, however, conceivable that energy transfer to B850 occurs *via* higher exciton states of the B850 pigment assembly that are near resonant with the B800 states (Ma *et al.* 1997; Koolhaas *et al.* 1998).

In a paper that appeared very recently it has been shown theoretically that a slight delocalization of the excitation energy in the B800 ring leads to an improvement of the robustness of the B800→B850 energy transfer (Cheng & Silbey, 2006). These conclusions are consistent with the experimental findings described above.

### 7.2.3 B850

In the case of the B850 band we have to consider the strong excitonic coupling between the Bchl*a* molecules in order to understand its optical spectra. As pointed out above the exciton states are characterized by the quantum number, $k^j$ ($j$=s, as) which can take the values 0, ±1, ±2, …, ±4. The lower part of this exciton manifold, i.e. the states $k^{\mathrm{as}} = 0, \pm 1, \pm 2$, is shown in the inset of Fig. 41. Due to the circular symmetry only the states $k^{\mathrm{as}} = \pm 1$ carry an appreciable oscillator strength which means that they dominate the optical spectra. Also as a result of this circular symmetry the transition moments of these two states are mutually orthogonal, as

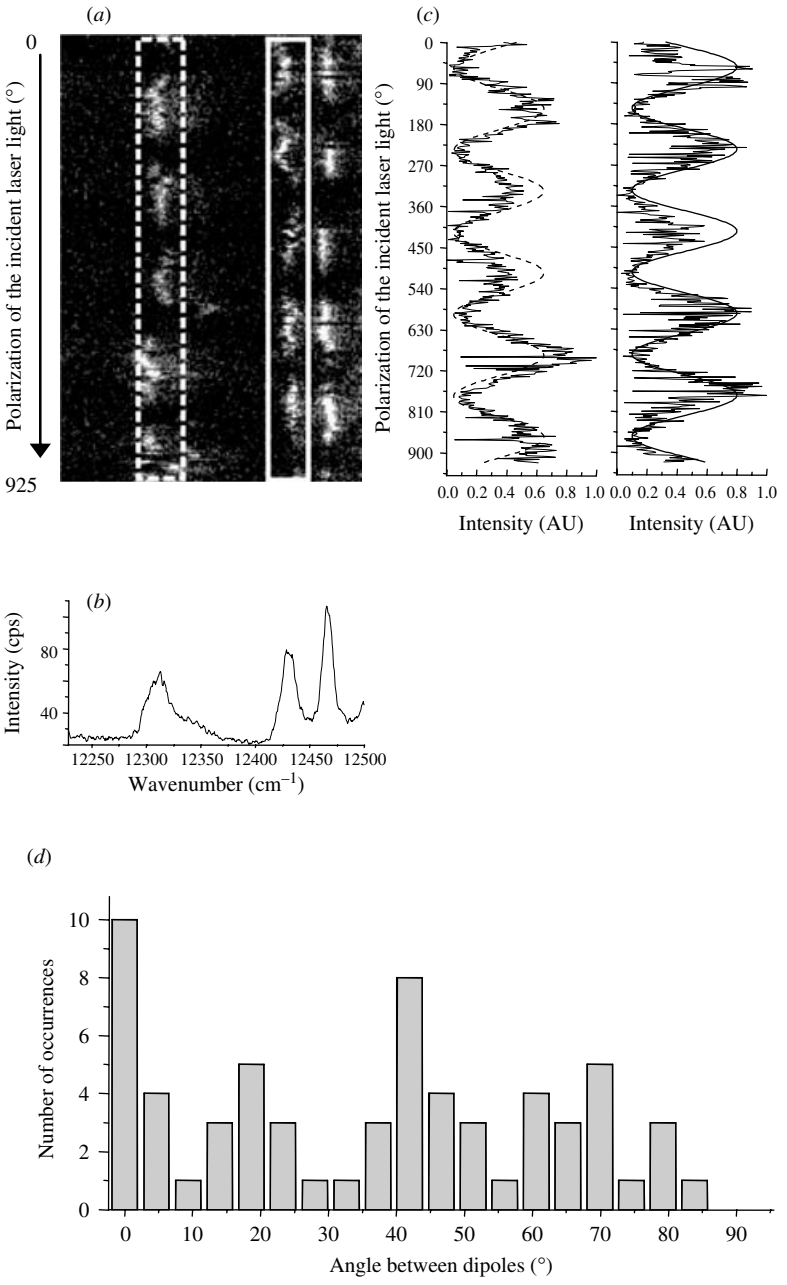


**Fig. 40.** (*a*) A two-dimensional representation of 513 fluorescence-excitation spectra from a part of the B800 band of an individual LH2 complex recorded consecutively at a scan speed of 45 $cm^{-1}$/s and an excitation intensity of 10 W/$cm^2$. The horizontal axis corresponds to wavelength, the vertical axis to polarization, and the grey scale gives the fluorescence intensity. Between two successive scans the polarization of the incident radiation has been turned by 1·8°. (*b*) Average of all 513 spectra. (*c*) Intensity of the fluorescence for the two absorptions indicated by the boxes in part (*a*) as a function of the polarization of the excitation. The full and dashed lines correspond to $\cos^2[\alpha(t)+\alpha]$-type functions fitted to the experimental data with phase angles, $\alpha$, of 148° and 57° respectively. (*d*) Histogram of mutual orientations of the transition–dipole moments from 88 absorption lines from 24 individual complexes. (From Hofmann *et al.* 2003b.)

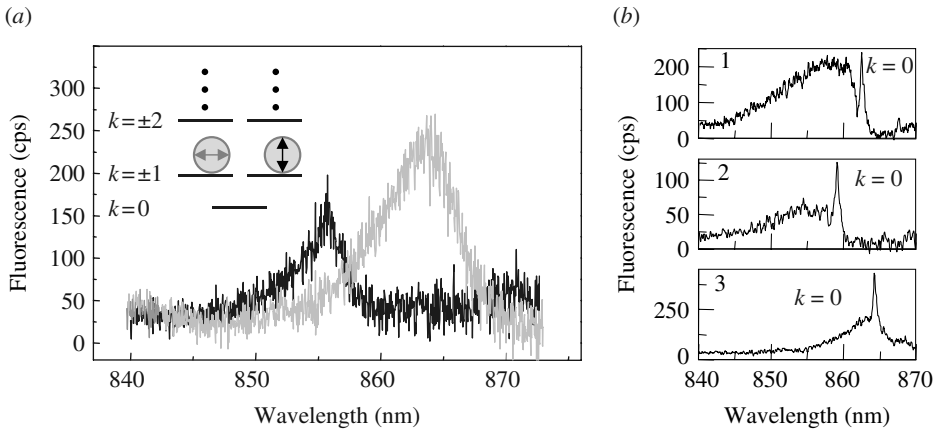


**Fig. 41.** (*a*) A fluorescence-excitation spectrum of the long-wavelength region of an individual LH2 complex for mutually orthogonal polarized excitation. The inset shows a schematic representation of the energy-level scheme of the lowest states in the excited-state manifold of the B850 ring in LH2 of *Rps. acidophila* for nine-fold rotational symmetry of the pigment arrangement. The grey circles indicate the initial population of a given excited state and the arrows the relative orientation of the transition–dipole moments in the plane of the ring. (*b*) Fluorescence-excitation spectra of the long wavelength part of the B850 band of three different complexes (1–3), featuring a very narrow transition at the red wing of the $k^{as} = \pm 1$ absorptions. The spectra are obtained by a summation of repetitively scanned spectra at a high scan rate, where the $k^{as} = 0$ transitions are aligned before summation to correct for spectral diffusion. (More details are given in Table 6 and Ketelaars *et al.* 2001.)

indicated by the two arrows in the inset. The respective fluorescence-excitation spectra of the B850 band taken with an individual LH2 complex are shown in Fig. 41*a*. These spectra have been obtained with excitations that had mutual orthogonal polarizations. Clearly, the data shows that the transition–dipole moments of these two transitions are perpendicular with respect to each other. Based on this observation and the fact that these bands are by far the most intense ones in absorption these transitions have been attributed to the $k^{as} = \pm 1$ exciton states (van Oijen *et al.* 1999b). The observed line widths of the bands reflect the ultra-fast relaxation ($\sim$100 fs) to the $k^{as} = 0$ exciton state, which is consistent with the time-resolved data as discussed in Section 5.3 (Sundström *et al.* 1999).

A crucial check for this assignment was the observation of the $k^{as} = 0$ exciton state. For this transition, which gains oscillator strength when there is any deviation from a perfectly symmetric Bchl*a* arrangement (both with respect to geometry and energetic equivalence), a relatively narrow absorption line is expected because the lifetime of the $k^{as} = 0$ state is $\sim$1 ns. Such a narrow line on the low-energy side of the B850 band has indeed been detected (Ketelaars *et al.* 2001) (Fig. 41*b*), which provides strong evidence that the description of the lowest electronically excited states of the B850 assembly in terms of the exciton model is justified. The spectral properties of the $k^{as} = 0$ transition observed with three individual LH2 complexes are summarized in Table 6. They have an oscillator strength that is 2–10% of the total oscillator strength in the B850 band, in good agreement with theoretical calculations (Mostovoy & Knoester, 2000). Although the statistics are poor, the data on the $k^{as} = 0$ transition in the three complexes suggests that the transition–dipole moment of the $k^{as} = 0$ state becomes stronger when the energy separation between the $k^{as} = 0$ and $k^{as} = \pm 1$ states increases. This is also in qualitative

**Table 6.** *The spectral properties of the narrow features shown in Fig. 41b.* $\delta E_{01}$ *denotes the spectral separation between the narrow line and the average spectral position of the two broad* $k^{as} = \pm 1$ *absorptions*

| Complex | Spectral position (wavenumber) | FWHM ($cm^{-1}$) | Relative oscillator strength (%) | $\delta E_{01}$ ($cm^{-1}$) |
|---|---|---|---|---|
| 1 | 11594 $cm^{-1}$ | 10 | 2 | 58 |
| 2 | 11637 $cm^{-1}$ | 13 | 9 | 93 |
| 3 | 11571 $cm^{-1}$ | 12 | 10 | 102 |

agreement with model calculations on this system (Wu *et al.* 1997b; Alden *et al.* 1997; Monshouwer *et al.* 1997; Timpmann *et al.* 2001).

However, for the circular arrangement of the pigments, the exciton model predicts that the $k^{as} = \pm 1$ states are degenerate, i.e. they have the same transition energy, and have the same intensity. From this experimental data on single LH2 complexes it is possible to obtain the energetic splitting of the $k^{as} = \pm 1$ states $\Delta E_{blue,\ red}$, the ratio of the integrated intensities $I_{blue}/I_{red}$, and the relative orientation of the two transition–dipole moments $\Delta\alpha_{blue,\ red}$, where blue (red) refers to the energetically higher (lower) absorption band(s). The distributions of these parameters are shown in the histograms in Fig. 42 (van Oijen *et al.* 1999b; Hofmann *et al.* 2004). As can be seen from Fig. 42 these parameters vary from complex to complex. The energetic separation $\Delta E_{blue,\ red}$ of the $k^{as} = \pm 1$ states is centered at 126 $cm^{-1}$ and has a width of 101 $cm^{-1}$ (FWHM). The centre value (FWHM) of the integrated intensity ratio $I_{blue}/I_{red}$ is 0·73 (0·54), and the mutual orientation of the transition–dipole moments $\Delta\alpha_{blue,red}$ is 91° (19°).

Analysis of this data lead to the conclusion that these distributions are a result of the B850 pigment ring deviating from perfect circular symmetry and that an elliptical distortion is the most probable distortion (Ketelaars *et al.* 2001; Matsushita *et al.* 2001). Based on fluorescence-polarization experiments two other groups came to similar conclusions (Bopp *et al.* 1999; Tietz *et al.* 2000). Experiments of Bopp *et al.* indicated, moreover, that these structural deformations fluctuate on a timescale of seconds at room temperature. However, it is reasonable to assume that such an elliptical distortion would also affect the conformation of the protein residues in the binding pocket of the chromophores. Since it is already known that for the B800 absorption lines relatively small structural changes in their pigment-binding pockets result in large spectral shifts (Zazubovich *et al.* 2002a) it is important to consider whether a moderate modulation of the individual B850 site energies would also be compatible with the experimental data. If such a modulation in site energies following an imposed structural deformation of the LH2 complex could explain the data then a smaller deviation from circular symmetry would be sufficient to account for the observations (which might be too small to be resolved by X-ray crystallography). This idea has been tested by comparing numerical simulations for three different models of disorder: (i) random diagonal disorder (energetic disorder), (ii) random diagonal disorder together with correlated off-diagonal disorder (structural disorder), and (iii) random and correlated diagonal disorder. Only a model (shown in Fig. 42 by the simulations) that takes into account random and correlated diagonal disorder (model iii) is in good agreement with the measured experimental distributions (Fig. 42). More details about these simulations can be found in Hofmann *et al.* (2004).

Biologists often worry about low-temperature spectroscopy on biomolecules. How can this data be relevant to physiological conditions? It is worth therefore remembering that most

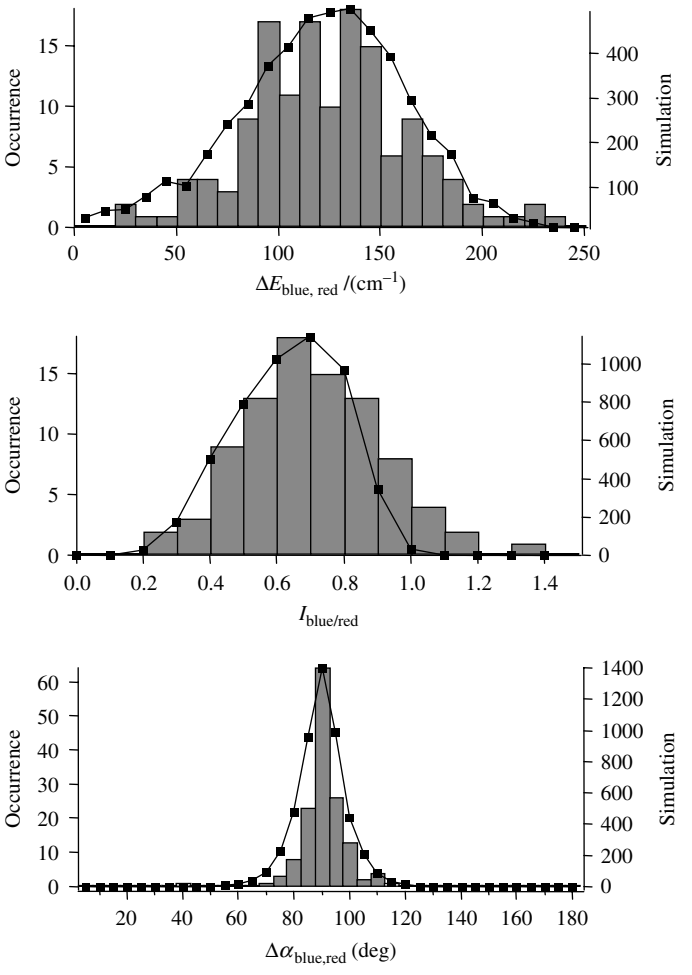


**Fig. 42.** Comparison of the experimental data (histograms) and simulations for a model that takes random and correlated diagonal disorder into account. From top to bottom: energetic separation $\Delta E_{\text{blue, red}}$ for 144 complexes, intensity ratio $I_{\text{blue}}/I_{\text{red}}$ for 88 complexes, and relative orientation of the transition–dipole moments $\Delta\alpha_{\text{blue, red}}$ for the two broad transitions in the B850 spectra for 144 complexes. The experimental data refer to the left vertical scale and the simulations refer to the right vertical scale. (Redrawn from Hofmann *et al.* 2004.)

of the 3D protein structures have been determined by X-ray crystallography under cryogenic conditions, and nobody questions the usefullness of these data.

If one is interested in studying the physical properties of proteins then the interplay of structural disorder and structural organization is key. One of the most important features of high-resolution low temperature experiments, such as these, is the possibility to probe structural heterogeneity in a very direct way *via* the associated spectral heterogeneity. Under ambient conditions, even for single molecules, the expected spectral changes will be completely masked because the homogeneous linewidth of the absorption bands often exceed those spectral changes. At low temperatures, in contrast, the spectral bands become sufficiently narrow, since most of the thermal contributions to the line broadening are frozen out, and the rates of the

processes that change the structure become sufficiently slow to be measured. Clearly, at low temperatures the observed rates for conformational changes do not reflect the dynamics of the protein in its native environment. However, working at cryogenic temperatures shifts the timescale for these fluctuations into a range that is experimentally accessible and offers the opportunity to study the organization of the protein energy landscape directly.

Finally, it is very interesting to realise that the detailed knowledge about semiconductor physics that was required to construct electronic devices like radios, computers, mobile phones, etc. was elucidated by low temperature solid-state physics. Clearly, these devices do not operate at cryogenic temperatures, yet the information obtained at low temperature underpins the operation of these devices at room temperature.

## 8. Quantum mechanics and the purple bacteria LH system

The B850 assembly of LH2 is an elegant example of the clever exploitation of quantum mechanics to produce an efficient LH system (Sumi, 2000, 2001).

The relatively strong interaction between the B850 Bchl*a* molecules causes a ladder of exciton states spread over $\sim$1200 cm$^{-1}$ in energy. The exciton band consists of 16 pairwise degenerate states enclosed by two non-degenerate states at the bottom and the top of the band. The circular arrangement of the pigments with a large in-plane component of the individual transition–dipole moments enforces by symmetry that the transition probability for each state of the lowest degenerate pair increases at the expense of all other exciton states by a factor $N$, where $N$ is the numer of dimers in the ring. After excitation of one of these states the energy relaxes on a 100 fs timescale to the lowest exciton state which features only a very small transition probability to the ground state. In other words the excitation energy is trapped for a time sufficiently long to favour energy transfer above wasteful fluorescence. Further, the transition–dipole moments of the $k = \pm 1$ exciton states can be excited with mutually orthogonal polarized light. This allows the B850 assembly to absorb light of any polarization within the plane of the ring. Moreover, the higher exciton states are not 'useless' because they do not carry a net transition–dipole moment, they can act as accepting states for energy transfer from the B800 molecules (Mukai *et al.* 1999; Sumi, 1999) (see Section 6).

The advantages of a circular array for LH and energy transfer become clear by comparison with a linear arrangement of the chromophores (or a circular geometry featuring a strong component of the transition–dipole moments along the $C_9$-symmetry axis of the ring). Such geometry yields an $N$-fold increase of the transition probability ($N$ corresponds to the number of molecules in the linear chain) for the lowest exciton state which can be excited exclusively with light that is linear polarized parallel to the direction of the dipole moment. In other words the absorption becomes less efficient while at the same time the probability for fluorescence is enhanced tremendously.

Another fascinating piece of evidence for the high degree of optimization of the antenna system is found when looking at the B800$\rightarrow$B850 energy-transfer rate as a function of the size of the fluctuations of the B850 site energies. Modelling the spread in site energies by a Gaussian distribution with a standard deviation $\Delta E$ yields that the B800$\rightarrow$B850 energy-transfer rate shows a broad maximum for $\Delta E \approx 100$ cm$^{-1}$–300 cm$^{-1}$ peaking at $\sim$230 cm$^{-1}$ (Sumi, 2000, 2001). It is worth noting that without disorder in the site energies this energy-transfer rate would be significantly smaller. The broad range over which the enhancement occurs testifies not only to the robustness against structural fluctuations but also that the antenna system takes

advantage of the fluctuations of the protein environment to fine-tune its energy-transfer properties.

Remarkably, the energetic disorder of the site energies is in the same order of magnitude as the thermal energy under ambient conditons which might be indicative that during the evolution of these complexes the disorder was exploited to further optimize the photosynthetic process.

In summary, owing to the size effects of the assembly the energy is allowed to enter the B850 exciton manifold via optically 'forbidden' states surpassing the quantum mechanical coherence which on the other hand is the cause for the vanishing total transition–dipole moment of the lowest excited state preventing wasteful fluorescence.

## 9. Appendix

In order to help to provide the general insights of such systems for mathematically literate non-specialists we present some additional information about quantum mechanics and the application of quatum mechanics to LH2. First we introduce some basic concepts and notations of quantum mechanics such as wavefunctions, operators and the Dirac notation. We have followed a pragmatic approach that has been simplified as much as possible without going into too many details about some of the mathematical prerequisites and potential obstacles. For an exact mathematical treatment, which is far beyond the scope of this Appendix, the interested readers are referred to any general textbook on quantum mechanics. The description given here has been adapted from Yariv (1982). Our aim is to familiarize the non-specialist reader with the main approximations and to develop the formalism for an example of gradually increasing complexity. In order to do so we describe the excitonic interaction within a dimer of two equivalent molecules and will progress towards a 'ring' consisting of three equivalent interacting dimers. We have chosen this example because this represents the smallest unit reminescent of the LH2 complex from *Rps. acidophila* that consists of nine interacting dimers. More experienced readers can visit the literature for a full treatment of the excitons in LH2 (Sauer *et al.* 1996; Alden *et al.* 1997; van Amerongen *et al.* 2000; Dempster *et al.* 2001; Jang *et al.* 2001; Matsushita *et al.* 2001; Didraga & Knoester, 2002).

### 9.1 A crash course on quantum mechanics

The basic ingredients of quantum mechanics are wavefunctions and operators. A wavefunction $\psi(x)$ contains all knowable information about a system and is usually normalized fulfilling

$$\int_V \psi^*(x) \cdot \psi(x)\, \mathrm{d}V = 1, \tag{A 1}$$

where $\psi^*(x)$ denotes the complex conjugate of the wavefunction and the integration is over the full space. Operators play a crucial role because they are closely connected to physically observable properties, commonly abbreviated as observables. Simply speaking an operator is an instruction that, when applied to a function, changes it to another function. For example the operator

$$\hat{A} = 1 + \frac{\partial}{\partial x} \tag{A 2}$$

means that

$$\hat{A}f(x) = f(x) + \frac{\partial}{\partial x} f(x). \tag{A 3}$$

Another example is the operator

$$\hat{H} = -\frac{\hbar^2}{2m} \underbrace{\left( \frac{\partial^2}{\partial x^2} + \frac{\partial^2}{\partial y^2} + \frac{\partial^2}{\partial z^2} \right)}_{\nabla^2} = -\frac{\hbar^2}{2m} \nabla^2, \tag{A 4}$$

which is the operator that corresponds to the kinetic energy of a particle of mass $m$. With each operator a set of numbers $\lambda_n$ and a set of functions $a_n(x)$ is associated such that

$$\hat{A}a_n(x) = \lambda_n a_n(x). \tag{A 5}$$

The numbers are called *eigenvalues* and the functions are called *eigenfunctions* of the operator $\hat{A}$. Mathematically it can be shown that operators that corresponds to a physically observable property satisfy the equation

$$\int_V f^*(x) \left( \hat{A} g(x) \right) \mathrm{d}V = \int_V \left( \hat{A} f(x) \right)^* g(x) \, \mathrm{d}V, \tag{A 6}$$

where $f(x)$ and $g(x)$ are two arbritrary functions. Such operators are termed *hermitian*. These operators have the interesting property that their eigenfunctions are orthogonal (provided that their eigenvalues are not equal). This means for $n \neq$m they obey the equation

$$\int_V a_n^*(x) \cdot a_m(x) \, \mathrm{d}V = 0. \tag{A 7}$$

Usually the eigenfunctions are chosen to be normalized, i.e.

$$\int_V a_n^*(x) \cdot a_n(x) \, \mathrm{d}V = 1, \tag{A 8}$$

and Eqs (A 7) and (A 8) are commonly summarized by

$$\int_V a_n^*(x) \cdot a_m(x) \, \mathrm{d}V = \delta_{nm}, \tag{A 9}$$

where $\delta_{nm} = 1$ if $n = m$ and $\delta_{nm} = 0$ if $n \neq m$. The symbol $\delta_{nm}$ is called the Kronecker delta. A set of eigenfunctions $a_n(x)$ of a hermitian operator possesses the important property that it can be used to expand any arbitrary function $\psi(x)$, i.e.

$$\psi(x) = \sum_n c_n a_n(x), \tag{A 10}$$

where the expansion coefficients $c_n$ are complex numbers that can be obtained from

$$c_n = \int_V a_n^*(x) \cdot \psi(x) \, \mathrm{d}V. \tag{A 11}$$

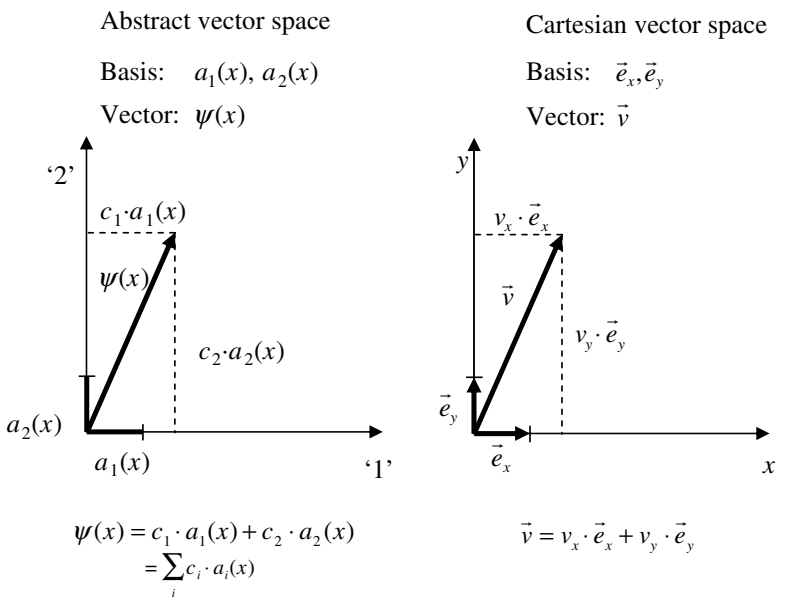


**Fig. 43.** Representation of abstract vector and Cartesian vector spaces, see text for details.

The function $\psi(x)$ can be thought of as an arbitrary vector (in an abstract vector space) and Eq. (A 11) expresses the expansion of that vector in terms of the orthonormal 'unit vectors' $a_n(x)$. Mathematically this is fully equivalent to the expansion of a real vector $\vec{v}$ as

$$\vec{v} = \sum_i v_i \cdot \vec{e}_i \quad (i = x, y, z), \tag{A 12}$$

where $\vec{e}_i$ are the unit vectors along the Cartesian coordinates [see Eqs (A 10) and (A 12)] as we have illustrated in Fig. 43. Given this similarity the 'vectors' $a_n(x)$ are called also a basis set (of the abstract vector space). If we associate the operator $\hat{A}$ with the physical variable (observable) $A$, in quantum mechanics the expectation value $\langle A \rangle$ of this variable is obtained by performing the integral

$$\langle A \rangle = \int_V \psi^*(x) \hat{A} \psi(x) \, \mathrm{d}V. \tag{A 13}$$

As an example we calculate the expectation value of the observable 'position'. The position operator $\hat{x}$ is given by the position $x$, i.e. $\hat{x} = x$. Thus

$$\langle x \rangle = \int_V \psi^*(x) \hat{x} \psi(x) \, \mathrm{d}V = \int_V \psi^*(x) x \psi(x) \, \mathrm{d}V = \int_V \underbrace{\psi^*(x)\psi(x)}_{|\psi(x)|^2} x \, \mathrm{d}V = \int_V |\psi(x)|^2 x \, \mathrm{d}V. \tag{A 14}$$

Comparing this result with the classical definition of the average value of a vector $\vec{v}$ subjected to a distribution $P(\vec{v})$ which is given by

$$\vec{v} = \int_V P(\vec{v})\,\vec{v}\,\mathrm{d}V, \tag{A 15}$$

tempts us to associate $|\psi(x)|^2\,\mathrm{d}V$ with the probability to find the particle inside the volume $\mathrm{d}V$.

It is interesting to analyse Eq. (A 13) in terms of the eigenfunctions of the operator $\hat{A}$. Accordingly we expand $\psi(x) = \sum_n c_n\,a_n(x)$ and rewrite Eq. (A 13) as

$$\langle A\rangle = \int_V \psi^*(x)\hat{A}\psi(x)\,\mathrm{d}V = \int_V \underbrace{\left(\sum_i c_i\,a_i(x)\right)^*}_{\psi^*(x)}\hat{A}\underbrace{\left(\sum_i c_j\,a_j(x)\right)}_{\psi(x)}\,\mathrm{d}V. \tag{A 16}$$

After exchanging the order of integration and summation, and taking advantage of the orthogonality of the eigenfunctions $a_n(x)$ [see Eq. (A 9)] one finally arrives at

$$\langle A\rangle = \sum_i \lambda_i |c_i|^2, \tag{A 17}$$

which shows that $\langle A\rangle$ is the 'average value' observed for the observable $A$ and this is why it is called the (quantum mechanical) expectation value. Certainly, the reader will have noticed that the notation used so far is very clumsy. Even more since most of the time it is not required to calculate any of the integrals in detail. A notation introduced by Dirac greatly simplifies the writing and the manipulations involved. If we consider the integral

$$\int_V f^*(x)\cdot g(x)\,\mathrm{d}V \tag{A 18}$$

than in Dirac notation this is expressed as

$$\langle f|g\rangle = \int_V f^*(x)\cdot g(x)\,\mathrm{d}V. \tag{A 19}$$

The individual functions f and g are represented by a 'ket-vector' $g \rightarrow |g\rangle$ and a 'bra-vector' $f^* \rightarrow \langle f|$, respectively. When a 'bra' and a 'ket' vector are joined to form a 'bracket' $\langle f \mid g\rangle$ this corresponds by definition to the integral (A 19). Consequently, operating on g with $\hat{A}$ is represented by $\hat{A}|g\rangle$ and $\int_V f^*(x)\hat{A}g(x)\,\mathrm{d}V = \langle f|\hat{A}|g\rangle$. In this notation the 'projection' of $\psi(x)$ on $a_n(x)$ is simply given by $\langle a_n(x)|\psi(x)\rangle = c_n$ and the expansion of any arbitrary state function can thus be expressed as

$$|\psi(x)\rangle = \sum_n \underbrace{c_n}_{\langle a_n(x)|\psi(x)\rangle}|a_n(x)\rangle = \sum_n (\langle a_n(x) \mid \psi(x)\rangle)|a_n(x)\rangle = \sum_n |a_n(x)\langle a_n(x) \mid \psi(x)\rangle. \tag{A 20}$$

Formally we can identify that the result of operating with the operator $\hat{I} = \sum_n |a_n(x)\rangle\langle a_n(x)|$ on an arbitrary function $|\psi(x)\rangle$ is to obtain back $|\psi(x)\rangle$. In other words $\hat{I}$ is the identity operator, i.e. $\hat{I}\,|\psi(x)\rangle = |\psi(x)\rangle$.

The Dirac notation offers the opportunity to write operators in a matrix representation. We will develop this representation on the example of the energy states of a dimer. Therefore we label the molecules in the dimer $n_\alpha$ and $n_\beta$ and denote by $|n_\alpha\rangle$ the state where molecule $n_\alpha$ is in the

electronically excited state while molecule $n_\beta$ is in the electronic ground state. Correspondingly $|n_\beta\rangle$ denotes the reversed situation. Then the two states $|n_\alpha\rangle$ and $|n_\beta\rangle$ form a basis set for the description of the excited states of the dimer, thus $\langle n_i|n_j\rangle = \delta_{ij}$. The quantum mechanical operator for the energy of a system is the Hamilton operator. Here we denote the Hamiltonian for the two non-interacting molecules by $\hat{H}_0$ and the Schrödinger equation for each molecule is given by

$$H_0|n_i\rangle = E_0|n_i\rangle \quad (i = \alpha,\ \beta), \tag{A 21}$$

where $E_0$ refers to the energy difference between the ground state and the excited state of the molecules. Taking advantage of the identity operator, which reads for this example $\hat{I} = |n_\alpha\rangle\langle n_\alpha| + |n_\beta\rangle\langle n_\beta|$ yields

$$H_0 = E_0|n_\alpha\rangle\langle n_\alpha| + E_0|n_\beta\rangle\langle n_\beta|. \tag{A 22}$$

Employing Eq. (A 21) we can verify that

$$\langle n_\alpha| \underbrace{H_0|n_\alpha\rangle}_{E_0|n_\alpha\rangle} = \langle n_\alpha|E_0|n_\alpha\rangle = E_0 \underbrace{\langle n_\alpha|n_\alpha\rangle}_{1} = E_0 \tag{A 23}$$

and similarly

$$\langle n_\beta|H_0|n_\beta\rangle = E_0 \tag{A 24}$$

holds. Moreover, we find

$$\langle n_\alpha| \underbrace{H_0|n_\beta\rangle}_{E_0|n_\beta\rangle} = \langle n_\alpha|E_0|n_\beta\rangle = E_0 \underbrace{\langle n_\alpha|n_\beta\rangle}_{0} = 0 \tag{A 25}$$

and

$$\langle n_\beta|H_0|n_\alpha\rangle = \langle n_\beta|E_0|n_\alpha\rangle = E_0 \underbrace{\langle n_\beta|n_\alpha\rangle}_{0} = 0. \tag{A 26}$$

A short-term notation for Eqs (A 23)–(A 26) is as follows

| $H_0$ | $\lvert n_\alpha\rangle$ | $\lvert n_\beta\rangle$ |
|---|---|---|
| $\langle n_\alpha\rvert$ | $E_\alpha$ | 0 |
| $\langle n_\beta\rvert$ | 0 | $E_\beta$ |

. (A 27)

The first row and first column of the table gives the 'bra' and the 'ket' vectors, and the matrix corresponds to the four entries next (under) the basis vectors respectively. Obviously the matrix that represents the Hamiltonian is diagonal. However, if in algebra a matrix is diagonal this is equivalent to the statement that the chosen basis states are the eigenstates and the diagonal elements are the eigenvalues of the system. Since here the matrix corresponds to the Hamilton operator, i.e. to the energy of the system, the eigenvalues are the energies of the respective eigenstates. In the next step we introduce an interaction, $V$, between molecules $n_\alpha$ and $n_\beta$

with the property $V_{\alpha\beta} = \langle n_\alpha | V | n_\beta \rangle = \langle n_\beta | V | n_\alpha \rangle = V_{\beta\alpha}$. This can be incorporated into the Hamiltonian as

$$H = E_0 |n_\alpha\rangle\langle n_\alpha| + E_0 |n_\beta\rangle\langle n_\beta| + V |n_\alpha\rangle\langle n_\beta| + V |n_\beta\rangle\langle n_\alpha|. \tag{A 28}$$

The matrix representation of this Hamiltonian in the same basis as above is given by

| $H$ | $\lvert n_\alpha\rangle$ | $\lvert n_\beta\rangle$ |
|---|---|---|
| $\langle n_\alpha \rvert$ | $E_0$ | $V_\mathrm{d}$ |
| $\langle n_\beta \rvert$ | $V_\mathrm{d}$ | $E_0$ |

. (A 29)

This Hamiltonian is no longer diagonal which is equivalent to (i) the chosen basis states where the excitation energy is localized on the individual molecules are not the eigenstates of the system and (ii) the entries on the diagonal are not the energies of the eigenstates and hence not the energies of the system of the two interacting molecules. Interestingly we arrived at this result without solving (or even writing down in detail) any of the integrals that are hidden in the Dirac notation. In order to obtain the proper eigenstates and energies of the system the Hamiltonian has to be diagonalized. For a $2 \times 2$ matrix this is mathematically not very demanding and here we give the result of this procedure:

| $H$ | $\lvert n^\mathrm{s}_{\alpha\beta}\rangle$ | $\lvert n^\mathrm{as}_{\alpha\beta}\rangle$ |
|---|---|---|
| $\langle n^\mathrm{s}_{\alpha\beta} \rvert$ | $E_\mathrm{s}$ | 0 |
| $\langle n^\mathrm{as}_{\alpha\beta} \rvert$ | 0 | $E_\mathrm{as}$ |

, (A 30)

with

$$|n^\mathrm{s}_{\alpha\beta}\rangle = \frac{1}{\sqrt{2}}\left(|n_\alpha\rangle + |n_\beta\rangle\right) \quad (E_\mathrm{s} = E_0 + V_\mathrm{d}) \tag{A 31}$$

and

$$\left|n^\mathrm{as}_{\alpha\beta}\right\rangle = \frac{1}{\sqrt{2}}\left(-|n_\alpha\rangle + |n_\beta\rangle\right) \quad (E_\mathrm{as} = E_0 - V_\mathrm{d}), \tag{A 32}$$

where 's', and 'as' abbreviate 'symmetric' and 'antisymmetric'. The new eigenstates are linear combinations of the states localized on the individual molecules. In the eigenstates the excitation energy is distributed equally over both molecules $n_\alpha$ and $n_\beta$. Moreover, the initial degeneracy of the states $|n_\alpha\rangle$ and $|n_\beta\rangle$ is lifted by the interaction and the states $|n^\mathrm{s}_{\alpha\beta}\rangle$ and $|n^\mathrm{as}_{\alpha\beta}\rangle$ are separated in energy by $2V_\mathrm{d}$.

In the simplest approximation the Coulomb interaction between the charges of neighbouring molecules may be described as interacting point dipoles. For the example shown in Fig. 44 we have chosen the mutual orientation of the dipoles according to the dimeric subunit within the B850 array of Bchl*a* molecules of LH2 from *Rps. acidophila* (McDermott *et al.* 1995). The transition–dipole moment to the ground states is determined by

$$\vec{M}(n^j_{\alpha\beta}) = \langle g | \vec{D} \left| n^j_{\alpha\beta} \right\rangle \quad (j = \mathrm{s}, \mathrm{as}) \tag{A 33}$$

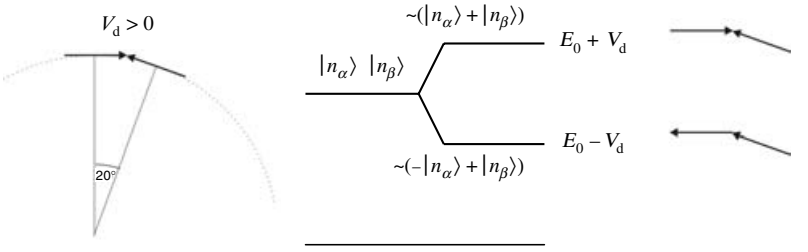


**Fig. 44.** From left to right: arrangement of two interacting molecular transition–dipole moments, energy levels and eigenstates of the two monomers (left) and the dimer (right), and mutual orientation of the transition–dipole moments in the respective eigenstates of the dimer. The geometry depicted corresponds to a dimeric subunit in the B850 ring of LH2 from *Rps. acidophila*.

which yields

$$\left.\begin{aligned}\vec{M}(n^{s}_{\alpha\beta}) &= \frac{1}{\sqrt{2}}\Big(\underbrace{\langle g|\vec{D}|n_\alpha\rangle}_{\vec{m}_0(n_\alpha)} + \underbrace{\langle g|\vec{D}|n_\alpha\rangle}_{\vec{m}_0(n_\beta)}\Big)\\ \vec{M}(n^{as}_{\alpha\beta}) &= \frac{1}{\sqrt{2}}\Big(\underbrace{-\langle g|\vec{D}|n_\alpha\rangle}_{\vec{m}_0(n_\alpha)} + \underbrace{\langle g|\vec{D}|n_\alpha\rangle}_{\vec{m}_0(n_\beta)}\Big)\end{aligned}\right\} \tag{A 34}$$

where $\vec{m}_0(n_i)$ refers to the transition–dipole moment of the respective individual molecule which are given by

$$\vec{m}_0(n_\alpha) = m_0\begin{pmatrix}1\\0\end{pmatrix} \quad \text{and} \quad \vec{m}_0(n_\beta) = m_0\begin{pmatrix}-\cos 20^\circ\\ \sin 20^\circ\end{pmatrix}$$

for the geometry chosen in the example. Insertion into (A 34) yields for the transition probabilities

$$\left.\begin{aligned}\left|\vec{M}(n^{s}_{\alpha\beta})\right|^2 &= \left(\frac{1}{\sqrt{2}}\left(\vec{m}_0(n_\alpha)+\vec{m}_0(n_\beta)\right)\right)^2 = 0.06\cdot m_0^2,\\ \left|\vec{M}(n^{as}_{\alpha\beta})\right|^2 &= \left(\frac{1}{\sqrt{2}}\left(-\vec{m}_0(n_\alpha)+\vec{m}_0(n_\beta)\right)\right)^2 = 1.94\cdot m_0^2,\end{aligned}\right\} \tag{A 35}$$

which shows that the transition probability to the lower state is $\sim 30$ times larger with respect to the transition probability to the upper state. This reflects the head-to-tail arrangement of the transition–dipole moments in the upper state where the individual dipoles are close to cancel each other.

## 9.2 Interacting dimers

To obtain the energies for a system of three interacting dimers we have to evaluate Eq. (8) for $N=3$, $k^s=0, \pm 1$ and $k^{as}=0, \pm 1$. In Fig. 45 we show the influence of the various contributions. First the intradimer interaction $V_d$ leads to splitting of the energies of the excited states of the individual molecules by an amount $2V_d$. For three dimers each of these states is threefold degenerate. If the interdimer interaction is taken into account as well this degeneracy is lifted

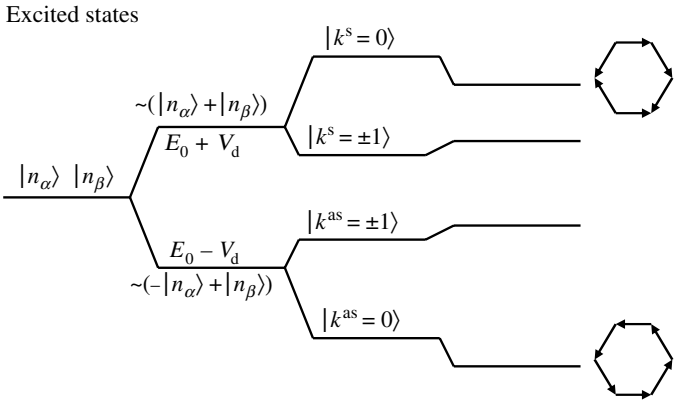


| Monomers | Isolated dimers | Interacting dimers | Interacting dimers |
|---|---|---|---|
| $E_\alpha = E_\beta$ | $E_\alpha = E_\beta$ | $E_\alpha = E_\beta$ | $E_\alpha = E_\beta$ |
| $V_d = 0$ | $V_d \neq 0$ | $V_d \neq 0$ | $V_d \neq 0$ |
| | $V_{ext} = 0$ | $V_{ext} \neq 0$ | $V_{ext} \neq 0$ |
| | | $W_\alpha = W_\beta = 0$ | $W_\alpha = W_\beta = W_0 \neq 0$ |

**Fig. 45.** Energy levels for six molecules that are treated as monomers, three non-interacting dimers, and three interacting dimers with and without next-nearest neighbour interaction (from left to right). The arrows on the right-hand side indicate the mutual orientation of the transition–dipole moments in the highest and lowest exciton state respectively.

in part. The $k^j = 0$ states get separated from the $k^j = \pm 1$ which remain degenerate. As long as the interdimer interaction is only included in the nearest-neighbour approximation (Fig. 45 centre) the pattern of the exciton states appears symmetric with respect to the monomer transition energy $E_0$. The total splitting amounts to $2\cdot(V_d + V_{ext})$ which is $\sim 4\cdot V_d$ since in the B850 $V_d$ and $V_{ext}$ are of the same order of magnitude. Inclusion of second-neighbour interactions shifts the energies of the exciton states in the 's' and 'as' manifold in opposite directions resulting in an asymmetric pattern for the energy level spacings. The energetic separation between the exciton states in the 'as' manifold becomes larger whereas the energetic separation between the exciton states in the 's' manifold becomes smaller. It should be noted that for the choosen geometry $V_d$, $V_{ext} > 0$ and $W_\alpha$, $W_\beta < 0$. However, for the B850 manifold of LH2 the second-neighbour interaction is in the order of 10% of the nearest-neighbour interaction hence its influence on the exciton energies is small.

## 10. Acknowledgements

We acknowledge generous financial support from the Biotechnology and Biological Sciences Research Council, U.K. (R.J.C., A.G.), the European Union (A.G., contract MEIF-CT-2005-00951),

the Volkswagen Foundation (J.K.) and the Bavarian Science Foundation (J.K.). We thank Shozo Shimonaka and Hideki Hashimoto (Department of Physics, Osaka City University) for providing Figure 14 and Mary Grace Galinato and Harry Frank (Department of Chemistry, University of Connecticut) for their help in compiling Figure 32.

## 11. References

Abrahams, J. P., Leslie, A. G., Lutter, R. & Walker, J. E. (1994). Structure at 2·8 Å resolution of F1-ATPase from bovine heart mitochondria. *Nature* **370**, 621–628.

Abresch, E. C., Axelrod, H. L. A., Beatty, J. T., Johnson, J. A., Nechushtai, R. & Paddock, M. L. (2005). Characterization of a highly purified, fully active, crystallizable RC-LH1-PufX core complex from *Rhodobacter sphaeroides*. *Photosynthesis Research* **86**, 61–70.

Alden, R. G., Johnson, E., Nagarajan, V., Parson, W. W., Law, C. J. & Cogdell, R. J. (1997). Calculations of spectroscopic properties of the LH2 bacteriochlorophyll-protein antenna complex from *Rhodopseudomonas acidophila*. *Journal of Physical Chemistry B* **101**, 4667–4680.

Allen, J. P., Feher, G., Yeates, T. O., Komiya, H. & Rees, D. C. (1987). Structure of the reaction center from *Rhodobacter sphaeroides* R-26: the cofactors. *Proceedings of the National Academy of Sciences USA* **84**, 5730–5734.

Allen, J. P., Feher, G., Yeates, T. O., Komiya, H. & Rees, D. C. (1988). Structure of the reaction center from *Rhodobacter sphaeroides* R-26: 5. Protein-cofactor (quinones and iron$^{2+}$) interactions. *Proceedings of the National Academy of Science USA* **85**, 8487–8491.

Allen, J. P., Feher, G., Yeates, T. O., Rees, D. C., Deisenhofer, J., Michel, H. & Huber, R. (1986). Structural homology of reaction centers from *Rhodopseudomonas sphaeroides* and *Rhodopseudomonas viridis* as determined by x-ray diffraction. *Proceedings of the National Academy of Sciences USA* **83**, 8589–8593.

Anderson, S., Dragnea, V., Masuda, S., Ybe, J., Moffat, K. & Bauer, C. (2005). Structure of a novel photoreceptor, the BLUF domain of AppA from *Rhodobacter sphaeroides*. *Biochemistry* **44**, 7998–8005.

Arellano, J. B., Raju, B. B., Naqvi, K. R. & Gillbro, T. (1998). Estimation of pigment stoichiometries in photosynthetic systems of purple bacteria: special reference to the (absence of) second carotenoid in LH2. *Photochemistry and Photobiology* **68**, 84–87.

Arluison, V., Seguin, J., Le Caer, J. P., Sturgis, J. N. & Robert, B. (2004). Hydrophobic pockets at the membrane interface: an original mechanism for membrane protein interactions. *Biochemistry* **43**, 1276–1282.

Arluison, V., Seguin, J. & Robert, B. (2002). Biochemical characterization of the dissociated forms from the core antenna proteins from purple bacteria. *Biochemistry* **41**, 11812–11819.

Armitage, J. P. & Hellingwerf, K. J. (2003). Light-induced behavioral responses ('phototaxis') in prokaryotes. *Photosynthesis Research* **76**, 145–155.

Bahatyrova, S., Frese, R. N., Siebert, C. A., Olsen, J. D., van der Werf, K. O., van Grondelle, R., Niederman, R. A., Bullough, P. A., Otto, C. & Hunter, C. N. (2004a). The native architecture of a photosynthetic membrane. *Nature* **430**, 1058–1062.

Bahatyrova, S., Frese, R. N., van der Werf, K. O., Otto, C., Hunter, C. N. & Olsen, J. D. (2004b). Flexibility and size heterogeneity of the LH1 light harvesting complex revealed by atomic force microscopy: functional significance for bacterial photosynthesis. *Journal of Biological Chemistry* **279**, 21327–21333.

Bakalis, L. D. & Knoester, J. (1999). Pump probe spectroscopy and the exciton delocalization length in molecular aggregates. *Journal of Physical Chemistry B* **103**, 6620–6628.

Bandilla, M., Ucker, B., Ram, M., Simonin, I., Gelhaye, E., McDermott, G., Cogdell, R. J. & Scheer, H. (1998). Reconstitution of the B800 bacteriochlorophylls in the peripheral light harvesting complex B800–850 of *Rhodobacter sphaeroides* 2.4.1 with Bchl *a* and modified (bacterio-)chlorophylls. *Biochimica et Biophysica Acta – Bioenergetics* **1364**, 390–402.

Barkigia, K. M., Chantranupong, L., Kehres, L. A., Smith, K. M. & Fajer, J. (1988). Structural and theoretical models of photosynthetic chromophores. Implications for redox, light absorption properties and vectorial electron flow. *Journal of the American Chemical Society* **110**, 7566–7567.

Barz, W. P., Francia, F., Venturoli, G., Melandri, B. A., Vermeglio, A. & Oesterhelt, D. (1995a). Role of the PufX protein in photosynthetic growth of *Rhodobacter sphaeroides* 1. PufX is required for efficient light-driven electron transfer and photophosphorylation under anaerobic conditions. *Biochemistry* **34**, 15235–15247.

Barz, W. P., Vermeglio, A., Francia, F., Venturoli, G., Melandri, B. A. & Oesterhelt, D. (1995b). Role of the PufX protein in photosynthetic growth of *Rhodobacter sphaeroides*. 2. PufX is required for efficient ubiquinone/ubiquinol exchange between the reaction center $Q_B$ site and the cytochrome $bc_1$ complex. *Biochemistry* **34**, 15248–15258.

Basche, T., Moerner, W. E., Orrit, M. & Wild, U. P. (1997). *Single Molecule Optical Detection, Imaging and Spectroscopy*. Munich: Verlag-Chemie.

Bauer, C. (1995). Regulation of photosynthesis gene expression. In *Anoxygenic Photosynthetic Bacteria*, vol. 2. *Advances in Photosynthesis* (eds. R. E. Blakenship, M. T. Madigan & C. E. Bauer), pp. 1221–1234. Dordrecht: Kluwer Academic Publishers.

Beekman, L. M. P., van Mourik, F., Jones, M. R., Visser, H. M., Hunter, C. N. & van Grondelle, R. (1994). Trapping kinetics in mutants of the photosynthetic purple bacterium *Rhodobacter sphaeroides*: Influence of the charge separation rate and consequences for the rate-limiting step in the light-harvesting process. *Biochemistry* **33**, 3143–3147.

Benini, S., Rypniewski, W. R., Wilson, K. S., Ciurli, S. & Mangani, S. (2001). Structure-based rationalization of urease inhibition by phosphate: novel insights into the enzyme mechanism. *Journal of Biological Inorganic Chemistry* **6**, 778–790.

Bergström, H., Sundström, V., van Grondelle, R., Gillbro, T. & Cogdell, R. (1988). Energy-transfer dynamics of isolated B800–850 and B800–820 pigment-protein complexes of *Rhodobacter sphaeroides* and *Rhodopseudomonas acidophila*. *Biochimica et Biophysica Acta – Bioenergetics* **936**, 90–98.

Bhoo, S. H., Davis, S. J., Walker, J., Karniol, B. & Vierstra, R. D. (2001). Bacteriophytochromes are photochromic histidine kinases using a biliverdin chromophore. *Nature* **414**, 776–779.

Bissig, I., Brunisholz, R. A., Suter, F., Cogdell, R. J. & Zuber, H. (1988). The complete amino acid sequences of the B800–850 antenna polypeptides from *Rhodopseudomonas acidophila* strain 7750. *Zeitschrift für Naturforschung, C: Bioscience* **43**, 77–83.

Bittl, R., Schlodder, E., Geisenheimer, I., Lubitz, W. & Cogdell, R. J. (2001). Transient EPR and absorption studies of carotenoid triplet formation in purple bacterial antenna complexes. *Journal of Physical Chemistry B* **105**, 5525–5535.

Böhmer, M. & Enderlein, J. (2003). Fluorescence spectroscopy of single molecules under ambient conditions: methodology and technology. *ChemPhysChem* **4**, 793–808.

Bopp, M. A., Jia, Y., Li, L., Cogdell, R. J. & Hochstrasser, R. M. (1997). Fluorescence and photobleaching dynamics of single light harvesting complexes. *Proceedings of the National Academy of Sciences USA* **94**, 10630–10635.

Bopp, M. A., Sytnik, A., Howard, T. D., Cogdell, R. J. & Hochstrasser, R. M. (1999). The dynamics of structural deformations of immobilized single light-harvesting complexes. *Proceedings of the National Academy of Sciences USA* **96**, 11271–11276.

Bowman, W. C., Du, S. Y., Bauer, C. E. & Kranz, R. G. (1999). In vitro activation and repression of photosynthesis gene transcription in *Rhodobacter capsulatus*. *Molecular Microbiology* **33**, 429–437.

Braatsch, S., Gomelsky, M., Kuphal, S. & Klug, G. (2002). A single flavoprotein, AppA, integrates both redox and light signals in *Rhodobacter sphaeroides*. *Molecular Microbiology* **45**, 827–836.

Braatsch, S. & Klug, G. (2004). Blue light perception in bacteria. *Photosynthesis Research* **79**, 45–57.

Braatsch, S., Moskvin, O. V., Klug, G. & Gomelsky, M. (2004). Responses of the *Rhodobacter sphaeroides* transcriptome to blue light under semiaerobic conditions. *Journal of Bacteriology* **186**, 7726–7735.

Braun, P., Gebhardt, R., Kwa, L. & Doster, W. (2005). High pressure near infrared study of the mutated light-harvesting complex LH2. *Brazilian Journal of Medical and Biological Research* **38**, 1273–1278.

Braun, P., Olsen, J. D., Strohmann, B., Hunter, C. N. & Scheer, H. (2002). Assembly of light-harvesting bacteriochlorophyll in a model transmembrane helix in its natural environment. *Journal of Molecular Biology* **318**, 1085–1095.

Braun, P., Vegh, A. P., von Jan, M., Strohmann, B., Hunter, C. N., Robert, B. & Scheer, H. (2003). Identification of intramembrane hydrogen bonding between 13(1) keto group of bacteriochlorophyll and serine residue alpha27 in the LH2 light-harvesting complex. *Biochimica et Biophysica Acta – Bioenergetics* **1607**, 19–26.

Brunisholz, R. A. & Zuber, H. (1992). Structure, function and organization of antenna polypeptides and antenna complexes from the three families of Rhodospirillaneae. *Journal of Photochemistry and Photobiology B* **15**, 113–140.

Burland, D. M. & Zewail, A. H. (1979). Coherent processes in molecular crystals. In *Advances in Chemical Physics*, vol. 40 (eds. I. Prigogine & S. A. Rice), pp. 369. New York: John Wiley and Sons Inc.

Bylina, E. J., Robles, S. J. & Youvan, D. C. (1988). Directed mutations affecting the putative bacteriochlorophyll-binding sites in the light-harvesting I antenna of *Rhodobacter capsulatus*. *Israel Journal of Chemistry* **28**, 73–78.

Cerullo, G., Polli, D., Lanzani, G., De Silvestri, S., Hashimoto, H. & Cogdell, R. J. (2002). Photosynthetic light harvesting by carotenoids: Detection of an intermediate excited state. *Science* **298**, 2395–2398.

Chachisvilis, M., Kühn, O., Pullerits, T. & Sundström, V. (1997). Excitons in photosynthetic purple bacteria: wavelike motion or incoherent hopping? *Journal of Physical Chemistry B* **101**, 7275–7283.

Cheng, Y. C. & Silbey, R. J. (2006). Coherence in the B800 ring of purple bacteria LH2. *Physical Review Letters* **96**, 028103-1–028103-4.

Cherezov, V., Clogston, J., Papiz, M. Z. & Caffrey, M. (2006). Room to move: crystallizing membrane

proteins in swollen lipidic mesophases. *Journal of Molecular Biology* **357**, 1605–1618.

Chernyak, V. & Mukamel, S. (1996). Collective coordinates for nuclear spectral densities in energy transfer and femtosecond spectroscopy of molecular aggregates. *Journal of Chemical Physics* **105**, 4565–4583.

Chory, J., Donohue, T. J., Varga, A. R., Staehelin, L. A. & Kaplan, S. (1984). Induction of the photosynthetic membranes of *Rhodopseudomonas sphaeroides*: biochemical and morphological studies. *Journal of Bacteriology* **159**, 540–554.

Christensen, R. L. (1999). The electronic states of carotenoids. In *Advances in Photosynthesis*, vol. 8 (*Photochemistry of Carotenoids*) (eds. H. A. Frank, A. J. Young, G. Britton & R. J. Cogdell), pp. 137–157. Dordrecht: Kluwer Academic Publishers.

Cogdell, R. J., Durant, I., Valentine, J., Lindsay, J. G. & Schmidt, K. (1983). The isolation and partial characterization of the light-harvesting pigment-protein complement of *Rhodopseudomonas acidophila*. *Biochimica et Biophysica Acta – Bioenergetics* **722**, 427–435.

Cogdell, R. J. & Frank, H. A. (1987). How carotenoids function in photosynthetic bacteria. *Biochimica et Biophysica Acta – Bioenergetics* **895**, 63–79.

Cogdell, R. J., Fyfe, P. K., Barrett, S. J., Prince, S. M., Freer, A. A., Isaacs, N. W., McGlynn, P. & Hunter, C. N. (1996). The purple bacterial photosynthetic unit. *Photosynthesis Research* **48**, 55–63.

Cogdell, R. J., Hawthornthwaite, A. M., Evans, M. B., Ferguson, L. A., Kerfeld, C., Thornber, J. P., Van Mourik, F. & van Grondelle, R. (1990). Isolation and characterization of an unusual antenna complex from the marine purple sulfur photosynthetic bacterium *Chromatium purpuratum* BN5500. *Biochimica et Biophysica Acta – Bioenergetics* **1019**, 239–244.

Cogdell, R. J., Hipkins, M. F., MacDonald, W. & Truscott, T. G. (1981). Energy transfer between the carotenoid and the bacteriochlorophyll within the B800–850 light harvesting pigment-protein complex of *Rhodopseudomonas sphaeroides*. *Biochimica et Biophysica Acta – Bioenergetics* **634**, 191–202.

Cogdell, R. J. & Scheer, H. (1985). Circular dichroism of light-harvesting complexes from purple photosynthetic bacteria. *Photochemistry and Photobiology* **42**, 669–678.

Cogdell, R. J., Zuber, H., Thornber, J. P., Drews, G., Gingras, G., Niederman, R. A., Parson, W. W. & Feher, G. (1985). Recommendations for the naming of photochemical reaction centers and light-harvesting pigment-protein complexes from purple photosynthetic bacteria. *Biochimica et Biophysica Acta – Bioenergetics* **806**, 185–186.

Comayras, F., Jungas, C. & Lavergne, J. (2005a). Functional consequences of the organization of the photosynthetic apparatus in *Rhodobacter sphaeroides*: I. quinone domains and excitation transfer in chromatophores and reaction center-antenna complexes. *Journal of Biological Chemistry* **280**, 11203–11213.

Comayras, F., Jungas, C. & Lavergne, J. (2005b). Functional consequences of the organization of the photosynthetic apparatus in *Rhodobacter sphaeroides*: II. A study of PufX$^-$ membranes. *Journal of Biological Chemistry* **280**, 11214–11223.

Cory, M. G., Zerner, M. C., Hu, X. & Schulten, K. (1998). Electronic excitations in aggregates of bacteriochlorophylls. *Journal of Physical Chemistry B* **102**, 7640–7650.

Cramer, W. A., Yan, J., Zhang, H., Kurisu, G. & Smith, J. L. (2005). Structure of the cytochrome $b_6f$ complex: new prosthetic groups, Q-space, and the 'hors d'oeuvres hypothesis' for assembly of the complex. *Photosynthesis Research* **85**, 133–143.

Crielaard, W., Visschers, R. W., Fowler, G. J. S., van Grondelle, R., Hellingwerf, K. J. & Hunter, C. N. (1994). Probing the B800 bacteriochlorophyll binding site of the accessory light-harvesting complex from *Rhodobacter sphaeroides* using site-directed mutants. I. Mutagenegenesis, effects on binding, function and electronic behaviour of its carotenoids. *Biochimica et Biophysica Acta – Bioenergetics* **1183**, 473–482.

Dahlbom, M., Pullerits, T., Mukamel, S. & Sundström, V. (2001). Exciton delocalization in the B850 light-harvesting complex: comparison of different measures. *Journal of Physical Chemistry B* **105**, 5515–5524.

Davis, C. M., Bustamante, P. L. & Loach, P. A. (1995). Reconstitution of the bacterial core light-harvesting complexes of *Rhodobacter sphaeroides* and *Rhodospirillum rubrum* with Isolated $\alpha$- and $\beta$-polypeptides, bacteriochlorophyll *a*, and carotenoid. *Journal of Biological Chemistry* **270**, 5793–5804.

Davis, S. J., Vener, A. V. & Vierstra, R. D. (1999). Bacteriophytochromes: Phytochrome-like photoreceptors from nonphotosynthetic eubacteria. *Science* **286**, 2517–2520.

Davydov, A. S. (1948). Theory of absorption spectra of molecular crystals [in Russian]. *Zhurnal Eksperimentalnoi I Teoreticheskoi Fiziki* **18**, 210–218.

Davydov, A. S. (1971). *Theory of Molecular Excitons*. New York: Plenum.

de Caro, C., Visschers, R. W., van Grondelle, R. & Völker, S. (1994). Inter- and Intraband energy transfer in LH2 antenna complexes of purple bacteria. A fluorescence line narrowing and hole-burning study. *Journal of Physical Chemistry* **98**, 10584–10590.

Deinum, G., Otte, S. C. M., Gardiner, A. T., Aartsma, T. J., Cogdell, R. J. & Amesz, J. (1991). Antenna organization of *Rhodopseudomonas acidophila*: a study of the excitation migration. *Biochimica et Biophysica Acta – Bioenergetics* **1060**, 125–131.

Deisenhofer, J., Epp, O., Miki, K., Huber, R. & Michel, H. (1984). X-ray structure analysis of a membrane protein complex. Electron density map at 3Å resolution

and a model of the chromophores of the photosynthetic reaction center from *Rhodopseudomonas viridis*. *Journal of Molecular Biololgy* **180**, 385–398.

Deisenhofer, J., Epp, O., Miki, K., Huber, R. & Michel, H. (1985). Structure of the protein subunits in the photosynthetic reaction center of *Rhodopseudomonas viridis* at 3Å resolution. *Nature* **318**, 618–624.

DeLano, W. L. (2004). PyMOL. Delano Scientific LLC.

Dempster, S. E., Jang, S. & Silbey, R. J. (2001). Single molecule spectroscopy of disordered circular aggregates: A perturbation analysis. *Journal of Physical Chemistry* **114**, 10015–10023.

Dexter, D. L. (1953). A theory of sensitized luminescence in solids. *Journal of Chemical Physics* **21**, 836–850.

Didraga, C. & Knoester, J. (2002). Exchange narrowing in circular and cylindrical molecular aggregates: degenerate *versus* nondegenerate states. *Chemical Physics* **275**, 307–318.

Donohue, T. J., Kiley, P. J. & Kaplan, S. (1988). The *puf* operon region of *Rhodobacter sphaeroides*. *Photosynthesis Research* **19**, 39–61.

Dracheva, T. V., Novoderezhkin, V. I. & Razjivin, A. P. (1997). Exciton delocalization in the light-harvesting LH2 complex from photosynthetic purple bacteria. *Photochemistry and Photobiology* **66**, 605–610.

Drews, G. (1996). Formation of the light-harvesting complex I (B870) of anoxygenic phototrophic purple bacteria. *Archives of Microbiology* **166**, 151–159.

Drews, G. & Golecki, J. R. (1995). Structure, molecular organization, and biosynthesis of membranes of purple bacteria. In *Anoxygenic Photosynthetic Bacteria*, vol. 2. *Advances in Photosynthesis* (eds. R. E. Blakenship, M. T. Madigan & C. E. Bauer), pp. 231–257. Dordrecht: Kluwer Academic Publishers.

Du, S., Bird, T. H. & Bauer, C. E. (1998). DNA binding characteristics of RegA. A constitutively active anaerobic activator of photosynthesis gene expression in *Rhodobacter capsulatus*. *Journal of Biochemical Chemistry* **273**, 18509–18513.

Duysens, L. N. M. (1952). Transfer of excitation energy in photosynthesis. State University of Utrecht.

Eccles, J. & Honig, B. (1983). Charged amino acids as spectroscopic determinants for chlorophyll *in vivo*. *Proceedings of the National Academy of Sciences USA* **80**, 4959–4962.

Eraso, J. M. & Kaplan, S. (1994). prrA, a putative response regulator involved in oxygen regulation of photosynthesis gene expression in *Rhodobacter sphaeroides*. *Journal of Bacteriology* **176**, 32–43.

Eraso, J. M. & Kaplan, S. (1995). Oxygen-insensitive synthesis of the photosynthetic membranes of *Rhodobacter-sphaeroides* – a mutant histidine kinase. *Journal of Bacteriology* **177**, 2695–2706.

Eraso, J. M. & Kaplan, S. (1996). Complex regulatory activities associated with the histidine kinase PrrB in expression of photosynthesis genes in *Rhodobacter sphaeroides* 2.4.1. *Journal of Bacteriology* **178**, 7037–7046.

Evans, K., Fordham-Skelton, A. P., Mistry, H., Reynolds, C. D., Lawless, A. M. & Papiz, M. Z. (2005). A bacteriophytochrome regulates the synthesis of LH4 complexes in *Rhodopseudomonas palustris*. *Photosynthesis Research* **85**, 169–180.

Evans, M. B., Hawthornthwaite, A. M. & Cogdell, R. J. (1990). Isolation and characterization of the different B800–850 light-harvesting complexes from low- and high-light grown cells of *Rhodopseudomonas palustris*, strain 2.1.6. *Biochimica et Biophysica Acta – Bioenergetics* **1016**, 71–76.

Farchaus, J. W. & Oesterhelt, D. (1989). A *Rhodobacter sphaeroides pufL, M* and *X* deletion mutant and its complementation in *trans* with a 5·3 kb *puf* operon shuttle fragment. *EMBO Journal* **8**, 47–54.

Fidder, H., Knoester, J. & Wiersma, D. A. (1991). Optical properties of disordered molecular aggregates: A numerical study. *Journal of Chemical Physics* **95**, 7880–7890.

Fiedor, L., Akahane, J. & Koyama, Y. (2004). Carotenoid-induced cooperative formation of bacterial photosynthetic LH1 complex. *Biochemistry* **43**, 16487–16496.

Fiedor, L. & Scheer, H. (2005). Trapping of an assembly intermediate of photosynthetic LH1 antenna beyond B820 subunit. Significance for the assembly of photosynthetic LH1 antenna. *Journal of Biological Chemistry* **280**, 20921–20926.

Firsov, N. N. & Drews, G. (1977). Differentiation of the intracytoplasmic membrane of *Rhodopseudomonas palustris* induced by variations of oxygen partial pressure of light intensity. *Archives of Microbiology* **115**, 299–306.

Foote, C. S. (1976). Photosensitizatized oxidation and singlet oxygen: consequences in biological systems. In *Free Radicals and Biological Systems* (ed. W. A. Pryor). New York: Academic Press.

Foote, C. S., Chang, Y. C. & Denny, R. W. (1970). Chemistry of singlet oxygen 10. Carotenoid quenching parallels biological protection. *Journal of the American Chemical Society* **92**, 5216–5218.

Foote, C. S. & Denny, R. W. (1968). Chemistry of singlet oxygen 7. Quenching by beta-carotene. *Journal of the American Chemical Society* **90**, 6233–6235.

Fotiadis, D., Qian, P., Philippsen, A., Bullough, P. A., Engel, A. & Hunter, C. N. (2004). Structural analysis of the reaction center light-harvesting complex I photosynthetic core complex of *Rhodospirillum rubrum* using atomic force microscopy. *Journal of Biological Chemistry* **279**, 2063–2068.

Fowler, G. J. S., Hess, S., Pullerits, T., Sundström, V. & Hunter, C. N. (1997). Role of $\beta$Arg-10 in the B800 bacteriochlorophyll and carotenoid pigment environment within the light-harvesting LH2 complex of *Rhodobacter sphaeroides*. *Biochemistry* **36**, 11282–11291.

Fowler, G. J. S., Sockalingum, G. D., Robert, B. & Hunter, C. N. (1994). Blue shifts in bacteriochlorophyll absorbance correlate with changed hydrogen bonding patterns in light-harvesting 2 mutants of *Rhodobacter sphaeroides* with alterations at $\alpha$-Tyr-44 and $\alpha$-Tyr-45. *Biochemical Journal* **299**, 695–700.

Fowler, G. J. S., Visschers, R. W., Grief, G. G., van Grondelle, R. & Hunter, C. N. (1992). Genetically modified photosynthetic antenna complexes with blueshifted absorbance bands. *Nature* **355**, 848–850.

Frank, H. A. & Cogdell, R. J. (1993). The photochemistry and function of carotenoids in photosynthesis. In *Carotenoids in Photosynthesis* (ed. A. J. Young), pp. 252–326. London, UK: Chapman & Hall.

Frank, H. A. & Cogdell, R. J. (1996). Carotenoids in photosynthesis. *Photochemistry Photobiology* **63**, 257–264.

Frank, H. A., Josue, J. S., Bautista, J. A., van der Hoef, I., Jansen, F. J., Lugtenburg, J., Wiederrecht, G. & Christensen, R. (2002). Spectroscopic and photochemical properties of open-chain carotenoids. *Journal of Physical Chemistry B* **106**, 2083–2092.

Fraser, N. J., Dominy, P. J., Ücker, B., Simonin, I., Scheer, H. & Cogdell, R. J. (1999). Selective release, removal, and reconstitution of bacteriochlorophyll *a* molecules into the B800 sites of LH2 complexes from *Rhodopseudomonas acidophila* 10050. *Biochemistry* **38**, 9684–9692.

Freer, A., Prince, S., Sauer, K., Papiz, M., Hawthornthwaite-Lawless, A., McDermott, G., Cogdell, R. & Isaacs, N. W. (1996). Pigment-pigment interactions and energy transfer in the antenna complex of the photosynthetic bacterium *Rhodopseudomonas acidophila*. *Structure* **4**, 449–462.

Freiberg, A., Allen, J. P., Williams, J. & Woodbury, N. W. (1996). Energy trapping and detrapping by wild type and mutant reaction centers of purple non-sulfur bacteria. *Photosynthesis Research* **48**, 309–319.

Freiberg, A., Godik, V. I., Pullerits, T. & Timpmann, K. E. (1988). Directed picosecond excitation transport in purple photosynthetic bacteria. *Chemical Physics* **128**, 227–235.

Frenkel, J. (1931a). On the transformation of light into heat in solids. I. *Physical Review* **37**, 17–44.

Frenkel, J. (1931b). On the transformation of light into heat in solids. II. *Physical Review* **37**, 1276–1294.

Frese, R. N., Olsen, J. D., Branvall, R., Westerhuis, W. H. J., Hunter, C. N. & Van Grondelle, R. (2000). The long-range supraorganization of the bacterial photosynthetic unit: a key role for PufX. *Proceedings of the National Academy of Sciences USA* **97**, 5197–5202.

Frese, R. N., Siebert, C. A., Niederman, R. A., Hunter, C. N., Otto, C. & van Grondelle, R. (2004). The long-range organization of a native photosynthetic membrane. *Proceedings of the National Academy of Sciences USA* **101**, 17994–17999.

Fromme, P., Yu, H. Q., DeRuyter, Y. S., Jolley, C., Chauhan, D. K., Melkozernov, A. & Grotjohann, I. (2006). Structure of photosystems I and II. *Comptes Rendus Chimie* **9**, 188–200.

Fujii, R., Fujino, T., Inaba, T., Nagae, H. & Koyama, Y. (2004). Internal conversion of $1B^{+}{}_{u} \rightarrow 1B^{-}{}_{u} \rightarrow 2A^{-}{}_{g}$ and fluorescence from the $1B_{u}^{-}$ state in all-*trans*-neurosporene as probed by up-conversion spectroscopy. *Chemical Physics Letters* **384**, 9–15.

Fujii, R., Ishikawa, T., Koyama, Y., Taguchi, M., Isobe, Y., Nagae, H. & Watanabe, Y. (2001). Fluorescence spectroscopy of all-*trans*-anhydrorhodovibrin and spirilloxanthin: detection of the $1B_{u}^{-}$ fluorescence. *Journal of Physical Chemistry A* **105**, 5348–5355.

Fujii, R., Onaka, K., Kuki, M., Koyama, Y. & Watanabe, Y. (1998). The $2A_{g}^{-}$ energies of all-trans-neurosporene and spheroidene as determined by fluorescence spectroscopy. *Chemical Physics Letters* **288**, 847–853.

Fulcher, T. K., Beatty, J. T. & Jones, M. R. (1998). Demonstration of the key role played by the PufX protein in the functional and structural organization of native and hybrid bacterial photosynthetic core complexes. *Journal of Bacteriology* **180**, 642–646.

Gall, A. (1994). Purification, characterisation and crystallisation from a range of Rhodospirillneae pigment-protein complexes, Ph.D. thesis, University of Glasgow, UK.

Gall, A., Cogdell, R. J. & Robert, B. (2003a). Influence of carotenoid molecules on the structure of the bacteriochlorophyll binding site in peripheral light-harvesting proteins from *Rhodobacter sphaeroides*. *Biochemistry* **42**, 7252–7258.

Gall, A., Ellervee, A., Sturgis, J. N., Fraser, N. J., Cogdell, R. J., Freiberg, A. & Robert, B. (2003b). Membrane protein stability: high pressure effects on the structure and chromophore-binding properties of the light-harvesting complex LH2. *Biochemistry* **42**, 13019–13026.

Gall, A., Fraser, N. J., Bellissent-Funel, M.-C., Scheer, H., Robert, B. & Cogdell, R. J. (1999). Bacteriochlorin-protein interactions in native B800–B850, B800 deficient and B800-Bchl$a_{p}$-reconstituted complexes from *Rhodopseudomonas acidophila*, strain 10050. *FEBS Letters* **449**, 269–272.

Gall, A., Gardiner, A. T., Cogdell, R. J. & Robert, B. (2006). Carotenoid stoichiometry in the LH2 crystal: no spectral evidence for the presence of the second molecule in the $\alpha/\beta$-apoprotein dimer. *FEBS Letters* **580**, 3841–3844.

Gall, A., Henry, S., Takaichi, S., Robert, B. & Cogdell, R. J. (2005). Preferential uptake of coloured-carotenoids occurs in the LH2 complexes from non-sulphur purple bacteria under carotenoid-limiting conditions. *Photosynthesis Research* **86**, 25–35.

Gall, A., Robert, B., Cogdell, R. J., Bellissent-Funel, M. C. & Fraser, N. J. (2001). Probing the binding sites

of exchanged chlorophyll a in LH2 by Raman and site-selection fluorescence spectroscopies. *FEBS Letters* **491**, 143–147.

Gardinaru, C. C., Kennis, J. T. M., Papagiannakis, E., van Stokkum, I. H. M., Cogdell, R. J., Fleming, G. R., Niederman, R. A. & van Grondelle, R. (2001). An unusal pathway of excitation energy deactivation in carotenoids: Singlet-to-triplet conversion on an unltrafst timescale in photosynthetic antenna. *Proceedings of the National Academy of Sciences USA* **98**, 2364–2369.

Gauden, M., Yeremenko, S., Laan, W., van Stokkum, I. H., Ihalainen, J. A., van Grondelle, R., Hellingwerf, K. J. & Kennis, J. T. M. (2005). Photocycle of the flavin-binding photoreceptor AppA, a bacterial transcriptional antirepressor of photosynthesis genes. *Biochemistry* **44**, 3653–3662.

Gentemann, S., Nelson, N. Y., Jaquinod, L., Nurco, D. J., Leung, S. H., Medforth, C. J., Smith, K. M., Fajer, J. & Holten, D. (1997). Variations and temperature dependence of the excited state properties of conformationally and electronically perturbed zinc and free base porphyrins. *Journal of Physical Chemistry B* **101**, 1247–1254.

Georgakopoulou, S., Frese, R. N., Johnson, E., Koolhaas, C., Cogdell, R. J., van Grondelle, R. & van Der Zwan, G. (2002). Absorption and CD spectroscopy and modeling of various LH2 complexes from purple bacteria. *Biophysical Chemistry* **82**, 2184–2197.

Georgakopoulou, S., van Grondelle, R. & van Der Zwan, G. (2004). Circular dichroism of carotenoids in bacterial light-harvesting complexes: experiments and modeling. *Biophysical Journal* **87**, 3010–3022.

Gerken, U., Lupo, D., Tietz, C., Wrachtrup, J. & Ghosh, R. (2003). Circular symmetry of the light-harvesting 1 complex from *Rhodospirillum rubrum* is not perturbed by interaction with the reaction center. *Biochemistry* **42**, 10354–10360.

Germeroth, L., Lottspeich, F., Robert, B. & Michel, H. (1993). Unexpected similarities of the B800–850 light-harvesting complex from *Rhodospirillum molischianum* to the B870 light-harvesting complexes from other purple photosynthetic bacteria. *Biochemistry* **32**, 5615–5621.

Ghosh, R., Hauser, H. & Bachofen, R. (1988). Reversible dissociation of the B873 light-harvesting complex from *Rhodospirillum rubrum* G9$^{+}$. *Biochemistry* **27**, 1004–1014.

Giesberger, G. (1947). Some observations on the culture, physiology and morphology of some brown-red *Rhodospirillum* species. *Antonie van Leeuwenhoek* **13**, 135–148.

Giraud, E., Fardoux, J., Fourrier, N., Hannibal, L., Genty, B., Bouyer, P., Dreyfus, B. & Vermeglio, A. (2002). Bacteriophytochrome controls photosystem synthesis in anoxygenic bacteria. *Nature* **417**, 202–205.

Giraud, E., Zappa, S., Jaubert, M., Hannibal, L., Fardoux, J., Adriano, J. M., Bouyer, P., Genty, B., Pignol, D. & Vermeglio, A. (2004). Bacteriophytochrome and regulation of the synthesis of the photosynthetic apparatus in *Rhodopseudomonas palustris*: pitfalls of using laboratory strains. *Photochemical and Photobiological Sciences* **3**, 587–591.

Giraud, E., Zappa, S., Vuillet, L., Adriano, J. M., Hannibal, L., Fardoux, J., Berthomieu, C., Bouyer, P., Pignol, D. & Vermeglio, A. (2005). A new type of bacteriophytochrome acts in tandem with a classical bacteriophytochrome to control the antennae synthesis in *Rhodopseudomonas palustris*. *Journal of Biological Chemistry* **280**, 32389–32397.

Glaeser, J. & Klug, G. (2005). Photo-oxidative stress in *Rhodobacter sphaeroides*: protective role of carotenoids and expression of selected genes. *Microbiology-Sgm* **151**, 1927–1938.

Glaeser, J. & Overmann, J. (1999). Selective enrichment and characterization of *Roseospirillum parvum*, gen. nov and sp nov., a new purple nonsulfur bacterium with unusual light absorption properties. *Archives of Microbiology* **171**, 405–416.

Golecki, J., Drews, G. & Buhler, R. (1979). The size and number of intramembrane particles in cells of the photosynthetic bacterium *Rhodopseudomonas capsulata* studied by freeze-fracture electron microscopy. *Cytobiologie* **18**, 381–389.

Gomelsky, M. & Klug, G. (2002). BLUF: a novel FAD-binding domain involved in sensory transduction in microorganisms. *Trends in Biochemical Sciences* **27**, 497–500.

Gregor, J. & Klug, G. (2002). Oxygen-regulated expression of genes for pigment binding proteins in *Rhodobacter capsulatus*. *Journal of Molecular Microbiology and Biotechnology* **4**, 249–253.

Gudowska-Nowak, E., Newton, M. D. & Fajer, J. (1990). Conformational and environmental-effects on bacteriochlorophyll optical spectra – correlations of calculated spectra with structural results. *Journal of Physical Chemistry* **94**, 5795–5801.

Ha, T., Enderle, T., Chemla, D. S., Selvin, P. R. & Weiss, S. (1997). Quantum jumps of single molecules at room temperature. *Chemical Physical Letters* **271**, 1–5.

Halloren, E., McDermott, G., Lindsay, J. G., Miller, C., Freer, A. A., Isaacs, N. W. & Cogdell, R. J. (1995). Studies on the light-harvesting complexes from the thermotolerant purple bacterium *Rhodopseudomonas cryptolactis*. *Photosynthesis Research* **44**, 149–155.

Han, Y. C., Braatsch, S., Osterloh, L. & Klug, G. (2004). A eukaryotic BLUF domain mediates light-dependent gene expression in the purple bacterium *Rhodobacter sphaeroides* 2.4.1. *Proceedings of the National Academy of Sciences USA* **101**, 12306–12311.

Hartigan, N., Tharia, H. A., Sweeney, F., Lawless, A. M. & Papiz, M. Z. (2002). The 7·5 Å electron density and spectroscopic properties of a novel low-light B800

LH2 from *Rhodopseudomonas palustris*. *Biophysical Journal* **82**, 963–977.

Hartwich, G., Fiedor, L., Simonin, I., Cmiel, E., Schaefer, W., Noy, D., Scherz, A. & Scheer, H. (1998). Metal-substituted bacteriochlorophylls. 1. Preparation and influence of metal and coordination on spectra. *Journal of the American Chemical Society* **120**, 3675–3683.

Haselkorn, R., Lapidus, A., Kogan, Y., Vlcek, C., Paces, J., Paces, V., Ulbrich, P., Pecenkova, T., Rebrekov, D., Milgram, A., Mazur, M., Cox, R., Kyrpides, N., Ivanova, N., Kapatral, M., Los, T., Lykidis, A., Mikhailova, N., Reznik, G., Vasieva, O. & Fonstein, M. (2001). The *Rhodobacter capsulatus* genome. *Photosynthesis Research* **70**, 43–52.

Hashimoto, H., Yanagi, K., Yoshizawa, M., Polli, D., Cerullo, G., Lanzani, G., De Silvestri, S., Gardiner, A. T. & Cogdell, R. J. (2004). The very early events following photoexcitation of carotenoids. *Archives of Biochemistry and Biophysics* **430**, 61–69.

Hayashi, H., Nakano, M. & Morita, S. (1982). Comparative studies of protein properties and bacteriochlorophyll contents of bacteriochlorophyll-protein complexes from spectrally different types of *Rhodopseudomonas palustris*. *Journal of Biochemistry* **92**, 1805–1811.

Heinemeyer, E. A. & Schmidt, K. (1983). Changes in carotenoid biosynthesis caused by variations of growth conditions in cultures of *Rps. acidophila* strain 7050. *Archives of Microbiology* **134**, 217–221.

Herek, J. L., Fraser, N. J., Pullerits, T., Martinsson, P., Polivka, T., Scheer, H., Cogdell, R. J. & Sundström, V. (2000). B800→B850 energy transfer mechanism in bacterial LH2 complexes investigated by B800 pigment exchange. *Biophysical Journal* **78**, 2590–2596.

Hess, S., Chachisvilis, M., Timpmann, K., Jones, M. R., Fowler, G. J. S., Hunter, C. N. & Sundström, V. (1995). Temporally and spectrally resolved sub-picosecond energy transfer within the peripheral antenna complex (LH2) and from LH2 to the core antenna complex in photosynthetic purple bacteria. *Proceedings of the National Academy of Sciences USA* **92**, 12333–12337.

Hess, S., Feldchtein, F., Babin, A., Nurgaleev, I., Pullerits, T., Sergeev, A. & Sundström, V. (1993). Femtosecond energy transfer within the LH2 peripheral antenna of the photosynthetic purple bacteria *Rhodobacter sphaeroides* and *Rhodopseudomonas palustris* LL. *Chemical Physical Letters* **216**, 247–257.

Hess, S., Visscher, K. J., Pullerits, T., Sundström, V., Fowler, G. J. S. & Hunter, C. N. (1994). Enhanced rates of subpicosecond energy transfer in blue-shifted light-harvesting LH2 mutants of *Rhodobacter sphaeroides*. *Biochemistry* **33**, 8300–8305.

Hoff, A. J. & Deisenhofer, J. (1997). Photophysics of photosynthesis. Structure and spectroscopy of reaction centers of purple bacteria. *Physics Reports* **287**, 1–247.

Hofmann, C., Aartsma, T. J. & Köhler, J. (2004). Energetic disorder and the B850-excition states of Individual light-harvesting 2 complexes from *Rhodopseudomonas acidophila*. *Chemical Physical Letters* **395**, 373–378.

Hofmann, C., Aartsma, T. J., Michel, H. & Kohler, J. (2003a). Direct observation of tiers in the energy landscape of a chromoprotein: a single-molecule study. *Proceedings of the National Academy of Sciences USA* **100**, 15534–15538.

Hofmann, C., Ketelaars, M., Matsushita, M., Michel, H., Aartsma, T. J. & Köhler, J. (2003b). Single-molecule study of the electronic couplings in a circular array of molecules: Light-harvesting-2 complex from *Rhodospirillum molischianum*. *Physical Review Letters* **90**, 013004-1–013004-4.

Hofmann, C., Michel, H., van Heel, M. & Kohler, J. (2005). Multivariate analysis of single-molecule spectra: Surpassing spectral diffusion. *Physical Review Letters* **94**, 195501-1–195501-4.

Hu, Q., Sturgis, J. N., Robert, B., Delagrave, S., Youvan, D. C. & Niederman, R. A. (1998). Hydrogen bonding and circular dichroism of bacteriochlorophylls in the *Rhodobacter capsulatus* light-harvesting 2 complex altered by combinatorial mutagenesis. *Biochemistry* **37**, 10006–10015.

Hu, X. C., Ritz, T., Damjanovic, A., Autenrieth, F. & Schulten, K. (2002). Photosynthetic apparatus of purple bacteria. *Quarterly Reviews of Biophysics* **35**, 1–62.

Hu, X. C., Ritz, T., Damjanovic, A. & Schulten, K. (1997). Pigment organization and transfer of electronic excitation in the photosynthetic unit of purple bacteria. *Journal of Physical Chemistry B* **101**, 3854–3871.

Hughes, J., Lamparter, T., Mittmann, F., Hartmann, E., Gartner, W., Wilde, A. & Borner, T. (1997). A prokaryotic phytochrome. *Nature* **386**, 663.

Hunter, C. N., Hundle, B. S., Hearst, J. E., Lang, H. P., Gardiner, A. T., Takaichi, S. & Cogdell, R. J. (1994). Introduction of new carotenoids into the bacterial photosynthetic apparatus by combining the carotenoid biosynthetic pathways of *Erwinia herbicola* and *Rhodobacter sphaeroides*. *Journal of Bacteriology* **176**, 3692–3697.

Hunter, C. N., Pennoyer, J. D., Sturgis, J. N., Farrelly, D. & Niederman, R. A. (1988). Oligomerization states and associations of light-harvesting pigment-protein complexes of *Rhodobacter sphaeroides* as analyzed by lithium dodecyl sulfate-polyacrylamide gel electrophoresis. *Biochemistry* **27**, 3459–3467.

Imhoff, J. F. (1995). Taxonomy and physiology of phototrophic purple bacteria and green sulfur bacteria. In *Anoxygenic Photosynthetic Bacteria*, vol. 2. *Advances in Photosynthesis* (eds. R. E. Blakenship, M. T. Madigan &

C. E. Bauer), pp. 1–15. Dordrecht: Kluwer Academic Publishers.

IMHOFF, J. F. (2001). Transfer of *Rhodopseudomonas acidophila* to the new genus *Rhodoblastus* as *Rhodoblastus acidophilus* gen. nov., comb. nov. *International Journal of Systematic and Evolutionary Microbiology* **51**, 1863–1866.

IMHOFF, J. F. & TRÜPER, H. G. (1980). *Chromatium purpuratum*, sp. nov, a new species of the Chromatiaceae. *Zentralblatt Fur Bakteriologie Mikrobiologie Und Hygiene I Abteilung Originale C-Allgemeine Angewandte Und Okologische Mikrobiologie* **1**, 61–69.

IUPAC (1987). Nomenclature of tetrapyrroles. *Journal of Pure and Applied Chemistry* **59**, 787–832.

JANG, S., DEMPSTER, S. E. & SILBEY, R. J. (2001). Characterization of the static disorder in the B850 band of LH2. *Journal of Physical Chemistry B* **105**, 6655–6665.

JANG, S., MARSHALL, D. N. & SILBEY, R. J. (2004). Multichromophoric Forster resonance energy transfer. *Physical Review Letters* **92**, 21830-1-1–218301-4.

JANOSI, L., KEER, H., KOSZTIN, I. & RITZ, T. (2005). Influence of subunit structure on the oligomerization state of light harvesting complexes: a free energy calculation study. *Chemical Physics* **323**, 117–128.

JAUBERT, M., ZAPPA, S., FARDOUX, J., ADRIANO, J. M., HANNIBAL, L., ELSEN, S., LAVERGNE, J., VERMEGLIO, A., GIRAUD, E. & PIGNOL, D. (2004). Light and redox control of photosynthesis gene expression in *Bradyrhizobium* – dual roles of two PpsR. *Journal of Biological Chemistry* **279**, 44407–44416.

JAY, F., LAMBILLOTTE, M., STARK, W. & MUEHLETHALER, K. (1984). The preparation and characterization of native photoreceptor units from the thylakoids of *Rhodopseudomonas viridis*. *EMBO Journal* **3**, 773–776.

JIANG, Z. Y., SWEM, L. R., RUSHING, B. G., DEVANATHAN, S., TOLLIN, G. & BAUER, C. E. (1999). Bacterial photoreceptor with similarity to photoactive yellow protein and plant phytochromes. *Science* **285**, 406–409.

JIMENEZ, R., DIKSHIT, S., BRADFORTH, S. E. & FLEMING, G. R. (1996). Electronic excitation transfer in the LH2 complex from *Rhodobacter sphaeroides*. *Journal of Physical Chemistry* **100**, 6825–6834.

JOO, T., JIA, Y., YU, J.-Y., JONAS, D. M. & FLEMING, G. R. (1996). Dynamics in isolated bacterial light harvesting antenna (LH2) of *Rhodobacter sphaeroides* at room temperature. *Journal of Physical Chemistry* **100**, 2399–2409.

JUNGAS, C., RANCK, J. L., RIGAUD, J. L., JOLIOT, P. & VERMEGLIO, A. (1999). Supramolecular organisation of the photosynthetic apparatus of *Rhodobacter sphaeroides*. *EMBO Journal* **18**, 534–542.

KAPLAN, S., ERASO, J. & ROH, J. H. (2005). Interacting regulatory networks in the facultative photosynthetic bacterium, *Rhodobacter sphaeroides* 2.4.1. *Biochemical Society Transactions* **33**, 51–55.

KARNIOL, B. & VIERSTRA, R. D. (2003). The pair of bacteriophytochromes from *Agrobacterium tumefaciens* are histidine kinases with opposing photobiological properties. *Proceedings of the National Academy of Sciences USA* **100**, 2807–2812.

KARRASCH, S., BULLOUGH, P. A. & GHOSH, R. (1995). The 8·5 Å. projection map of the light-harvesting complex I from *Rhodospirillum rubrum* reveals a ring composed of 16 subunits. *EMBO Journal* **14**, 631–638.

KATONA, G., ANDREASSON, U., LANDAU, E. M., ANDREASSON, L. E. & NEUTZE, R. (2003). Lipidic cubic phase crystal structure of the photosynthetic reaction centre from *Rhodobacter sphaeroides* at 2·35 Å resolution. *Journal of Molecular Biology* **331**, 681–692.

KEHOE, J. W., MEADOWS, K. A., PARKES-LOACH, P. S. & LOACH, P. A. (1998). Reconstitution of core light-harvesting complexes of photosynthetic bacteria using chemically synthesized polypeptides. 2. Determination of structural features that stabilize complex formation and their implications for the structure of the subunit complex. *Biochemistry* **37**, 3418–3428.

KENNIS, J. T. M., STRELTSOV, A. M., PERMENTIER, H., AARTSMA, T. J. & AMESZ, J. (1997a). Exciton coherence and energy transfer in the LH2 antenna complex of *Rhodopseudomonas acidophila* at low temperature. *Journal of Physical Chemistry B* **101**, 8369–8374.

KENNIS, J. T. M., STRELTSOV, A. M., VULTO, S. I. E., AARTSMA, T. J., NOZAWA, T. & AMESZ, J. (1997b). Femtosecond dynamics in isolated LH2 complexes of various species of purple bacteria. *Journal of Physical Chemistry B* **101**, 7827–7834.

KETELAARS, M., VAN OIJEN, A. M., MATSUSHITA, M., KÖHLER, J., SCHMIDT, J. & AARTSMA, T. J. (2001). Spectroscopy on the B850 band of individual light-harvesting 2 complexes of *Rhodopseudomonas acidophila*; I. experiments and monte-carlo simulations. *Biophysical Journal* **80**, 1591–1603.

KHOROSHILOVA, N., POPESCU, C., MUNCK, E., BEINERT, H. & KILEY, P. J. (1997). Iron-sulfur cluster disassembly in the FNR protein of *Escherichia coli* by O-2: [4Fe-4S] to [2Fe-2S] conversion with loss of biological activity. *Proceedings of the National Academy of Sciences USA* **94**, 6087–6092.

KILEY, P. J., VARGA, A. & KAPLAN, S. (1988). Physiological and structural analysis of light-harvesting mutants of *Rhodobacter sphaeroides*. *Journal of Bacteriology* **170**, 1103–1115.

KIMURA, A. & KAKITANI, T. (2003). Theoretical analysis of the energy gap dependence of the reconstituted B800→B850 excitation energy transfer rate in bacterial LH2 complexes. *Journal of Physical Chemistry B* **107**, 7932–7939.

KINOSITA, K. (1999). Real time imaging of rotating molecular machines. *FASEB Journal* **13**, 201–208.

KITAMURA, K., TOKUNAGA, M., WANE, A. H. & YANAGIDA, T. (1999). A single myosin head moves along an actin filament with regular steps of 5·3 nanometres. *Nature* **397**, 129–134.

KLUG, G. & COHEN, S. N. (1988). Pleiotropic effects of localized *Rhodobacter capsulatus puf* operon deletions on production of light-absorbing pigment-protein complexes. *Journal of Bacteriology* **170**, 5814–5821.

KNOX, R. S. (1963). *Theory of Excitons*. New York: Academic Press.

KOBLIZEK, M., SHIH, J. D., BREITBART, S. I., RATCLIFFE, E. C., KOLBER, Z. S., HUNTER, C. N. & NIEDERMAN, R. A. (2005). Sequential assembly of photosynthetic units in *Rhodobacter sphaeroides* as revealed by fast repetition rate analysis of variable bacteriochlorophyll *a* fluorescence. *Biochimica et Biophysica Acta – Bioenergetics* **1706**, 220–231.

KOEPKE, J., HU, X., MUENKE, C., SCHULTEN, K. & MICHEL, H. (1996). The crystal structure of the light-harvesting complex II (B800–850) from *Rhodospirillum molischianum*. *Structure* **4**, 581–597.

KOLACZKOWSKI, S. V., HAYES, J. M. & SMALL, G. J. (1994). A Theory of dispersive kinetics in the energy-transfer of antenna complexes. *Journal of Physical Chemistry* **98**, 13418–13425.

KOMIYA, H., YEATES, T. O., REES, D. C., ALLEN, J. P. & FEHER, G. (1988). Structure of the reaction center from *Rhodobacter sphaeroides* R-26 and 2.4.1: 6. Symmetry relations and sequence comparisons between different species. *Proceedings of the National Academy of Sciences USA* **85**, 9012–9016.

KOOLHAAS, M. H. C., FRESE, R. N., FOWLER, G. J. S., BIBBY, T. A., GEORGAKOPOULOU, S., ZWAN, G. V. D., HUNTER, C. N. & VAN GRONDELLE, R. (1998). Identification of the upper exciton component of the B850 bacteriochlorophylls of the LH2 antenna complex, using a B800-free mutant of *Rhodobacter sphaeroides*. *Biochemistry* **37**, 4693–4698.

KOYAMA, Y., KUKI, M., ANDERSSON, P. O. & GILLBRO, T. (1996). Singlet excited states and the light-harvesting function of carotenoids in bacterial photosynthesis. *Photochemisty and Photobiolgy* **63**, 243–256.

KOYAMA, Y., RONDONUWU, F. S., FUJII, R. & WATANABE, Y. (2004). Light-harvesting function of carotenoids in photo-synthesis: The roles of the newly found $1B_u^-$ state. *Biopolymers* **74**, 2–18.

KRIKUNOVA, M., KUMMROW, A., VOIGT, B., RINI, M., LOKSTEIN, H., MOSKALENKO, A., SCHEER, H., RAZJIVIN, A. & LEUPOLD, D. (2002). Fluorescence of native and carotenoid-depleted LH2 from *Chromatium minutissimum*, originating from simultaneous two-photon absorption in the spectral range of the presumed (optically 'dark') $S_1$ state of carotenoids. *FEBS Letters* **528**, 227–29.

KRINSKY, N. I. (1978). Non-photosynthetic functions of carotenoids. *Philosophical Transactions of the Royal Society of London Series B – Biological Sciences* **284**, 581–590.

KRUEGER, B. P., SCHOLES, G. D. & FLEMING, G. R. (1998). Calculation of couplings and energy-transfer pathways between the pigments of LH2 by the *ab initio* transition density cube method. *Journal of Physical Chemistry B* **102**, 5378–5387.

KRUEGER, B. P., SCHOLES, G. D., GOULD, I. R. & FLEMING, G. R. (1999). Carotenoid-mediated B800 B850 coupling in LH2. *PhysChemComm* **2**, 34–40.

KUHN, O. & SUNDSTRÖM, V. (1997). Pump-probe spectroscopy of dissipative energy transfer dynamics in photosynthetic antenna complexes: A density matrix approach. *Journal of Chemical Physics* **107**, 4154–4164.

KUKURA, P., MCCAMANT, D. W. & MATHIES, R. A. (2004). Femtosecond time-resolved stimulated Raman spectroscopy of the S-2 $^1B_u^+$ excited state of beta-carotene. *Journal of Physical Chemistry A* **108**, 5921–5925.

KULZER, F. & ORRIT, M. (2004). Single-molecule optics. *Annual Review of Physical Chemistry* **55**, 585–611.

KURISU, G., ZHANG, H., SMITH, J. L. & CRAMER, W. A. (2003). Structure of the cytochrome $b_6f$ complex of oxygenic photosynthesis: tuning the cavity. *Science* **302**, 1009–1014.

KWA, L. G., GARCIA-MARTIN, A., VEGH, A. P., STROHMANN, B., ROBERT, B. & BRAUN, P. (2004). Hydrogen bonding in a model bacteriochlorophyll-binding site drives assembly of light harvesting complex. *Journal of Biological Chemistry* **279**, 15067–15075.

KYNDT, J. A., FITCH, J. C., MEYER, T. E. & CUSANOVICH, M. A. (2005). *Thermochromatium tepidum* photoactive yellow protein/bacteriophytochrome/diguanylate cyclase: characterization of the PYP domain. *Biochemistry* **44**, 4755–4764.

KYNDT, J. A., MEYER, T. E. & CUSANOVICH, M. A. (2004). Photoactive yellow protein, bacteriophytochrome, and sensory rhodopsin in purple phototrophic bacteria. *Photochemical and Photobiological Sciences* **3**, 519–530.

LAAN, W., GAUDEN, M., YEREMENKO, S., VAN GRONDELLE, R., KENNIS, J. T. M., & HELLINGWERF, K. J. (2006). On the mechanism of activation of the BLUF domain of AppA. *Biochemistry* **45**, 51–60.

LANG, H. P. & HUNTER, C. N. (1994). The relationship between carotenoid biosynthesis and the assembly of the light-harvesting LH2 complex in *Rhodobacter sphaeroides*. *Biochemical Journal* **298**, 197–205.

LAPOUGE, K., NÄVEKE, A., GALL, A., SEGUIN, J., SCHEER, H., STURGIS, J. & ROBERT, B. (1999). Conformation of bacteriochlorophyll molecules in photosynthetic proteins from purple bacteria. *Biochemistry* **38**, 11115–11121.

LAPOUGE, K., NÄVEKE, A., ROBERT, B., SCHEER, H. & STURGIS, J. N. (2000). Exchanging cofactors in the core antennae from purple bacteria: structure and properties of Zn-bacteriopheophytin-containing LH1. *Biochemistry* **39**, 1091–1099.

LARIMER, F. W., CHAIN, P., HAUSER, L., LAMERDIN, J., MALFATTI, S., DO, L., LAND, M. L., PELLETIER, D. A., BEATTY, J. T., LANG, A. S., TABITA, F. R., GIBSON, J. L., HANSON, T. E., BOBST, C., TORRES, J., PERES, C., HARRISON, F. H., GIBSON, J. & HARWOOD, C. S. (2004).

Complete genome sequence of the metabolically versatile photosynthetic bacterium *Rhodopseudomonas palustris*. *Nature Biotechnology* **22**, 55–61.

Law, C. J. & Cogdell, R. J. (1998). The effect of chemical oxidation on the fluorescence of the LH1 (B880) complex from the purple bacterium *Rhodobium marinum*. *FEBS Letters* **432**, 27–30.

Leegwater, J. A. (1996). Coherent versus incoherent energy transfer and trapping in photosynthetic antenna complexes. *Journal of Physical Chemistry* **100**, 14403–14409.

Leupold, D., Stiel, H., Teuchner, K., Nowak, F., Sandner, W., Uecker, B. & Scheer, H. (1996). Size enhancement of transition dipoles to one- and two-exciton bands in a photosynthetic antenna. *Physical Review Letters* **77**, 4675–4678.

Lilburn, T. G. & Beatty, J. T. (1992). Suppressor mutants of the photosynthetically incompetent *puf*X deletion mutant *Rhodobacter capsulatus* DRC6 (pTL2). *FEMS Microbiological Letters* **100**, 155–160.

Lilburn, T. G., Haith, C. E., Prince, R. C. & Beatty, J. T. (1992). Pleiotropic effects of *pufX* gene deletion on the structure and function of the photosynthetic apparatus of *Rhodobacter capsulatus*. *Biochimica et Biophysica Acta – Bioenergetics* **1100**, 160–170.

Lin, C. (2000). Plant blue-light receptors. *Trends in Plant Science* **5**, 337–342.

Linnanto, J., Korppi-Tommola, J. E. I., Helenius, V. M. (1999). Electronic states, absorption spectrum and circular dichroism spectrum of the photosynthetic bacterial LH2 antenna of *Rhodopseudomonas acidophila* as predicted by exciton theory and semiempirical calculations. *Journal of Physical Chemistry B* **103**, 8739–8750.

Loach, P. A. & Parkes-Loach, P. S. (1995). Structure-function relationships in core light-harvesting complexes (LHI) as determined by characterization of the structural subunit and by reconstitution experiments. In *Anoxygenic Photosynthetic Bacteria*, vol. 2. *Advances in Photosynthesis* (eds. R. E. Blakenship, M. T. Madigan & C. E. Bauer), pp. 437–71. Dordrecht: Kluwer Academic Publishers.

Losi, A. (2004). The bacterial cunerparts of plant phototropins. *Photochemical and Photobiological Sciences* **3**, 566–574.

Lu, H. P., Xun, L. & Xie, S. (1998). Single molecule enzymatic dynamics. *Science* **282**, 1877–1882.

Lutz, M. & Robert, B. (1988). Chlorophylls and the photosynthetic membrane. In *Biological applications of Raman spectroscopy*, vol. III (ed. T. G. Spiro), pp. 347–411. Indianapolis, USA: John Wiley and Sons Inc.

Ma, Y.-Z., Cogdell, R. J. & Gillbro, T. (1997). Energy transfer and exciton annihilation in the B800–850 antenna complex of the photosynthetic purple bacterium *Rhodopseudomonas acidophila* (strain 10050). A fentosecond transient absorption study. *Journal of Physical Chemistry B* **101**, 1087–1095.

MacKenzie, C., Choudhary, M., Larimer, F. W., Predki, P. F., Stilwagen, S., Armitage, J. P., Barber, R. D., Donohue, T. J., Hosler, J. P., Newman, J. E., Shapleigh, J. P., Socket, R. E., Zeilstra-Ryalls, J. & Kaplan, S. (2001). The home stretch, a first analysis of the nearly competed genome of *Rhodobacter sphaeroides* 2.4.1. *Photosynthesis Research* **70**, 19–41.

MacPherson, A. N., Arellano, J. B., Fraser, N. J., Cogdell, R. J. & Gillbro, T. (2001). Efficient energy transfer from the carotenoid $S_2$ state in a photosynthetic light-harvesting complex. *Biophysical Journal* **80**, 923–930.

Masuda, S. & Bauer, C. E. (2002). AppA is a blue light photoreceptor that antirepresses photosynthesis gene expression in *Rhodobacter sphaeroides*. *Cell* **110**, 613–623.

Matsushita, M., Ketelaars, M., van Oijen, A. M., Köhler, J., Aartsma, T. J. & Schmidt, J. (2001). Spectroscopy on the B850 band of individual light-harvesting 2 complexes of *Rhodopseudomonas acidophila*; II. Exciton states of an elliptically deformed ring aggregate. *Biophysical Journal* **80**, 1604–1614.

Matsuzaki, S., Zazubovich, V., Fraser, N. J., Cogdell, R. J. & Small, G. J. (2001). Energy transfer dynamics in LH2 complexes of *Rhodopseudomonas acidophila* containing only one B800 molecule. *Journal of Physical Chemistry B* **105**, 7049–7056.

McDermott, G., Prince, S. M., Freer, A. A., Hawthornthwaite-Lawless, A. M., Papiz, M. Z., Cogdell, R. J. & Isaacs, N. W. (1995). Crystal structure of an integral membrane light-harvesting complex from photosynthetic bacteria. *Nature* **374**, 517–521.

McGlynn, P., Westerhuis, W. H. J., Jones, M. R. & Hunter, C. N. (1996). Consequences for the organization of reaction center-light harvesting antenna 1 (LH1) core complexes of *Rhodobacter sphaeroides* arising from deletion of amino acid residues from the C terminus of the LH1 $\alpha$ polypeptide. *Journal of Biological Chemistry* **271**, 3285–3292.

McLuskey, K., Prince, S. M., Cogdell, R. J. & Isaacs, N. W. (2001). The crystallographic structure of the B800–820 LH3 light-harvesting complex from the purple bacteria *Rhodopseudomonas acidophila* strain 7050. *Biochemistry* **40**, 8783–8789.

Meadows, K. A., Parkes-Loach, P. S., Kehoe, J. W. & Loach, P. A. (1998). Reconstitution of core light-harvesting complexes of photosynthetic bacteria using chemically synthesized polypeptides. 1. Minimal requirements for subunit formation. *Biochemistry* **37**, 3411–3417.

Meckenstock, R. U., Brunisholz, R. A. & Zuber, H. (1992a). The light-harvesting core-complex and the B820-subunit from *Rhodopseudomonas marina*. Part I. Purification and characterisation. *FEBS Letters* **311**, 128–134.

MECKENSTOCK, R. U., KRUSCHE, K., BRUNISHOLZ, R. A. & ZUBER, H. (1992b). The light-harvesting core-complex and the B820-subunit from *Rhodopseudomonas marina*. Part II. Electron microscopic characterisation. *FEBS Letters* **311**, 135–138.

MECKENSTOCK, R. U., KRUSCHE, K., STAEHELIN, L. A., CYRKLAFF, M. & ZUBER, H. (1994). The six fold symmetry of the B880 light-harvesting complex and the structure of the photosynthetic membranes of *Rhodopseudomonas marina*. *Biological Chemistry Hoppe-Seyler* **375**, 429–438.

MEIER, T., CHERNYAK, V. & MUKAMEL, S. (1997). Multiple exciton coherence sizes in photosynthetic antenna complexes viewed by pump-probe spectroscopy. *Journal of Physical Chemistry B* **101**, 7332–7342.

MILLER, K. R. (1979). Structure of a bacterial photosynthetic membrane. *Proceedings of the National Academy of Sciences USA* **76**, 6415–6419.

MILLER, K. R. (1982). Three-dimensional structure of a photosynthetic membrane. *Nature* **300**, 53–55.

MOERNER, W. E. & BASCH, T. (1993). Optical spectroscopy of single impurity molecules in solids. *Angewandte Chemie International Edition* (in English) **32**, 457–476.

MOERNER, W. E. & KADOR, L. (1989). Optical detection and spectroscopy of single molecules in a solid. *Physical Review Letters* **62**, 2535–2538.

MONGER, T. G., COGDELL, R. J. & PARSON, W. W. (1976). Triplet states of bacteriochlorophyll and carotenoids in chromatophores of photosynthetic bacteria. *Biochimica et Biophysica Acta – Bioenergetics* **449**, 136–153.

MONSHOUWER, R., ABRAHAMSON, M., VAN MOURIK, F. & VAN GRONDELLE, R. (1997). Superradiance and exciton delocalization in bacterial photosynthetic light-harvesting systems. *Journal of Physical Chemistry B* **101**, 7241–7248.

MONSHOUWER, R., DE ZARATE, I. O., VAN MOURIK, F., PICOREL, R., COGDELL, R. J. & VAN GRONDELLE, R. (1995). Energy transfer in the LH 2 complex of *Rb. sphaeroides* and *Rps. acidophila* studied by sub picosecond absorption spectroscopy. In *Photosynthesis: Light Biosphere, Proceedings of the 10th International Photosynthesis Congress* (ed. P. Mathis), pp. 91–94. Dordrecht: Kluwer.

MOSER, C. C., PAGE, C. C., COGDELL, R. J., BARBER, J., WRAIGHT, C. A. & DUTTON, P. L. (2003). Length, time, and energy scales of photosystems. *Advances in Protein Chemistry* **63**, 71–109.

MOSLEY, C., SUZUKI, J. & BAUER, C. (1994). Identification and molecular genetic characterization of a sensor kinase responsible for coordinately regulating light harvesting and reaction center gene expression in response to anaerobiosis *Journal of Bacteriology* **176**, 7566–7573 [published Erratum appears in *Journal of Bacteriology* (1995), **177**, 3359].

MOSTOVOY, M. V. & KNOESTER, J. (2000). Statistics of optical spectra from single ring aggregates and its application to LH2. *Journal of Physical Chemistry B* **104**, 12355–12364.

MUKAI, K., ABE, S. & SUMI, H. (1999). Theory of rapid excitation energy transfer from B800 to optically forbidden exciton states of B850 in the antenna system LH2 of photosynthic purple bacteria. *Journal of Physical Chemistry B* **103**, 6096–6102.

MUSEWALD, C., HARTWICH, G., LOSSAU, H., GILCH, P., POLLINGER-DAMMER, F., SCHEER, H. & MICHEL-BEYERLE, M. E. (1999). Ultrafast photophysics and photochemistry of [Ni]-bacteriochlorophyll *a*. *Journal of Physical Chemistry B* **103**, 7055–7060.

MUSEWALD, C., HARTWICH, G., POELLINGER-DAMMER, F., LOSSAU, H., SCHEER, H. & MICHEL-BEYERLE, M. E. (1998). Time-resolved spectral investigation of bacteriochlorophyll *a* and its transmetalated derivatives [Zn]-Bacteriochlorophyll *a* and [Pd]-Bacteriochlorophyll *a*. *Journal of Physical Chemistry B* **102**, 8336–8342.

NAGAE, H., KAKITANI, T., KATOH, T. & MIMURO, M. (1993). Calculation of the excitation transfer-matrix elements between the $S_2$ or $S_1$ ctate of carotenoid and the $S_2$ or $S_1$ state of bacteriochlorophyll. *Journal of Chemical Physics* **98**, 8012–8023.

NAGARAJAN, V. & PARSON, W. W. (1997). Excitation energy transfer between the B850 and B875 antenna complexes of *Rhodobacter sphaeroides*. *Biochemistry* **36**, 2300–2306.

NAKAMURA, R., FUJII, R., NAGAE, H., KOYAMA, Y. & KANEMATSU, Y. (2004). Vibrational relaxation in the $1B_u^+$ state of carotenoids as determined by Kerr-gate fluorescence spectroscopy. *Chemical Physics Letters* **400**, 7–14.

NISHIMURA, K., RONDONUWU, F. S., FUJII, R., AKAHANE, J., KOYAMA, Y. & KOBAYASHI, T. (2004). Sequential singlet internal conversion of $1B_u^+ \rightarrow 3A_g \rightarrow 1B_u \rightarrow 2A_g \Rightarrow (1A_g^-$ ground) in all-trans-spirilloxanthin revealed by two-dimensional sub-5-fs spectroscopy. *Chemical Physics Letters* **392**, 68–73.

NOVODEREZHKIN, V. I., MONSHOUWER, R. & VAN GRONDELLE, R. (1999). Exciton (de)localization in the LH2 antenna of *Rhodobacter sphaeroides* as revealed by relative difference absorption measurements of the LH2 antenna and the B820 subunit. *Journal of Physical Chemistry B* **103**, 10540–10548.

OH, J. I. & KAPLAN, S. (2001). Generalized approach to the regulation and integration of gene expression. *Molecular Microbiology* **39**, 1116–1123.

OH, J.-I. & KAPLAN, S. (2000). Redox signaling: globalization of gene expression. *EMBO Journal* **19**, 4237–4247.

OH, J. I., KO, I. J. & KAPLAN, S. (2004). Reconstitution of the *Rhodobacter sphaeroides* $cbb_3$-PrrBA signal transduction pathway *in vitro*. *Biochemistry* **43**, 7915–7923.

OLSEN, J. D., ROBERT, B., SIEBERT, C. A., BULLOUGH, P. A. & HUNTER, C. N. (2003). Role of the C-terminal extrinsic region of the alpha polypeptide of the

light-harvesting 2 complex of *Rhodobacter sphaeroides*: a domain swap study. *Biochemistry* **42**, 15114–15123.

Olsen, J. D., Sockalingum, G. D., Robert, B. & Hunter, C. N. (1994). Modification of a hydrogen bond to a bacteriochlorophyll a molecule in the light-harvesting 1 antenna of *Rhodobacter sphaeroides*. *Proceedings of the National Academy of Sciencs USA* **91**, 7124–7128.

Olsen, J. D., Sturgis, J. N., Westerhuis, W. H. J., Fowler, G. J. S., Hunter, C. N. & Robert, B. (1997). Site-directed modification of the ligands to the bacteriochlorophylls of the light-harvesting LH1 and LH2 complexes of *Rhodobacter sphaeroides*. *Biochemistry* **36**, 12625–12632.

Orrit, M. & Bernard, J. (1990). Single pentacene molecules detected by fluorescence excitation in a *p*-terphenyl crystal. *Physical Review Letters* **65**, 2716–2719.

Orrit, M., Bernard, J. & Personov, R. I. (1993). High-resolution spectroscopy of organic molecules in solids: from fluorescence line narrowing and hole burning to single molecule spectroscopy. *Journal of Physical Chemistry B* **97**, 10256–10268.

Pandit, A., van Stokkum, I., Georgakopoulou, S., van der Zwan, G. & van Grondelle, R. (2003). Investigations of intermediates appearing in the reassociation of the light-harvesting 1 complex of *Rhodospirillum rubrum*. *Photosynthesis Research* **75**, 235–248.

Pandit, A., Visschers, R. W., van Stokkum, I. H. M., Kraayenhof, R. & van Grondelle, R. (2001). Oligomerization of light-harvesting I antenna peptides of *Rhodospirillum rubrum*. *Biochemistry* **40**, 12913–12924.

Papagiannakis, E., Das, S. K., Gall, A., Van Stokkum, I. H. M., Robert, B., VanGrondelle, R., Frank, H. A. & Kennis, J. T. M. (2003). Light harvesting by carotenoids Incorporated into the B850 light-harvesting complex from *Rhodobacter sphaeroides* R-26·1: Excited-state relaxation, ultrafast triplet formation, and energy transfer to bacteriochlorophyll. *Journal of Physical Chemistry B* **107**, 5642–5649.

Papagiannakis, E., Kennis, J. T. M., van Stokkum, I. H. M., Cogdell, R. J. & van Grondelle, R. (2002). An alternative carotenoid-to-bacteriochlorophyll energy transfer pathway in photosynthetic light harvesting. *Proceedings of the National Academy of Sciences USA* **99**, 6017–6022.

Papiz, M. Z., Prince, S. M., Howard, T., Cogdell, R. J. & Isaacs, N. W. (2003). The structure and thermal motion of the B800–850 LH2 complex from *Rps. acidophila* at 2·0 Å resolution and 100K: New structural features and functionally relevant motions. *Journal of Molecular Biolology* **326**, 1523–1538.

Pappas, C. T., Sram, J., Moskvin, O. V., Ivanov, P. S., Mackenzie, R. C., Choudhary, M., Land, M. L., Larimer, F. W., Kaplan, S. & Gomelsky, M. (2004). Construction and validation of the *Rhodobacter sphaeroides* 2.4.1 DNA microarray: Transcriptome flexibility at diverse growth modes. *Journal of Bacteriology* **186**, 4748–4758.

Parkes-Loach, P. S., Law, C. J., Recchia, P. A., Kehoe, J., Nehrlich, S., Chen, J. & Loach, P. A. (2001). Role of the core region of the PufX protein in inhibition of reconstitution of the core light-harvesting complexes of *Rhodobacter sphaeroides* and *Rhodobacter capsulatus*. *Biochemistry* **40**, 5593–5601.

Parkes-Loach, P. S., Majeed, A. P., Law, C. J. & Loach, P. A. (2004). Interactions stabilizing the structure of the core light-harvesting complex (LH1) of photosynthetic bacteria and Its subunit (B820). *Biochemistry* **43**, 7003–7016.

Parkes-Loach, P. S., Sprinkle, J. R. & Loach, P. A. (1988). Reconstitution of the B873 light-harvesting complex of *Rhodospirillum rubrum* from the separately isolated $\alpha$- and $\beta$-polypeptides and bacteriochlorophyll *a*. *Biochemistry* **27**, 2718–2727.

Pfennig, N. (1967). Photosynthetic bacteria. *Annual Review of Microbiology* **21**, 285–325.

Pfennig, N. (1978). General physiology and ecology of photosyntheic bacteria. In *The Photosynthetic Bacteria* (eds. R. K. Clayton & W. R. Sistrom), pp. 3–18. New York: Plenum Publishing Coporation.

Phillips-Jones, M. K. & Hunter, C. N. (1994). Cloning and nucleotide sequence of *regA*, a putative response regulator gene of *Rhodobacter sphaeroides*. *FEMS Microbiology Letters* **116**, 269–275.

Plakhotnik, T., Donley, E. A. & Wild, U. P. (1997). Single molecule spectroscopy. *Annual Review of Physical Chemistry* **48**, 181–212.

Polivka, T. & Sundström, V. (2004). Ultrafast dynamics of carotenoid excited states – from solution to natural and artificial systems. *Chemical Reviews* **104**, 2021–2071.

Polivka, T., Zigmantas, D., Herek, J. L., He, Z., Pascher, T., Pullerits, T., Cogdell, R. J., Frank, H. A. & Sundström, V. (2002). The carotenoid $S_1$ state in LH2 complexes from purple bacteria *Rhodobacter sphaeroides* and *Rhodopseudomonas acidophila*: $S_1$ energies, dynamics, and carotenoid radical formation. *Journal of Physical Chemistry B* **106**, 11016–11025.

Polli, D., Cerullo, G., Lanzani, G., De Silvestri, S., Yanagi, K., Hashimoto, H. & Cogdell, R. J. (2004). Conjugation length dependence of internal conversion in carotenoids: Role of the intermediate state. *Physical Review Letters* **93**, 163002-1-163002-4.

Prince, S. M., Papiz, M. Z., Freer, A. A., McDermott, G., Hawthornthwaite-Lawless, A. M., Cogdell, R. J. & Isaacs, N. W. (1997). Apoprotein structure in the LH2 complex from *Rhodopseudomonas acidophila* strain 10050: modular assembly and protein pigment interactions. *Journal of Molecular Biology* **268**, 412–423.

Pugh, R. J., McGlynn, P., Jones, M. R. & Hunter, C. N. (1998). The LH1-RC core complex of *Rhodobacter sphaeroides*: interaction between components, time-dependent assembly, and topology of the PufX

protein. *Biochimica et Biophysica Acta – Bioenergetics* **1366**, 301–316.

Pullerits, T., Chachisvillis, M. & Sundström, V. (1996). Exciton delocalization length in the B850 antenna of *Rhodobacter sphaeroides*. *Journal of Physical Chemistry* **100**, 10787–10792.

Pullerits, T., Hess, S., Herek, J. L. & Sundström, V. (1997). Temperature dependence of excitation transfer in LH2 of *Rhodobacter sphaeroides*. *Journal of Physical Chemistry B* **101**, 10560–10567.

Pullerits, T. & Sundström, V. (1996). Photosynthetic light harvesting pigment-protein complexes: towards understaning how and why. *Accounts of Chemical Research* **29**, 381–389.

Qian, P., Hunter, C. N. & Bullough, P. A. (2005). The 8·5 Å projection structure of the core RC-LH1-PufX dimer of *Rhodobacter sphaeroides*. *Journal of Molecular Biology* **349**, 948–960.

Ray, J. & Makri, N. (1999). Short range coherence in the energy transfer of photosynthetic light harvesting systems. *Journal of Physical Chemistry A* **103**, 9417–9422.

Rebane, K. K. (1970). *Impurity Spectra in Solids*. New York: Plenum Press.

Recchia, P. A., Davis, C. M., Lilburn, T. G., Beatty, J. T., Parkes-Loach, P. S., Hunter, C. N. & Loach, P. A. (1998). Isolation of the PufX protein from *Rhodobacter capsulatus* and *Rhodobacter sphaeroides*: Evidence for its interaction with the $\alpha$-polypeptide of the core light-harvesting complex. *Biochemistry* **37**, 11055–11063.

Reddy, N., Picorel, R. & Small, G. J. (1992a). B896 and B870 components of the *Rhodobacter sphaeroides* antenna: a hole burning study. *Journal of Physical Chemistry* **96**, 6458–6464.

Reddy, N. R. S., Cogdell, R. J., Zhao, L. & Small, G. J. (1993). Nonphotochemical hole burning of the B800–B850 antenna complex of *Rhodopseudomonas acidophila*. *Photochemistry and Photobiology* **57**, 35–39.

Reddy, N. R. S., Lyle, P. A. & Small, G. J. (1992b). Applications of spectral hole burning spectroscopies to antenna and reaction center complexes. *Photosynthesis Research* **31**, 167–194.

Reddy, N. R. S., Manson, N. B. & Krausz, E. R. (1987). Two-Laser spectral hole burning in a colour centre in diamond. *Journal of Luminesance* **38**, 46–47.

Reddy, N. R. S., Small, G. J., Seibert, M. & Picorel, R. (1991). Energy transfer dynamics of the B800–B850 antenna complex of *Rhodobacter sphaeroides*: a hole burning study. *Chemical and Physical Letters* **181**, 391–399.

Reddy, N. R. S., Wu, H.-M., Jankowiak, R., Picorel, R., Cogdell, R. J. & Small, G. J. (1996). High pressure studies of energy transfer and strongly coupled bacteriochlorophyll dimers in photosynthetic protein complexes. *Photosynthesis Research* **48**, 277–289.

Reslewic, S., Zhou, S., Place, M., Zhang, Y., Briska, A., Goldstein, S., Churas, C., Runnheim, R., Forrest, D., Lim, A., Lapidus, A., Han, C. S., Roberts, G. P. & Schwartz, D. C. (2005). Whole-genome shotgun optical mapping of *Rhodospirillum rubrum*. *Applied and Environmental Microbiology* **71**, 5511–5522.

Richter, P., Cortez, N. & Drews, G. (1991). Possible role of the highly conserved amino acids Trp-8 and Pro-13 in the N-terminal segment of the pigment-binding polypeptide LH$\alpha$ of *Rhodobacter capsulatus*. *FEBS Letters* **285**, 80–84.

Rigler, R., Orrit, M. & Basche, T. (2001). Single molecule spectroscopy. In *Nobel Conference Lectures*, vol. 67. *Springer Series in Chemical Physics*. Springer-Verlag, Berlin.

Robert, B. (1996). Resonance Raman studies in photosynthesis – chlorophyll and carotenoid molecules. In *Biophysical Techniques in Photosynthesis*, vol. 3. *Advances in photosynthesis* (eds. A. Amez & A. Hoff), pp. 161–276. Amsterdam: Kluwer Academic Publishers.

Robert, B., Cogdell, R. J. & van Grondelle, R. (2003). The Light-harvesting system of purple bacteria. In *Light-harvesting Antennas in Photosynthesis*, vol. 13. *Advances in Photosynthesis* (eds. B. B. Green & W. W. Parson), pp. 169–194. Dordrecht: Kluwer Academic Publishers.

Robert, B. & Lutz, M. (1985). Structure of antenna complexes of several Rhodospirillales from their resonance Raman spectra. *Biochimica et Biophysica Acta – Bioenergetics* **807**, 10–23.

Robinson, G. W. (1970). Electronic and vibrational excitons in molecular crystals. *Annual Review of Physical Chemistry* **21**, 429–474.

Roh, J. H., Smith, W. E. & Kaplan, S. (2004). Effects of oxygen and light intensity on transcriptome expression in *Rhodobacter sphaeroides* 2.4.1 – redox active gene expression profile. *Journal of Biological Chemistry* **279**, 9146–9155.

Rondonuwu, F. S., Yokoyama, K., Fujii, R., Koyama, Y., Cogdell, R. J. & Watanabe, Y. (2004). The role of the $11B_u^-$ state in carotenoid-to-bacteriochlorophyll singlet-energy transfer in the LH2 antenna complexes from Rhodobacter sphaeroides G1C, *Rhodobacter sphaeroides* 2.4.1, *Rhodospirillum molischianum* and *Rhodopseudomonas acidophila*. *Chemical Physics Letters* **390**, 314–322.

Roszak, A. W., Howard, T. D., Southall, J., Gardiner, A. T., Law, C. J., Isaacs, N. W. & Cogdell, R. J. (2003). Crystal structure of the RC-LH1 core complex from *Rhodopseudomonas palustris*. *Science* **302**, 1969–1972.

Rutkauskas, D., Novoderezhkin, V., Cogdell, R. J. & van Grondelle, R. (2005). Fluorescence spectroscopy of conformational changes of single LH2 complexes. *Biophysical Journal* **88**, 422–435.

Sabaty, M., Jappe, J., Olive, J. & Vermeglio, A. (1994). Organization of electron transfer components in *Rhodobacter sphaeroides* forma sp. *denitrificans* whole cells. *Biochimica et Biophysica Acta – Bioenergetics* **1187**, 313–323.

Sage, C. R., Rutenber, E. E., Stout, T. J. & Stroud, R. M. (1996). An essential role for water in an enzyme

reaction mechanism: the crystal structure of the thymidylate synthase mutant E58Q. *Biochemistry* **35**, 16270–16281.

Salverda, J. M., van Mourik, F., van der Zwan, G. & van Grondelle, R. (2000). Energy transfer in the B800 rings of the peripheral bacterial light-harvesting complexes of *Rhodopseudomomas acidophila* and *Rhodosprillium molischianum* with photon echo techiques. *Journal of Physical Chemistry B* **104**, 11395–11408.

Sauer, K., Cogdell, R. J., Prince, S. M., Freer, A., Isaacs, N. W. & Scheer, H. (1996). Structure-based calculations of the optical spectra of the LH2 bacteriochlorophyll-protein complex from *Rhodopseudomonas acidophila*. *Photochemistry and Photobiology* **64**, 564–576.

Sauer, K., Smith, J. R. L. & Schultz, A. J. (1966). Dimerization of chlorophyll *a*, chlorophyll *b* and bacteriochlorophyll in solution. *Journal of the American Chemical Society* **88**, 2681–2688.

Scheer, H. (1991). *Chlorophylls*. Boca Raton, FL: CRC Press.

Scheuring, S., Busselez, J. & Levy, D. (2005). Structure of the dimeric PufX-containing core complex of *Rhodobacter blasticus* by *in situ* atomic force microscopy. *Journal of Biological Chemistry* **280**, 1426–1431.

Scheuring, S., Francia, F., Busselez, J., Melandri, B. A., Rigaud, J. L. & Levy, D. (2004a). Structural role of PufX in the dimerization of the photosynthetic core complex of *Rhodobacter sphaeroides*. *Journal of Biological Chemistry* **279**, 3620–3626.

Scheuring, S., Reiss-Husson, F., Engel, A., Rigaud, J. L. & Ranck, J. L. (2001). High-resolution AFM topographs of *Rubrivivax gelatinosus* light-harvesting complex LH2. *EMBO Journal* **20**, 3029–3035.

Scheuring, S., Rigaud, J. L. & Sturgis, J. N. (2004b). Variable LH2 stoichiometry and core clustering in native membranes of *Rhodospirillum photometricum*. *EMBO Journal* **23**, 4127–4133.

Scheuring, S., Seguin, J., Marco, S., Levy, D., Robert, B. & Rigaud, J.-L. (2003). Nanodissection and high-resolution imaging of the *Rhodopseudomonas viridis* photosynthetic core complex in native membranes by AFM. *Proceedings of the National Academy of Sciences USA* **100**, 1690–1693.

Schmidt, T., Schütz, G. J., Baumgartner, W., Gruber, H. J. & Schindler, H. (1996). Imaging of single molecule diffusion. *Proceedings of the National Academy of Sciences USA* **93**, 2926–2929.

Scholes, G. D. & Fleming, G. R. (2000). On the mechanism of light-harvesting in photosynthetic purple bacteria: B800 to B850 energy transfer. *Journal of Physical Chemistry B* **104**, 1854–1868.

Scholes, G. D., Gould, I. R., Cogdell, R. J. & Fleming, G. R. (1999). *Ab initio* molecular orbital calculations of electronic couplings in the LH2 bacterial light-harvesting complex of *Rhodopseudomonas acidophila*. *Journal of Physical Chemistry B* **103**, 2543–2553.

Scholes, G. D., Jordanides, X. J. & Fleming, G. R. (2001). Adapting the Förster theory of energy transfer for modeling dynamics in aggregated molecular assemblies. *Journal of Physical Chemistry B* **105**, 1640–1651.

Sganga, M. W. & Bauer, C. E. (1992). Regulatory factors controlling photosynthetic reaction center and light-harvesting gene expression in *Rhodobacter capsulatus*. *Cell* **68**, 945–954.

Shreve, A. P., Trautman, J. K., Frank, H. A., Owens, T. G. & Albrecht, A. C. (1991). Femtosecond energy-transfer processes in the B800–850 light-harvesting complex of *Rhodobacter sphaeroides* 2.4.1. *Biochimica et Biophysica Acta – Bioenergetics* **1058**, 280–288.

Siebert, C. A., Qian, P., Fotiadis, D., Engel, A., Hunter, C. N. & Bullough, P. A. (2004). Molecular architecture of photosynthetic membranes in *Rhodobacter sphaeroides*: the role of PufX. *EMBO Journal* **23**, 690–700.

Silbey, R. J. (1976). Electronic transfer in molecular crystals. *Annual Review of Physical Chemistry* **27**, 203–223.

Sistrom, W. R. (1978). Phototaxis and chemotaxis. In *Photosynthetic Bacteria* (ed. R. K. Clayton), pp. 899–905. New York: Plenum.

Small, G. J. (1995). On the validity of the standard model for primary charge separation in the bacterial reaction center. *Chemical Physics* **197**, 239–257.

Stadtwald-Demchick, R., Turner, F. R. & Gest, H. (1990). *Rhodopseudomonas cryptolactis*, sp. Nov., a new thermotolerant species of budding phototrophic purple bacteria. *FEMS Microbiology Letters* **71**, 117–121.

Stahlberg, H., Dubochet, J., Vogel, H. & Ghosh, R. (1998). Are the light-harvesting I complexes from *Rhodospirillum rubrum* arranged around the reaction center in a square geometry? *Journal of Molecular Biology* **282**, 819–831.

Stark, W., Jay, F. & Muehlethaler, K. (1986). Localization of reaction center and light harvesting complexes in the photosynthetic unit of *Rhodopseudomonas viridis*. *Archives of Microbiology* **146**, 130–133.

Stock, A. M., Robinson, V. L. & Goudreau, P. N. (2000). Two-component signal transduction. *Annual Review of Biochemistry* **69**, 183–215.

Stock, D., Leslie, A. G. N. W. & Walker, J. E. (1999). Molecular architecture of the rotary motor in ATP synthase. *Science* **286**, 1700–1705.

Stroebel, D., Choquet, Y., Popot, J. L. & Picot, D. (2003). An atypical haem in the cytochrome $b_6f$ complex. *Nature* **426**, 413–418.

Sturgis, J. N., Gall, A., Ellervee, A., Freiberg, A. & Robert, B. (1998). The effect of pressure on the bacteriochlorophyll *a* binding sites of the core antenna complex from *Rhodospirillum rubrum*. *Biochemistry* **37**, 14875–14880.

Sturgis, J. N., Jirsakova, V., Reiss-Husson, F., Cogdell, R. J. & Robert, B. (1995). Structure and properties of

the bacteriochlorophyll binding site in peripheral light-harvesting complexes of purple bacteria. *Biochemistry* **34**, 517–523.

STURGIS, J. N. & ROBERT, B. (1994). Thermodynamics of membrane polypeptide oligomerization in light-harvesting complexes and associated structural changes. *Journal of Molecular Biology* **238**, 445–454.

STURGIS, J. N. & ROBERT, B. (1997). Pigment binding-site and electronic properties in light-harvesting proteins of purple bacteria. *Journal of Physical Chemistry B* **101**, 7227–7231.

SUMI, H. (1999). Theory on rates of excitation energy transfer between molecular aggregates through distributed transition dipoles with application to the antenna system in bacterial photosynthesis. *Journal of Physical Chemistry B* **103**, 252–260.

SUMI, H. (2000). Structural strategies in the antenna system of photosynthesis on the basis of quantum-mechanical coherence among pigments. *Journal of Luminescence* **87**, 71–76.

SUMI, H. (2001). Bacterial photosynthesis begins with quantum-mechanical coherence. *Chemical Record* **1**, 480–493.

SUNDSTRÖM, V., PULLERITS, T. & VAN GRONDELLE, R. (1999). Photosynthetic light-harvesting: Reconciling dynamics and structure of purple bacterial LH2 reveals function of photosynthetic unit. *Journal of Physical Chemistry B* **103**, 2327–2346.

SUNDSTRÖM, V. & VAN GRONDELLE, R. (1995). Kinetics of excitation transfer and trapping in purple bacteria. In *Anoxygenic Photosynthetic Bacteria*, vol. 2. *Advances in Photosynthesis* (eds. R. E. Blankenship, M. T. Madigan & C. E. Bauer), pp. 350–372. Dordrecht: Kluwer Academic Publishers.

SUNDSTRÖM, V., VAN GRONDELLE, R., BERGSTRÖM, H., AAKESSON, E. & GILLBRO, T. (1986). Excitation-energy transport in the bacteriochlorophyll antenna systems of *Rhodospirillum rubrum* and *Rhodobacter sphaeroides*, studied by low-intensity picosecond absorption spectroscopy. *Biochimica et Biophysica Acta – Bioenergetics* **851**, 431–446.

SWEM, L. R., ELSEN, S., BIRD, T. H., SWEM, D. L., KOCH, H.-G., MYLLYKALLIO, H., DALDAL, F. & BAUER, C. E. (2001). The RegB/RegA two-component regulatory system controls synthesis of photosynthesis and respiratory electron transfer components in *Rhodobacter capsulatus*. *Journal of Molecular Biology* **309**, 121–138.

TADROS, M. H., KATSIOU, E., HOON, M. A., YURKOVA, N. & RAMJI, D. P. (1993). Cloning of a new antenna gene cluster and expression analysis of the antenna gene family of *Rhodopseudomonas palustris*. *European Journal of Biochemistry* **217**, 867–875.

TADROS, M. H. & WATERKAMP, K. (1989). Multiple copies of the coding regions for the light-harvesting B800–850 $\alpha$- and $\beta$-polypeptides are present in the *Rhodopseudomonas palustris* genome. *EMBO Journal* **8**, 1303–1308.

TAKAICHI, S. (1999). Carotenoids and carotenogenesis in anoxygenic photosynthetic bacteria. In *The photochemistry of carotenoids*, vol. 8. *Advances in photosynthesis* (eds. H. A. Frank, A. J. Young, G. Britton & R. J. Cogdell), pp. 39–69. Dordrecht: Kluwer Academic Publishers.

TAKEMOTO, J. & LASCELLES, J. (1973). Coupling between bacteriochlorophyll and membrane protein synthesis in *Rhodopseudomonas spheroides*. *Proceedings of the National Academy of Sciences USA* **70**, 799–803.

TARS, M., ELLERVEE, A., KUKK, P., LAISAAR, A., SAARNAK, A. & FREIBERG, A. (1994). Photosynthetic proteins under high pressure. *Lietuvos fizikos žurnalas* **34**, 320–328.

TAVAN, P. & SCHULTEN, K. (1986). The low-lying electronic excitations in long polyenes: A PPP-MRD-CI study. *Journal of Chemical Physics* **85**, 6602–6609.

TAYLOR, B. L. & ZHULIN, I. B. (1999). PAS domains: internal sensors of oxygen, redox potential, and light. *Microbiology and Molelcular Biology Review* **63**, 479–506.

THARIA, H. A., NIGHTINGALE, T. D., PAPIZ, M. Z. & LAWLESS, A. M. (1999). Characterisation of hydrophobic peptides by RP-HPLC from different spectral forms of LH2 isolated from *Rps. palustris*. *Photosynthesis Research* **61**, 157–167.

THOULESS, D. J. (1974). Electrons in disordered systems and the theory of localization. *Physics Reports* **13**, 93–142.

TIETZ, C., CHEKLOV, O., DRÄBENSTEDT, A., SCHUSTER, J. & WRACHTRUP, J. (1999). Spectroscopy on single light harvesting complexes at low temperature. *Journal of Physical Chemistry B* **103**, 6328–6333.

TIETZ, C., GERKEN, U., JELEZKO, F. & WRACHTRUP, J. (2000). Polarization measurements on single pigment protein complexes. *Single Molecules* **1**, 67–72.

TIMPMANN, K., ELLERVEE, A., PULLERITS, T., RUUS, R., SUNDSTRÖM, V. & FREIBERG, A. (2001). Short-range exciton couplings in LH2 photosynthetic antenna proteins studied by high hydrostatic pressure absorption spectroscopy. *Journal of Physical Chemistry B* **105**, 8436–8444.

TODD, J. B., PARKES-LOACH, P. S., LEYKAM, J. F. & LOACH, P. A. (1998). *In vitro* reconstitution of the core and peripheral light-harvesting complexes of *Rhodospirillum molischianum* from separately isolated components. *Biochemistry* **37**, 17458–17468.

TODD, J. B., RECCHIA, P. A., PARKES-LOACH, P. S., OLSEN, J. D., FOWLER, G. J. S., MCGLYNN, P., HUNTER, C. N. & LOACH, P. A. (1999). Minimal requirements for in vitro reconstitution of the structural subunit of light-harvesting complexes of photosynthetic bacteria. *Photosynthesis Research* **62**, 85–98.

TOROPYGINA, O. A., MAKHNEVA, Z. K. & MOSKALENKO, A. A. (2003). Reconstitution of carotenoids into the light-harvesting complex B800–850 of *Chromatium minutissimum*. *Biochemistry – Moscow* **68**, 901–911.

TRETIAK, S., MIDDLETON, C., CHERNYAK, V. & MUKAMEL, S. (2000a). Bacteriochlorophyll and carotenoid excitonic

couplings in the LH2 system of purple bacteria. *Journal of Physical Chemistry B* **104**, 9540–9553.

Tretiak, S., Middleton, C., Chernyak, V. & Mukamel, S. (2000b). Exciton Hamiltonian for the bacteriochlorophyll system in the LH2 antenna complex of purple bacteria. *Journal of Physical Chemistry* B **104**, 4519–4528.

Trissl, H.-W. (1996). Antenna organization in purple bacteria investigated by means of fluorescence induction curves. *Photosynthesis Research* **47**, 175–185.

Tronrud, D. E., Schmid, M. F. & Matthews, B. W. (1986). Structure and X-ray amino acid sequence of a bacteriochlorophyll a protein from *Prosthecochloris aestuarii* refined at 1·9 Å resolution. *Journal of Molecular Biology* **188**, 443–454.

Trinkunas, G. & Freiberg, A. (2006). A disordered polaron model for polarized fluorescence excitation spectra of LH1 and LH2 bacteriochlorophyll antenna aggregates. *Journal of Luminescence* **119**, 105–115.

Urboniene, V., Vrublevskaja, O., Gall, A., Trinkunas, G., Robert, B. & Valkunas, L. (2005). Temperature broadening of LH2 absorption in glycerol solution. *Photosynthesis Research* **86**, 49–59.

van Amerongen, H., Valkunas, L. & Grondelle, V. (2000). *Photosynthetic Excitons*. Singapore: World Scientific.

van der Laan, H., Schmidt, T., Visschers, R. W., Visscher, K. J., van Grondelle, R. & Volker, S. (1990). Energy transfer in the B800–850 antenna complex of purple bacteria *Rhodobacter sphaeroides*: a study by spectral hole-burning. *Chemical Physical Letters* **170**, 231–238.

van Gammeren, A. J., Buda, F., Hulsbergen, F. B., Kiihne, S., Hollander, J. G., Egorova-Zachernyuk, T. A., Fraser, N. J., Cogdell, R. J. & de Groot, H. J. (2005). Selective chemical shift assignment of B800 and B850 bacteriochlorophylls in uniformly [$^{13}$C, $^{15}$N]-labeled light-harvesting complexes by solid-state NMR spectroscopy at ultra-high magnetic field. *Journal of the American Chemical Society* **127**, 3213–3219.

van Grondelle, R., Bergström, H., Sundström, V. & Gillbro, T. (1987). Energy transfer within the bacteriochlorophyll antenna of purple bacteria at 77 K, studied by picosecond absorption recovery. *Biochimica et Biophysica Acta – Bioenergetics* **894**, 313–326.

van Grondelle, R., Dekker, J. P., Gillbro, T. & Sundström, V. (1994). Energy transfer and trapping in photosynthesis. *Biochimica et Biophysica Acta – Bioenergetics* **1187**, 1–65.

van Grondelle, R. & Novoderezhkin, V. I. (2006). Energy transfer in photosynthesis: experimental insights and quantitative models. *Physical Chemistry Chemical Physics* **8**, 793–807.

van Heel, M., Gowen, B., Matadeen, R., Orlova, E. V., Finn, R., Pape, T., Cohen, D., Stark, H., Schmidt, R., Schatz, M. & Patwardhan, A. (2000). Single-particle electron cryo-microscopy: towards atomic resolution. *Quarterly Reviews of Biophysics* **33**, 307–369.

van Oijen, A. M., Ketelaars, M., Köhler, J., Aartsma, T. J. & Schmidt, J. (1998). Spectroscopy of single light-harvesting complexes from purple photosynthetic bacteria at 1·2 K. *Journal of Physcal Chemistry B* **102**, 9363–9366.

van Oijen, A. M., Ketelaars, M., Köhler, J., Aartsma, T. J. & Schmidt, J. (1999a). Spectroscopy of individual LH2 complexes of *Rhodopseudomonas acidophila*: Localized excitations in the B800 band. *Chemical Physics* **247**, 53–60.

van Oijen, A. M., Ketelaars, M., Köhler, J., Aartsma, T. J. & Schmidt, J. (1999b). Unraveling the electronic structure of individual photosynthetic pigment-protein complexes. *Science* **285**, 400–402.

van Oijen, A. M., Ketelaars, M., Köhler, J., Aartsma, T. J. & Schmidt, J. (2000). Spectroscopy of Individual LH2 complexes of *Rhodopseudomonas acidophila*: Diagonal disorder, sample heterogeneity, spectral diffusion, and energy transfer in the B800 band. *Biophysical Journal* **78**, 1570–1577.

Vegh, A. P. & Robert, B. (2002). Spectroscopic characterisation of a tetrameric subunit form of the core antenna protein from *Rhodospirillum rubrum*. *FEBS Letters* **528**, 222–226.

Visscher, K. J., Bergström, H., Sundström, V., Hunter, C. N. & van Grondelle, R. (1989). Temperature dependence of energy transfer from the long wavelength antenna BChl-869 to the reaction center in *Rhodospirillum rubrum*, *Rhodobacter sphaeroides* (w.t. and M21 mutant) from 77 to 177 K, studied by picosecond absorption spectroscopy. *Photosynthesis Research* **22**, 211–217.

Visschers, R. W., Crielaard, W., Fowler, G. J. S., Hunter, C. N. & Grondelle, R. V. (1994). Probing the B800 bacteriochlorophyll binding site of the accessory light-harvesting complex from *Rhodobacter sphaeroides* using site-directed mutants. II. A low-temperature spectroscopy study of structural aspects of the pigment-protein conformation. *Biochimica et Biophysica Acta – Bioenergetics* **1183**, 483–490.

Visschers, R. W., Germeroth, L., Michel, H., Monshouwer, R. & van Grondelle, R. (1995). Spectroscopic properties of the light-harvesting complexes from *Rhodospirillum molischianum*. *Biochimica et Biophysica Acta – Bioenergetics* **1230**, 147–154.

Visschers, R. W., Nunn, R., Calkoen, F., Van Mourik, F., Hunter, C. N., Rice, D. W. & van Grondelle, R. (1992). Spectroscopic characterization of B820 subunits from light-harvesting complex I of *Rhodospirillum rubrum* and *Rhodobacter sphaeroides* prepared with the detergent n-octyl-rac-2,3-dipropylsulfoxide. *Biochimica et Biophysica Acta – Protein Structure and Molecular Enzymology* **1100**, 259–266.

WAKAO, N., YOKOI, N., ISOYAMA, N., HIRAISHI, A., SHIMADA, K., KOBAYASHI, M., KISE, H., IWAKI, M., ITOH, S., TAKAICHI, S. & SAKURAI, Y. (1996). Discovery of natural photosynthesis using Zn-containing bacteriochlorophyll in an aerobic bacterium *Acidiphilium rubrum*. *Plant Cell Physiology* **37**, 889–893.

WALKER, C. J. & WILLOWS, R. D. (1997). Mechanism and regulation of Mg-chelatase. *Biochemical Journal* **327**, 321–333.

WESTERHUIS, W. H. J., HUNTER, C. N., VAN GRONDELLE, R. & NIEDERMAN, R. A. (1999). Modeling of oligomeric-state dependent spectral heterogeneity in the B875 light-harvesting complex of *Rhodobacter sphaeroides* by numerical simulation. *Journal of Physical Chemistry B* **103**, 7733–7742.

WESTERHUIS, W. H. J., STURGIS, J. N., RATCLIFFE, E. C., HUNTER, C. N. & NIEDERMAN, R. A. (2002). Isolation, size estimates, and spectral heterogeneity of an oligomeric series of light-harvesting 1 complexes from *Rhodobacter sphaeroides*. *Biochemistry* **41**, 8698–8707.

WILLOWS, R. D., GIBSON, L. C. D., KANANGARA, C. G., HUNTER, C. N. & VONWETTSTEIN, D. (1996). Three separate proteins constitute the magnesium chelatase of *Rhodobacter sphaeroides*. *European Journal of Biochemistry* **235**, 438–443.

WOHLLEBEN, W., BUCKUP, T., HEREK, J. L., COGDELL, R. J. & MOTZKUS, M. (2003). Multichannel carotenoid deactivation in photosynthetic light harvesting as identified by an evolutionary target analysis. *Biophysical Journal* **85**, 442–450.

WOLF, H. C. (1967). Energy transfer in organic molecular crystals: a survey of experiments. *Advances in Atomic and Molecular Physics* **3**, 119–142.

WRACHTRUP, J., AARTSMA, T. J., KÖHLER, J., KETELAARS, M., VAN OIJEN, A. M., MATSUSHITA, M., SCHMIDT, J., TIETZ, C. & JELEZKO, F. (2002). Spectroscopy of individual photosynthetic pigment-protein complexes. In *Single Molecule Detection in Solution, Methods and Application* (eds. C. Zander, J. Enderlein & R. A. Keller), pp. 185–229. Berlin: Wiley-VCH.

WU, H.-M., RATSEP, M., JANKOWIAK, R., COGDELL, R. J. & SMALL, G. J. (1997a). Comparison of the LH2 antenna complexes of *Rhodopseudomonas acidophila* (strain 10050) and *Rhodobacter sphaeroides* by high-pressure absorption, high-pressure hole burning, and temperature-dependent absorption spectroscopies. *Journal of Physical Chemistry B* **101**, 7641–7653.

WU, H.-M., RATSEP, M., JANKOWIAK, R., COGDELL, R. J. & SMALL, G. J. (1998). Hole-burning and absorption studies of the LH1 antenna complex of purple bacteria: effects of pressure and temperature. *Journal of Physical Chemistry B* **102**, 4023–4034.

WU, H.-M., RATSEP, M., LEE, I.-J., COGDELL, R. J. & SMALL, G. J. (1997b). Exciton level structure and energy disorder of the B850 ring of the LH2 antenna complex. *Journal of Physical Chemistry B* **101**, 7654–7663.

WU, H.-M., SAVIKHIN, S., REDDY, N. R. S., JANKOWIAK, R., COGDELL, R. J., STRUVE, W. S. & SMALL, G. J. (1996). Femtosecond and hole-burning studies of B800's excitation energy relaxation dynamics in the LH2 antenna complex of *Rhodopseudomonas acidophila* (strain 10050). *Journal of Physical Chemistry* **100**, 12022–12033.

WU, H.-M. & SMALL, G. J. (1998). Symmetry-based analysis of the effects of random energy disorder on the excitonic level structure of cyclic arrays: application to photosynthetic antenna complexes. *Journal of Physical Chemistry B* **102**, 888–898.

XIE, S. & TRAUTMAN, J. K. (1998). Optical studies of single molecules at room temperature. *Annual Review of Physical Chemistry* **49**, 441–480.

YANG, M., AGARWAL, R. & FLEMING, G. R. (2001). The mechanism of energy transfer in the antenna of photosynthetic purple bacteria. *Journal of Photochemistry and Photobiology A: Chemistry* **142**, 107–119.

YARIV, A. (1982). *Quantum Mechanics: An introduction to Theory and Applications of Quantum Mechanics*. New York: Wiley.

YEATES, T. O., KOMIYA, H., CHIRINO, A., REES, D. C., ALLEN, J. P. & FEHER, G. (1988). Structure of the reaction center from *Rhodobacter sphaeroides* R-26 and 2.4.1: Part 4. Protein-cofactor (bacteriochlorophyll, bacteriopheophytin, and carotenoid) interactions. *Proceedings of the National Academy of Sciences USA* **85**, 7993–7997.

YEATES, T. O., KOMIYA, H., REES, D. C., ALLEN, J. P. & FEHER, G. (1987). Structure of the reaction center from *Rhodobacter sphaeroides* R-26: Part 3. Membrane-protein interactions. *Proceedings of the National Academy of Sciences USA* **84**, 6438–6442.

YOUNG, C. S. & BEATTY, J. T. (2003). Multi-level regulation of purple bacterial light-haresting complexes. In *Light-harvesting Antennas in Photosynthesis*, vol. 13. *Advances in Photosynthesis* (eds. B. B. Green & W. W. Parson), pp. 449–470. Dordrecht: Kluwer Academic Publishers.

YURKOV, V. V. & BEATTY, J. T. (1998). Aerobic anoxygenic phototrophic bacteria. *Microbiology and Molecular Biology Reviews* **62**, 695–724.

ZANDER, C., ENDERLEIN, J. & KELLER, R. A. (2002). *Single Molecule Detection in Solution, Methods and Application*, pp. 371. Berlin: Wiley-VCH.

ZAZUBOVICH, V., JANKOWIAK, R. & SMALL, G. J. (2002a). A high-pressure spectral hole burning study of correlation between energy disorder and excitonic couplings in the LH 2 complex from *Rhodopseudomonas acidophila*. *Journal of Physical Chemistry B* **106**, 6802–6814.

ZAZUBOVICH, V., JANKOWIAK, R. & SMALL, G. J. (2002b). On B800→B800 energy transfer in the LH2 complex of purple bacteria. *Journal of Luminescence* **98**, 123–129.

ZEILSTRA-RYALLS, J. H. & KAPLAN, S. (2004). Oxygen intervention in the regulation of gene expression: the photosynthetic bacterial paradigm. *Cellular and Molecular Life Sciences* **61**, 417–436.

Zhang, F. G., Gillbro, T., van Grondelle, R. & Sundström, V. (1992a). Dynamics of energy transfer and trapping in the light-harvesting antenna of *Rhodopseudomonas viridis*. *Biophysical Journal* **61**, 694–703.

Zhang, F. G., van Grondelle, R. & Sundström, V. (1992b). Pathways of energy flow through the light-harvesting antenna of the photosynthetic purple bacterium *Rhodobacter sphaeroides*. *Biophysical Journal* **61**, 911–920.

Zhang, J. P., Inaba, T., Watanabe, Y. & Koyama, Y. (2000). Sub-picosecond time-resolved absorption spectroscopy of all-*trans*-neurosporene in solution and bound to the LH2 complex from *Rhodobacter sphaeroides* G1C. *Chemical Physics Letters* **331**, 154–162.

Zhang, W. M., Meier, T., Chernyak, V. & Mukamel, S. (1998). Exciton-migration and three-pulse femtosecond optical spectroscopies of photosynthetic antenna complexes. *Journal of Chemical Physics* **108**, 7763–7774.

Zhao, Y., Meier, T., Zhang, W. M., Chernyak, V. & Mukamel, S. (1999). Superradiance coherence sizes in single molecule spectroscopy of LH2 antenna. *Journal of Physical Chemistry B* **103**, 3954–3962.

Zuber, H. & Cogdell, R. J. (1995). Structure and organization of purple bacterial antenna complexes. In *Anoxygenic Photosynthetic Bacteria*, vol. 2. *Advances in Photosynthesis* (eds. R. E. Blakenship, M. T. Madigan & C. E. Bauer), pp. 315–348. Dordrecht: Kluwer Academic Publishers.